# REPORT DOCUMENTATION PAGE

*Form Approved*
*OMB No. 0704-0188*



| 1. AGENCY USE ONLY *(Leave blank)* | 2. REPORT DATE | 3. REPORT TYPE AND DATES COVERED |
|---|---|---|
| | 10 Jul 97 | |

**4. TITLE AND SUBTITLE**
THE OUTER RADIUS TANGENTIAL WINDS OF TROPICAL CYCLONES

**5. FUNDING NUMBERS**

**6. AUTHOR(S)**
STEPHEN B. COCKS

**7. PERFORMING ORGANIZATION NAME(S) AND ADDRESS(ES)**
COLORADO STATE UNIVERSITY FORT COLLINS, COLORADO

**8. PERFORMING ORGANIZATION REPORT NUMBER**
97-081

**9. SPONSORING/MONITORING AGENCY NAME(S) AND ADDRESS(ES)**
DEPARTMENT OF THE AIR FORCE
AFIT/CI
2950 P STREET
WRIGHT-PATTERSON AFB OH 45433-7765

**10. SPONSORING/MONITORING AGENCY REPORT NUMBER**

**11. SUPPLEMENTARY NOTES**

**12a. DISTRIBUTION AVAILABILITY STATEMENT**



**12b. DISTRIBUTION CODE**

**13. ABSTRACT** *(Maximum 200 words)*



| 14. SUBJECT TERMS | 15. NUMBER OF PAGES |
|---|---|
| | 102 |
| | 16. PRICE CODE |

| 17. SECURITY CLASSIFICATION OF REPORT | 18. SECURITY CLASSIFICATION OF THIS PAGE | 19. SECURITY CLASSIFICATION OF ABSTRACT | 20. LIMITATION OF ABSTRACT |
|---|---|---|---|
| | | | |

THESIS

# THE OUTER RADIUS TANGENTIAL WINDS OF TROPICAL CYCLONES

Submitted by

Stephen B. Cocks

Department of Atmospheric Science

In partial fulfillment of the requirements

for the degree of Master of Science

Colorado State University

Fort Collins, Colorado

Summer, 1997

## ABSTRACT OF THESIS

## THE OUTER RADIUS TANGENTIAL WINDS OF TROPICAL CYCLONES

Knowledge of the strength and horizontal extent of damaging winds from the center of a tropical cyclone is crucial for coastline preparations, forecasting coastal flooding and shipping interests. This study attempts to improve our understanding, estimation and prediction of the outer wind profiles of typhoons. The mean radii of 30 knot (R30), 50 knot (R50) and 65 knot (R65) winds are calculated using aircraft reconnaissance, satellite and synoptic data for 35 tropical cyclones during approximately 300 different time periods. By examining the change in the outer wind profile with time and central pressure, three cyclone classes were noted. One class of cyclones experiences a R30 increase which persists at least one day past its maximum intensity; these are termed "delayed." Another class experiences a trend in R30 that follows the trend in the central pressure; these are termed as "simultaneous". Similar differences were noted for R50 and R65 in simultaneous and delayed cyclones. However, the differences in the two cyclone classes diminish as one goes closer to the inner core. A less common class of cyclone had R30 values that were very large from the beginning of their formation and remained large throughout most of its life cycle. These were designated "gyre" cyclones.

Changes in outer winds as related to time of year, cyclone direction of motion, cyclone size and intensity are discussed for these cyclone classes. Composites of each cyclone class were created and the life cycle of the outer winds, central pressure, eye size, and synoptic size were investigated. Composites of synoptic surface maps showed distinct pressure patterns existed for each cyclone class. A surface pressure index was created which shows promise of early on distinguishing between simultaneous and delayed cyclones. Using

the information developed from previous research and these composite studies, multiple regression equations were developed to estimate various outer wind profiles (R30, R50 and R65).

Stephen B. Cocks
Department of Atmospheric Science
Colorado State University
Fort Collins, Colorado 80523
Summer, 1997

## ACKNOWLEDGEMENTS

In my childhood I have always wanted to study hurricanes, tornadoes, and, in general, weather. Since then I studied severe weather in Oklahoma for six years and at present have studied about typhoons with one of the most notable scientists in the field of tropical meteorology. Therefore, I would like to thank Dr. William M. Gray for giving me the chance to work on this research topic. I also much appreciated the help of Drs. Raymond Zehr and John Knaff and Mr. Frank Wells of the Joint Typhoon Warning Center in Guam for their helpful discussions on my research topic. Expert computer help was always at my beckon with Mr. William Thorson and Rick Taft nearby. I am very grateful for their quick response to my research needs. I could not have done this thesis without the able and most professional help of Mrs. Barbara Brumit, Judy Sorbie-Dunn, and Mr. John Sheaffer. I could not have graduated without the help of Kathy, Sarah and John Cocks, my wife and children. They endured many evenings without daddy being able to spend time with them. Finally, I would like to thank God, the Creator of heaven and earth, who enabled me to fulfill my childhood dreams.

TABLE OF CONTENTS

## LIST OF FIGURES

## LIST OF TABLES

## LIST OF SYMBOLS AND ACRONYMS

CYCLONE: Tropical Cyclone from tropical depression to super-typhoon intensity.

ERxx: The estimated radius of 'xx' not winds. For example, ER30 is the estimated radius of 30 knot winds.

ER04: The equivalent size of the 1004 mb isobar for a tropical cyclone.

GMS: Japan's Geostationary Meteorological Satellite

Intensity: Minimum sea -level pressure of the cyclone measured in whole millibars (mb).

JTWC: Joint Typhoon Warning Center (U.S. Air Force and Navy ) based in Guam.

MSLP: Stands for minimum sea level pressure in mb.

MI: The maximum intensity of the cyclone.

NGR: Negative growth rate associated with the composite life cycle of simultaneous and delayed cyclones.

NGRG: Negative growth rate associated with the composite life cycle of simultaneous and delayed cyclones.

PRxx: The predicted radius of 'xx' knot winds. For example, PR50 is the predicted radius of 50 knot winds.

OCS: Outer Core Strength: Time and area weighted average of wind speed relative to a moving cyclone within a range of 1 to 2.5 degrees from the center.

R30: Average Radius of 30 knot surface, or 35 knot 700 mb winds.

R50: Average Radius of 50 knot surface, or 59 knot 700mb winds.

R65: Average Radius of 65 knot surface, or 76 knot 700mb winds.

R08, R04, R00, R96: These are the latitude adjusted radii of the 1008, 1004, 1000, and 996 mb isobars around the center of a tropical cyclone.

SGR: Slow growth rate associated with the composite life cycle of simultaneous and delayed cyclones.

STGR: Steady growth rate associated with the composite life cycle of simultaneous and delayed cyclones.

STGRG: Steady growth rate associated with the composite life cycle of gyre cyclones.

# Chapter 1

## INTRODUCTION

The origin of the word "typhoon" is associated with the Chinese expression "ta-feng" which means "great wind" (ESCAP/WMO Review, 1985). Typhoons in the northwestern Pacific are some of the largest and most intense cyclones that occur on the globe. Typhoon Tip (October, 1979) not only held the record for the lowest minimum pressure observed in a tropical cyclone (870 mb), but at one point it's radius of 30 knot (15 $ms^{-1}$) winds (R30) extended over 600 n mi (970 km) from the center. It's radius of 50 knot winds (R50) extended over 150 n mi (240 km) from the storm center (JTWC 1979). Tip was one of the largest and most intense tropical cyclones ever observed. However, typhoons of similar intensities can have vastly different outer radius wind strengths. For instance, Abby 1983 had an average R30 of 324 n mi (520 km), while Orchid 1983 had an average R30 of 143 n mi (230 km), over two times smaller in radius and five times smaller in the areal coverage of winds $\geq$ 30 knots. Yet both of these storms had a minimum central pressure (MSLP) of 928 mb at the time their R30 was measured. Likewise storms of similar sizes can have vastly different intensities. For example Holly 1984 whose R30 of 320 n mi (515 km) was roughly the same size of Abby. But Holly's MSLP was 990 mb, 62 mb higher than Abby's. Therefore, the size of a typhoon cannot be based on intensity alone. Research is needed to find other ways of estimating the size.

Most attention has been focused on the cyclone's inner-core maximum intensity. However, various cyclone forecast units realize the importance of knowing the outer radius wind strengths as well. This is important because:

1. Emergency evacuations and preparations for a tropical cyclone typically end when gale force winds reach the coastline. Knowledge of when 30 knot (15 $ms^{-1}$) winds will cross the coastline is critical.

2. The larger tropical cyclones will pose a greater threat of coastal flooding than smaller ones.

3. Shipping interests need to know the extent of changing winds (R30 and R50) from the center of a tropical cyclone to keep from endangering their crews and cargo.

Research using satellite data has attempted to determine the tropical cyclone's outer wind profile. Kidder, Vonder Haar, and Gray (1978) devised a technique that uses microwave sounder data to estimate surface wind speeds around tropical cyclones. The microwave sounder senses warm anomalies above the tropical cyclone. Since warming in the upper troposphere is responsible for the surface pressure drop in tropical cyclones, then these warm anomalies can be hydrostatically converted into surface pressure. Surface wind speeds can then be deduced by assuming gradient wind balance. Kidder et al. 1980 refined this technique, and tested it on an independent data set. The results were good, but difficulties in obtaining microwave data remain to this day. One problem is that microwave sounders are mounted on polar orbiting satellites which have a limited viewing angle, therefore covering only one swath of the earth four times a day. This provides at most a 50% chance that a tropical cyclone will be sufficiently viewed by the satellite to use this technique. Also, if the microwave sounder is looking too far out towards the sides of the cyclone, the resolution becomes too poor to estimate R30 and R50 (Kidder and Vonder Haar 1995).

Microwave scatterometer data has been used to estimate the winds around tropical cyclones. Experiments in the 1960s indicated that there exists a relationship between the surface wind and the back-scattered radar return from the sea surface. The wind causes waves of all wavelengths to occur on the sea surface. The microwave scatterometer pulses microwave radiation towards the sea surface in wavelengths not affected by precipitation.

Sea waves, near the wavelength of the scatterometer, backscatter radiation which can be measured by the scatterometer. This information can be converted into near surface wind speeds and direction (Schroeder et al. 1982; Jones et al. 1982; Stewart 1985). These wind speed and direction measurements are highly reliable and useful. Hawkins and Black (1983), Jones and Zec (1997), Hawkins and Helveston (1997) and others have applied this technology for retrieving the surface winds in tropical cyclones. However, microwave scatterometers are mounted on polar orbiting satellites. This means that this technique is subject to the same data availability problems as the microwave sounder. This problem could possibly be solved in the near future with the addition of more scatterometers on polar orbiting satellites.

The tracking of low-level cloud elements on satellite imagery has also been used to estimate the typhoon's surface wind field (Rodgers et al. 1979, Ottshima et al. 1991, Uchida et al. 1991). Recently, with the advent of high resolution visible GOES and GMS satellite data tropical cyclone low level winds have been more closely estimated by tracking low level cloud elements. Again this provides additional information, but there are limitations. Ray Zehr (oral communication) has noted with many hurricanes, information on gale and hurricane force winds are not available using this technique. High and mid level clouds may obscure the low level clouds preventing any estimates of the wind speeds.

Frank and Gray (1980) used rawinsonde compositing methods to deduce that on average higher outer radius winds are more common with intense tropical cyclones. But there is a wide variation with individual cyclones. Also, higher winds for a given radius are more likely on the right side of the storm (Table 1.1) due to the cyclone's motion. Merrill (1982) made comparisons of small and large tropical cyclones. Using measurements of the cyclone's radius of outer closed isobar (ROCI) on a surface map, he found that the larger storms in both the northwest Pacific and the Atlantic basins generally occur in October and November. In general, the larger cyclones tended to be in the vicinity of the monsoon trough or between two anticyclones along a frontal boundary which extends

equatorwards. These cyclones often grew in size as they traveled northward (Figs. 1.1 a,b). But this relationship is far from a standard one. When Merrill correlated ROCI against the storm's maximum sustained winds and found a variance of only 10 percent (Figs. 1.2 a,b).

Table 1.1: (a) Percent of estimated sea surface winds $> 15ms^{-1}$ on left and right sides of tropical cyclones in the West Pacific. Numbers in parenthesis are total observations from Frank and Gray 1980).

| | Radius (deg latitude) | | | | | | | | | | | | | |
|---|---|---|---|---|---|---|---|---|---|---|---|---|---|---|
| Maximum winds | 1 – 2° | | 2 – 3° | | 3 – 4° | | 4 – 5° | | 5 – 6° | | 6 – 7° | | 7 – 8° | |
| $(ms^{-1})$ | L | R | L | R | L | R | L | R | L | R | L | R | L | R |
| 18-32 | 30 | 33 | 10 | 38 | 6 | 5 | 5 | 13 | 2 | 5 | 5 | 7 | 2 | 3 |
| | (30) | (12) | (40) | (34) | (02) | (38) | (74) | (67) | (88) | (96) | (95) | (103) | (106) | (113) |
| 33-51 | 36 | 75 | 21 | 64 | 20 | 45 | 4 | 22 | 6 | 14 | 4 | 10 | 1 | 2 |
| | (11) | (16) | (29) | (25) | (51) | (53) | (55) | (64) | (84) | (73) | (97) | (91) | (106) | (98) |
| >51 | 71 | 55 | 42 | 65 | 26 | 39 | 16 | 25 | 9 | 14 | 3 | 9 | 2 | 9 |
| | (14) | (22) | (33) | (31) | (53) | (41) | (61) | (71) | (77) | (80) | (70) | (89) | (86) | (118) |

Table 1.1: (b) Same as Table. 1.1 except for the West Indies (from Frank and Gray 1980).

| | Radius (deg latitude) | | | | | | | | | | | | | |
|---|---|---|---|---|---|---|---|---|---|---|---|---|---|---|
| Maximum winds | 1 – 2° | | 2 – 3° | | 3 – 4° | | 4 – 5° | | 5 – 6° | | 6 – 7° | | 7 – 8° | |
| $(ms^{-1})$ | L | R | L | R | L | R | L | R | L | R | L | R | L | R |
| 18-32 | 11 | 18 | 6 | 11 | 0 | 6 | 0 | 2 | 1 | 0 | 0 | 2 | 0 | 2 |
| | (19) | (22) | (35) | (44) | (45) | (48) | (75) | (63) | (76) | (62) | (76) | (62) | (87) | (81) |
| 33-51 | 17 | 60 | 0 | 27 | 0 | 20 | 4 | 7 | 3 | 2 | 0 | 1 | 0 | 0 |
| | (12) | (20) | (25) | (26) | (43) | (55) | (29) | (58) | (64) | (64) | (69) | (71) | (83) | (77) |
| >51 | 25 | 58 | 29 | 35 | 5 | 32 | 0 | 16 | 0 | 4 | 0 | 1 | 0 | 0 |
| | (8) | (19) | (21) | (20) | (19) | (37) | (27) | (45) | (55) | (53) | (51) | (69) | (51) | (77) |

Weatherford (1985) correlated the cyclone's R30 against MSLP and found that although a weak relationship existed, there was too much scatter for use in operational forecasting (Fig. 1.3a). The correlation of R50 and MSLP showed the two variables were essentially independent (Fig. 1.3b). A parameter known as the outer core strength (OCS), the mean tangential wind from 1° to 2.5° from the cyclone center, was created and was found to be highly correlated to R30 (Fig. 1.4). She concluded that the cyclone's outer wind core was only weakly related to the inner core. However,for a given eye size, a good relationship exists between intensity and R30. She hypothesized that if the size of a storm's eye and it's intensity could be known, then the outer core mean wind strength

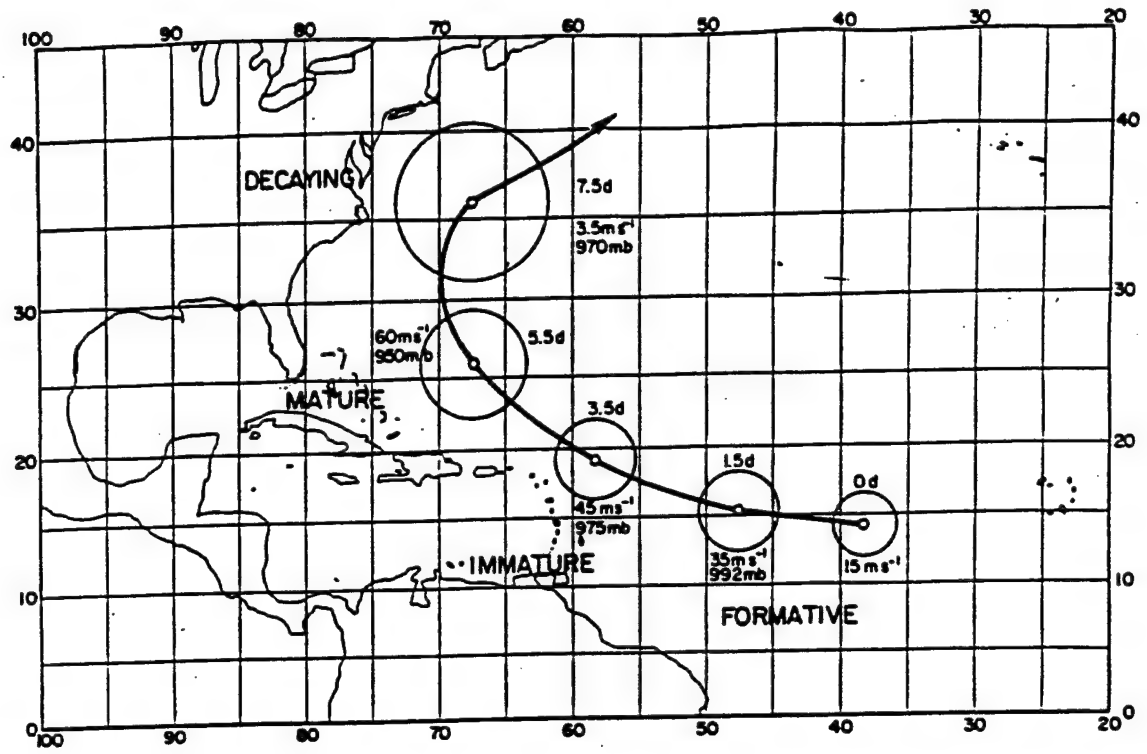


Figure 1.1: (a) Average changes of size and intensity of 12 recurving Atlantic hurricanes. The circle has the same radius as the average outer closed isobar (from Merrill 1982).

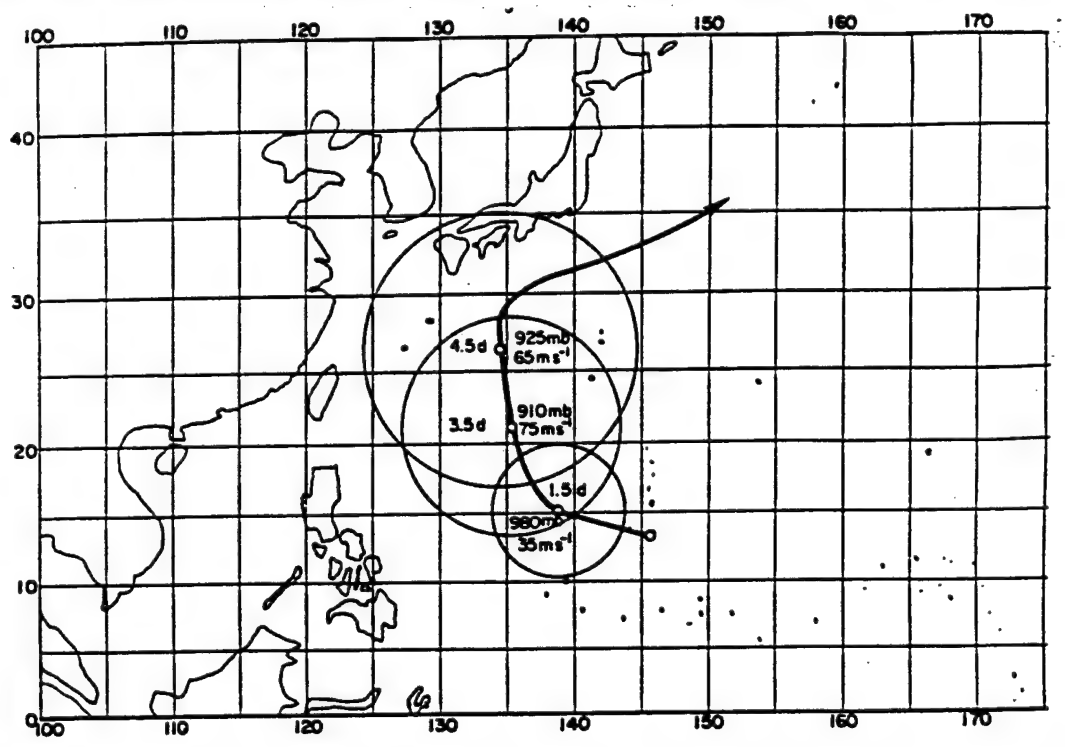


Figure 1.1: (b) Same as Fig. 1.1a except for six October supertyphoons (from Merrill 1982).

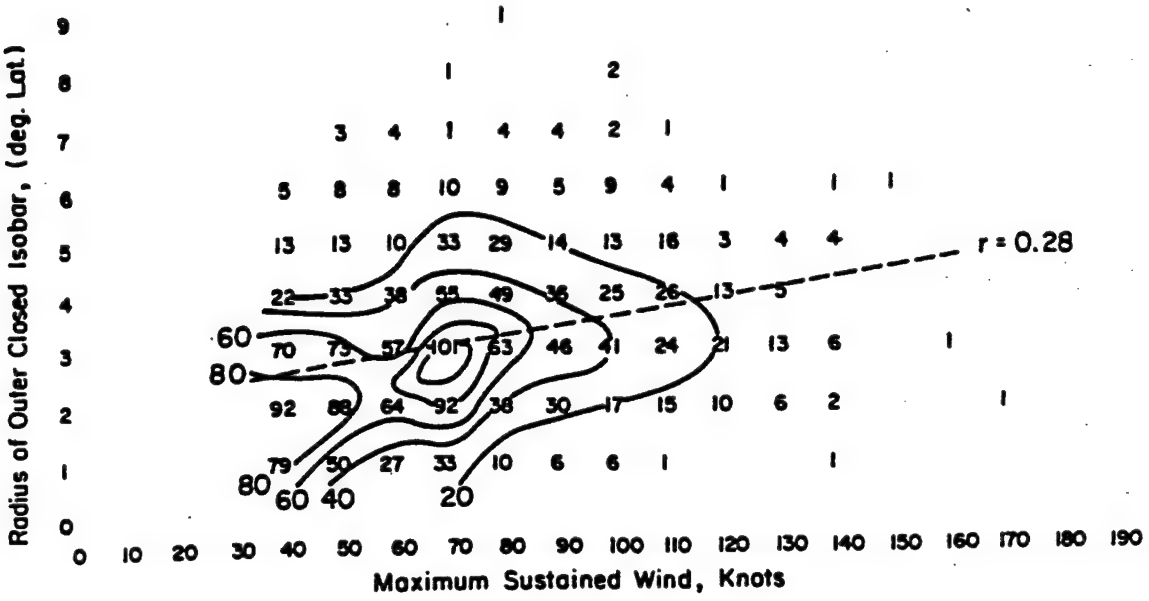


Figure 1.2: (a) Tropical cyclone size as a function of maximum sustained wind for Atlantic tropical cyclones, 1957-1977. Observations are tabulated in classes of 1° latitude and 10 knots (or $5ms^{-1}$). The least square line is fitted to the raw data (from Merrill 1982).

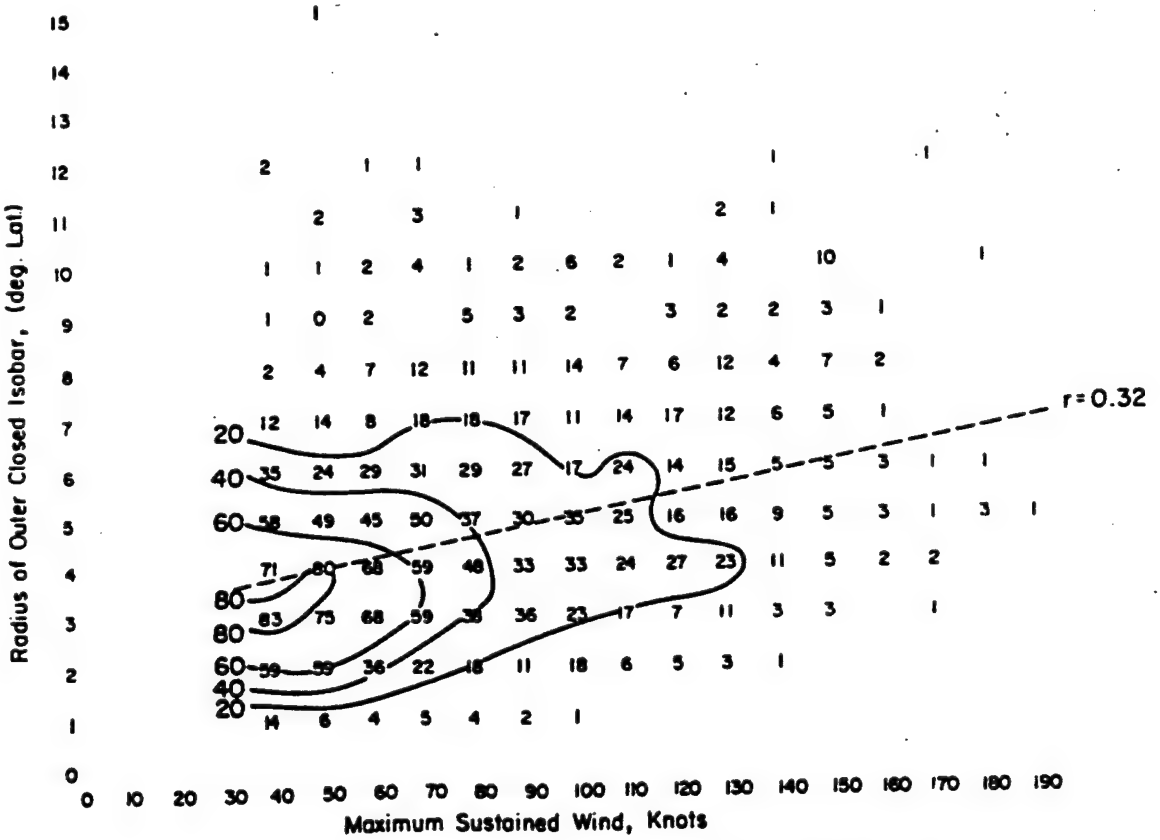


Figure 1.2: (b) Same as Fig. 1.2a except for Pacific tropical cyclones.

(OCS) and R30 could be estimated (Fig. 1.5). Weatherford (1989) also found that, on average, the cyclone's OCS continues to grow past maximum intensity (MI). Her research suggested that typically the OCS will continue to grow until the eye disappears.

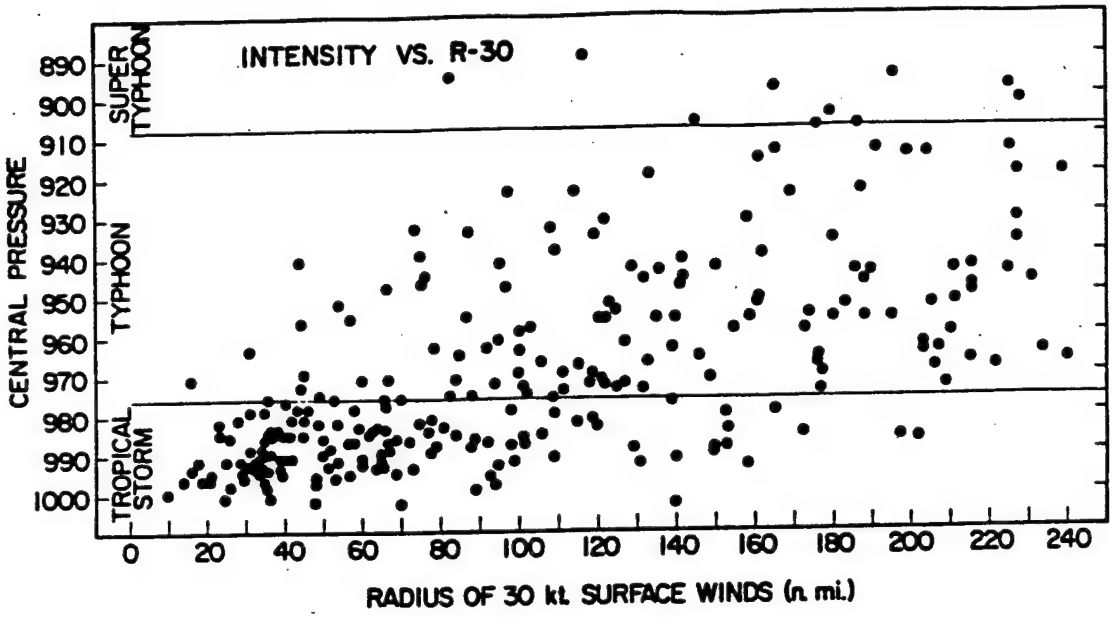


Figure 1.3: (a) Intensity (minimum sea-level pressure) versus the radius of 30 kts (15 $ms^{-1}$); (from Weatherford 1985).

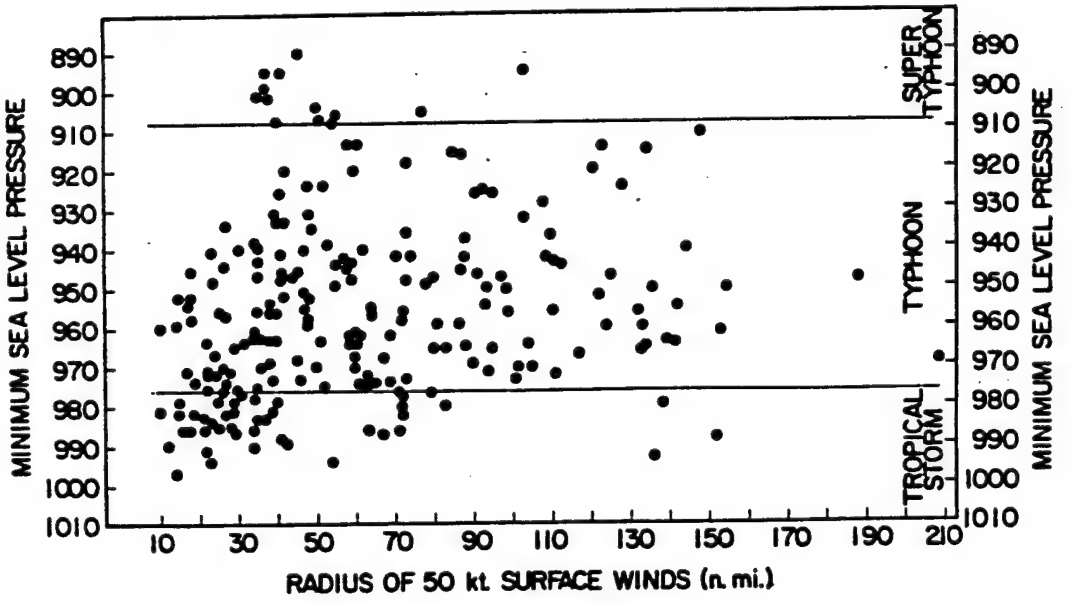


Figure 1.3: (b) Intensity (minimum sea-level pressure) versus the radius of 50 knot ($25ms^{-1}$) wind speed scatter diagram (from Weatherford 1985).

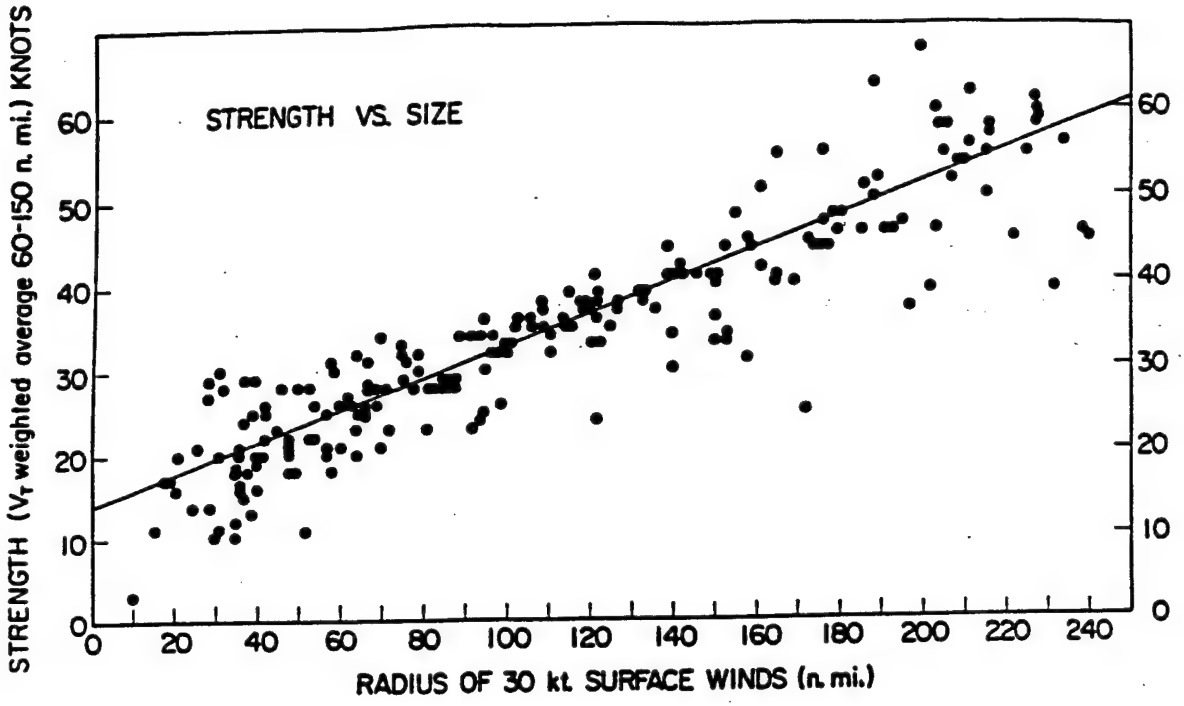


Figure 1.4: Outer core strength versus R30 (from Weatherford 1985).

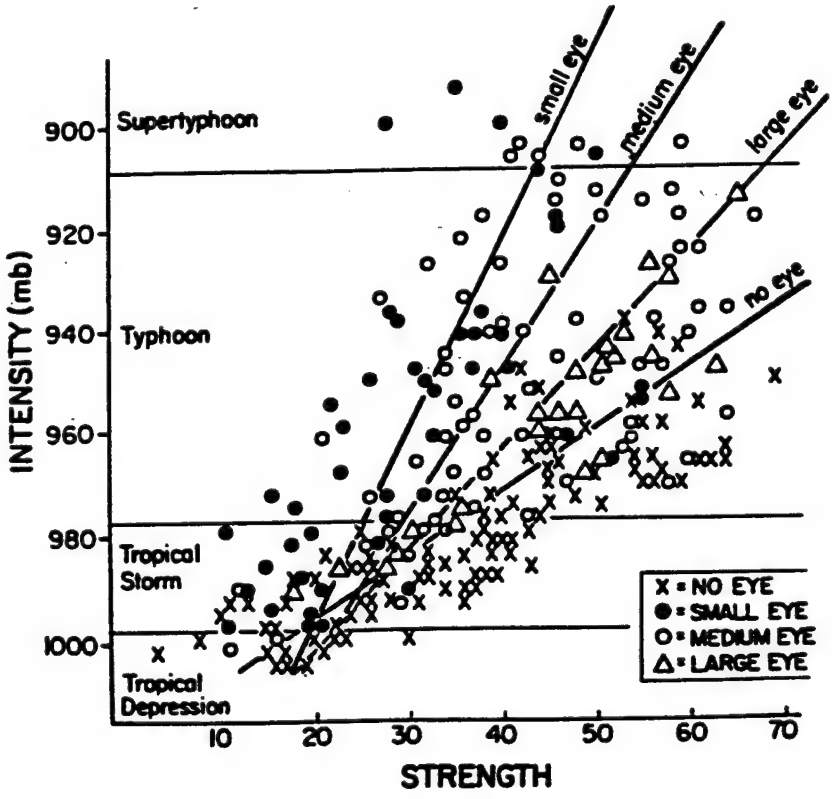


Figure 1.5: Relationship of MSLP versus OCS for a given eye size (from Weatherford 1985).

Wei and Gray (1989) used satellite observations to investigate the outer winds of tropical cyclones. The size of the cyclone's visible cloud shield was measured and then related to R30 (Fig. 1.6). Although this technique had some success the measurement of the cyclone's cloud shield was subjective. Shoemaker (1989) used infrared satellite observations to look for relationships to the cyclone's R30. He, like Weatherford, noticed that some tropical cyclones continued to grow for a time past their maximum intensity. However, there were some cyclones that decreased in size either just before or at maximum intensity. He named these cyclones "simultaneous", and the latter "delayed." His researched showed that 24–72 hr running means of convection colder than −25°C was somewhat correlated with the cyclones R30.

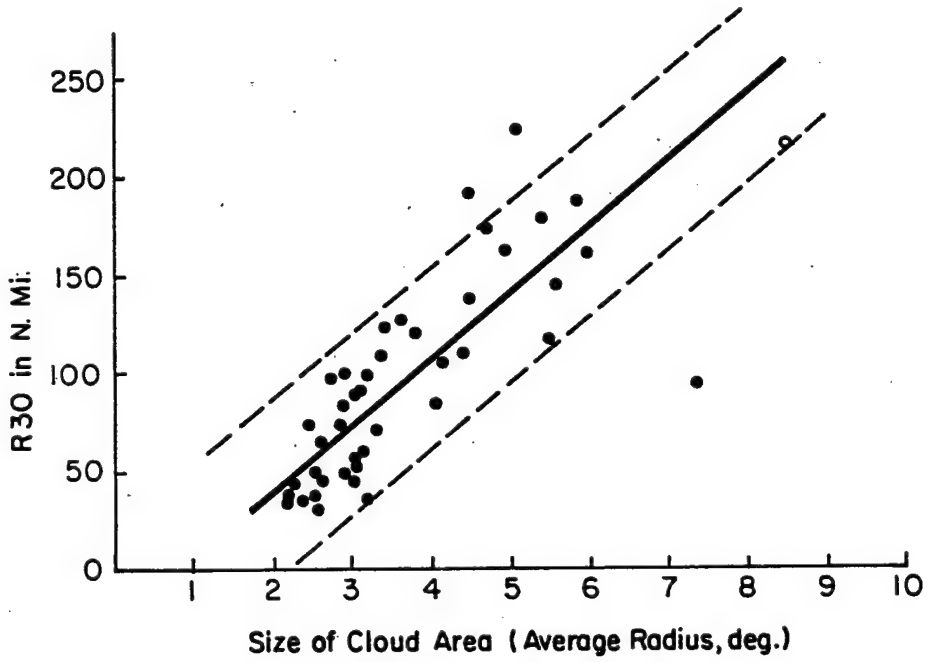


Figure 1.6: Relationship between the mean radius of 700 mb 35 kt (17.5 $ms^{-1}$)wind and the mean radius of satellite observed cloud shield size (Wei and Gray 1989).

One technique used by the Joint Typhoon Warning Center (JTWC) in Guam for forecasting outer wind radii is known as the Holland-Martin method (Frank Wells, oral communication). This technique uses the area of the −65°C cloud shield, the isobaric

value of the outer closed isobar, and the cyclone central pressure within an analytic model developed by Holland (1980). However, Shoemaker (1989) found very little correlation between R30 and the number of cloud pixels colder than −50°C or −75°C. Also, this technique was based upon relatively small tropical cyclones with outer winds dropping off rapidly with radius (Rupp and Lander 1996).

In each case, significant progress was made toward understanding and estimating the tropical cyclones outer wind profile. But there is still room for more research into understanding, estimating and predicting future changes in the outer wind profiles of tropical cyclones. Zehr (1997), on the subject of estimating the outer winds, states "An appropriate approach to the problem may be to develop surface wind analysis techniques using routinely available data as a first guess field, which can be refined by a hierarchy of additional data sources depending on their availability and location to the tropical cyclone."

This paper will focus on the growth of the outer winds in tropical cyclones. It will further investigate the two cases of outer wind profiles found by Shoemaker (1989). It will also try to correlate surface synoptic patterns to different cyclone strengths. Additionally, findings from previous research will be pooled together to develop regression equations used to estimate the cyclones outer winds. These regression equations can be used to provide a "first guess" for the tropical cyclone's outer winds. Additional satellite and synoptic observations can be used to adjust the estimates. Finally, a forecast scheme for prediction of the outer wind profile of tropical cyclones will be developed.

# Chapter 2

# THE DATA SET

## 2.1 Data Set Description

Over 400 aircraft reconnaissance missions were used to study the outer wind profiles of typhoons in the northwest Pacific during the years 1980 through 1984. The reconnaissance missions were performed by U.S. Air Force WC 130 aircraft with wind, pressure and 700 mb height data recorded. Weatherford (1985) describes how the missions were flown, and how the data was collected. She was instrumental in gathering and processing this data set. GMS satellite data was also available for the years 1983 and 1984. A description of the satellite data set and processing procedures can be found in Shoemaker 1989.

## 2.2 Data Methods

### 2.2.1 Flight and Surface Wind Plots

Over 400 flight data plots were processed with observations navigated to the center of the moving cyclone. The wind data were plotted relative to the moving direction and speed of the moving cyclone system. Figure 2.1 shows the typical flight pattern, and the number of observations that were reported on each radial leg and flight mission. Almost all of the missions were flown at the 700 mb level. Note that the data was typically collected no further out than 250 n mi (403 km) from the cyclone center. This meant that R30 for the larger storms could not always be determined using aircraft data alone. Also, some flights did not report data as often as Fig. 2.1 indicates. This caused occasional gaps in the flight data, which made R30, R50, and R65 difficult to analyze. To alleviate these difficulties, surface and rawinsonde observations on synoptic weather maps were used in conjunction with aircraft reconnaissance data to cross analyze and come up with the

cyclone's best R30, R50, and R65. Over 550 Japanese Meteorological Agency synoptic weather maps were used to provide this additional synoptic data. These maps included surface observations and analysis at 12 and 00Z, the cyclone's position, and the central pressure were determined from the aircraft's reconnaissance flights. In addition, 700 mb rawinsonde observations at 12Z were available. When using the synoptic data for these wind analysis, first preference was given to the 700 mb rawinsonde observations since they were identical to the flight level of the aircraft. If this wasn't available, surface reports from ships at sea were used since they are least affected by land induced friction. If ship reports were not available, land observations were used.

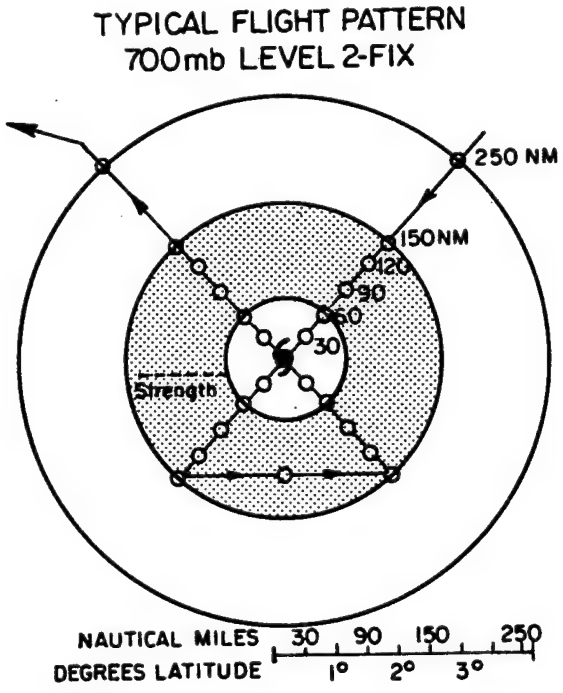


Figure 2.1: Typical flight pattern of USAF reconnaissance of NW Pacific typhoons.

R30, R50, and R65 at the 700 mb level of each storm observation were analyzed for either 4 quadrant or 8 octant averages. There were a few cases where 2 radial leg averages were used to make measurements, but it was less than 10 percent of the overall data set.

Additionally, if the cyclones R30, R50 or R65 measurement didn't surround the cyclone by at least 180 degrees, this case was not utilized. Finally, there were times where R50 and R65 could not be measured although it probably existed. In these cases, R50, R65 were left undetermined. Once R30, R50,and R65 were analyzed, surface wind speeds were assumed to be 85 percent of that at 700 mb (Frank and Gray 1980).

It should be stressed that the 700 mb wind profile was analyzed. The 700 mb and surface outer wind radii were usually well related to each other while the cyclone was over the open ocean, but significant departures could be noted in specific octants which were over land. This is because surface friction is typically higher over land than over water. Thus, one might think that the wind radii at 700 mb could be an overestimate of the surface wind over land than over the sea. However, over the land it is quite possible for winds at the 700 mb level to be brought down to the surface as strong gusts via convective downdrafts (Frank and Gray 1980). Therefore, it is assumed that over land the 700 mb wind profile may be a representative measure of the radial extent of 30, 50 and 65 knot (15, 25, and $33ms^{-1}$, respectively) wind gusts. This study does not make a distinction between the two.

In addition to wind speed and direction, the reconnaissance flights recorded the minimum 700 mb height obtained at the center. Weatherford (1985) found that the 700 mb height, and the minimum central pressure were highly correlated. Therefore, the 700 mb height from the center can be converted to a central pressure via this empirical formula and very accurate central pressure readings obtained. This study uses exclusively 700 mb height observations in proxy of pressure since they were more often available. Another parameter measured was the amount of time (in days) that elapsed since the beginning of the cyclone's life cycle. The beginning was approximately when the cyclone first obtained tropical storm intensity (996 mb). These times varied from about three to eleven days for individual cyclones.

### 2.2.2 Measurement of Cyclone Size on the Synoptic Weather Map (ER04)

Over 400 surface synoptic weather maps were used to measure another important parameter of the tropical cyclone: the radius of the outer two closed isobars. The isobaric values measured were the radius of the 1008 (R08), 1004 (R04), and 1000 (R00)mb isobars. The following rules were used to make the measurements:

- If the outer closed isobar is distinctly deformed in a preferential direction and it encircles 75% or more of the cyclone, then retrace the outer closed isobar so it will follow the next closed isobar (see Fig. 2.2a,b,c).
- If the outer closed isobar is generally deformed, measure the semi-major and semi-minor axis, and find the average radius (see Fig. 2.2d).
- Once the isobar no longer encircles at least 75 percent of the cyclone, that isobar is no longer considered the outer closed isobar. That particular isobar will not be measured again until it completely encloses the cyclone again.

It should be noted that a few measurements were used without nearby observations to provide at least some sort of continuity. However, over 90% of the data did have at least one supporting or verified observation. Once these measurements were made, a 12 hour running mean was created to smooth the data. Data were corrected for longitude convergence due to latitude. For instance, 60 n mi ($\sim$ 97 km) exists between meridians around 5° latitude, but this value is reduced to 52 n mi (84 km) at 30° latitude.

Over 725 outer closed isobar measurements were made. Of these measurements 46% were made of R04, 29% of R00 and 25% of R08 mb. This meant that most of the time, the 1004 mb isobar was one of the outer two closed isobars around the tropical cyclone. An inherent problem with these measurements is as the cyclone intensifies it's outer closed isobar typically opens up. If the outer closed isobar is used as a measure of a cyclone's size only, it would appear that the cyclone became smaller when actually it did not. So, it is desirable to convert every outer isobaric value to a reference pressure value. Since the largest number of measurements were of R04 mb, the 1004 mb isobar was chosen as

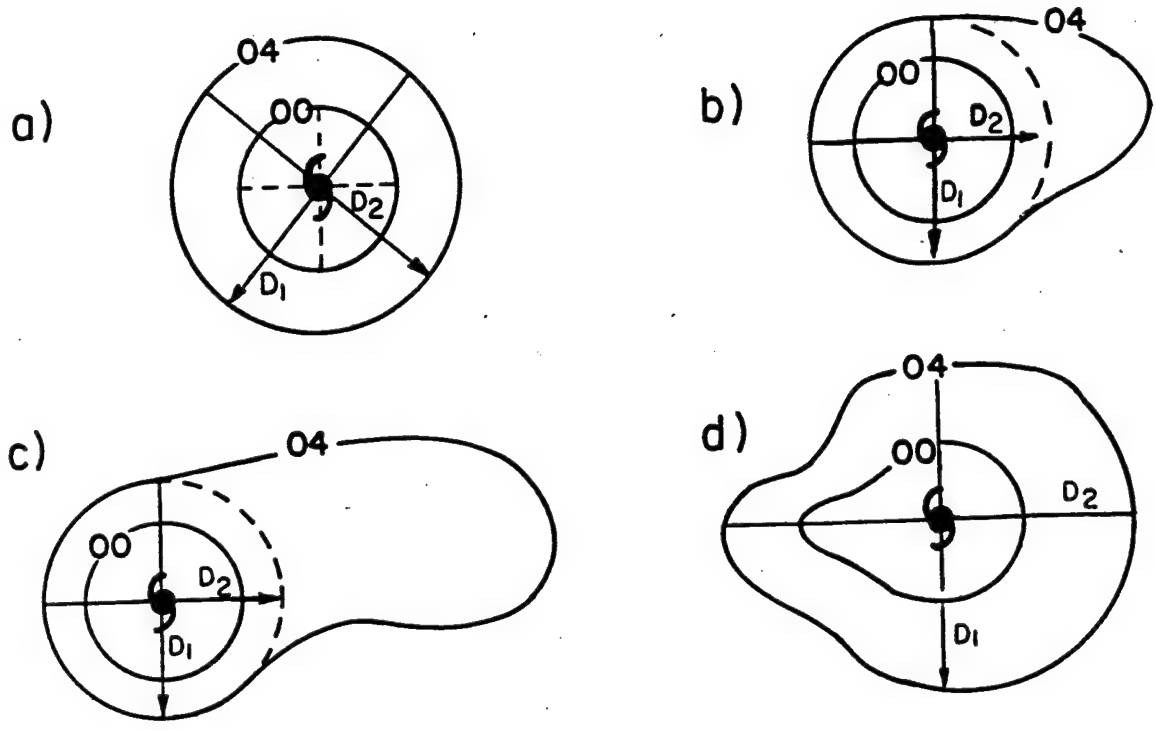


$$\text{Average Radius} = \frac{D_1 + D_2}{4}$$

Figure 2.2: Methods for measuring the outer closed isobar under different synoptic conditions.

the reference value to which outer closed isobars are to be referred. To do this, R08 and R00 were correlated to R04 (see Table 2.1). The standard deviation of the errors from the regression equations ranged from 0.6 to 0.7°. The difference between R08 and R04, as well as R04 and R00, were 1.9 and 1.5° respectively. Therefore, since the standard deviation of the errors are approximately 2.5 times less then R08 minus R04 and R04 minus R00 differences, it was possible to convert 00 and 08 values to a common reference value of R04.

Table 2.1: Correlation test, number of observations, correlation coefficient, variance and conversion equation for converting R08 and R00 values to ER04.

| Test | No. of Observations | Correlation R | $R^2$ | Conversion Equation |
|---|---|---|---|---|
| R08 vs R04 | 146 | 88% | 78% | (Eq. 2.1) ER04 = 0.75*R08 - 0.75 |
| R04 vs R00 | 167 | 90% | 82% | (Eq. 2.2) ER04 = 1.13*R00 + 1.21 |

Thus, R08 and R00 were converted to an Equivalent Radius of 1004 mb isobar (ER04) for all data. This new variable proved very useful as a measure of the cyclone's size throughout it's life cycle.

### 2.2.3 Surface Synoptic Patterns

In order to quantify surface synoptic patterns for various storms, surface pressure was measured at roughly 450, 675, and 900 n mi (725, 1087, and 1449 km, respectively) from the center of the storm along the 290, 315, 360, 045, 070 radials. These measurements were made for each day from two days before to two days after Maximum Intensity (MI). The pressures were then averaged for the three radii along each radial.

### 2.2.4 Satellite Data

The constraint on the satellite data set was to use cyclones whose centers were between latitude and longitude belts below 32°N, and between 115°E and 168°E (see Fig. 2.3). Temperature thresholds used for counting satellite pixels in this study were very similar to Shoemaker 1989 who used threshold values of: 0°C, 25°C, 50°C, and 65°C. Once pixels were counted they were divided by the total number of pixels possible for a particular

radius and multiplied by 100. The number of pixels for a given radius is shown in Table 2.2. This gave the percent areal coverage of pixels colder than a certain temperature threshold. Additionally, 24-hour running means were created to eliminate diurnal affects in the tropical cyclone's convection which was noted by McBride and Gray (1980a,b) as well as Zehr (1987). Also, 48-hour running means were created since a previous study by Shoemaker (1989) showed some correlation with R15 using these averages. Fifteen different tropical cyclones for 1250 time periods were included in this data set.

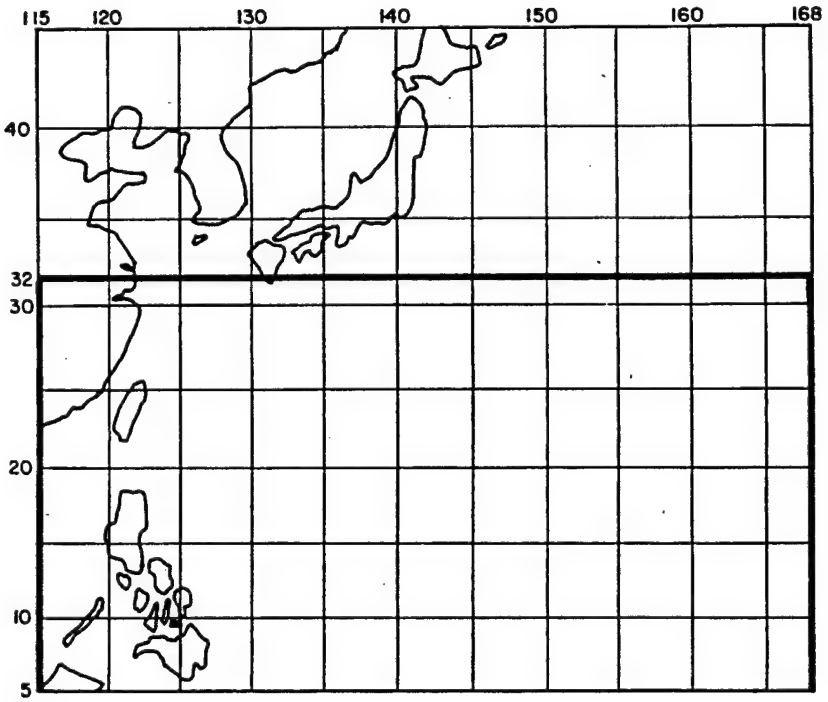


Figure 2.3: Area (outlined in black) that satellite data for tropical cyclones were included in the study.

Table 2.2: Radii (in degrees latitude) and total equivalent pixel counts used for the analysis of GMS data.

| Degrees Latitude | Total Pixels |
|---|---|
| 0-4 | 6082 |
| 2-4 | 4562 |
| 0-6 | 13977 |
| 2-6 | 12457 |

## 2.3 Frequency Distribution of the Data

Thirty-five typhoons between the period 1981–1984 were selected for the study. This represents roughly 60 percent of the typhoons that occurred during that time period. The prerequisite for the selection was that enough measurements of R30 were available to see each cyclone's growth and decay with time. Also, observations of cyclones whose center had crossed over land were removed from the data set. Figure 2.4 shows the distribution of the data set with respect to maximum intensity. It shows that the data set had a below average number of minimal and moderate typhoons (MSLP > 940 mb). This means the data set may be somewhat biased towards the more intense storms ( MSLP < 940 mb). This reflects the fact that these cyclones had longer life spans, usually more intense inner core circulations and outer radius wind profiles that were more persistent and were easier to measure. Many of the weaker typhoons just didn't have enough data information to analyze the life cycle of the R30, R50, or R65.

Distributions of R30, R50, R65, and aircraft measured eye sizes are shown in Figs. 2.5–2.7. The R30, and R50 distribution is somewhat similar to that shown in Shoemaker 1989 with the exception that larger values were obtained since synoptic weather maps were used. Looking at the R50 and R65 distributions would give one the impression of a bi-modal pattern. However, the distributions are including observations of storms without a measured R50 or R65. In the R65 distribution, the 'zero' category was the most frequent. This doesn't mean that typhoons never developed 65 knot winds (33 $ms^{-1}$). It just shows that measurable R65 was available for a shorter period of the cyclone's lifetime. The distribution for aircraft measured eye sizes showed that the most frequent radius was

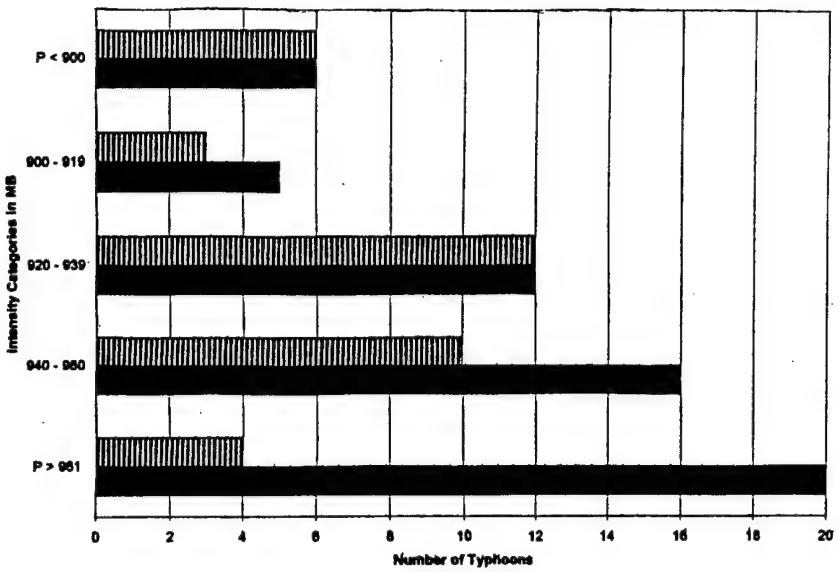


Figure 2.4: The number of typhoons in various intensity categories for the years 1980, 1981, 1983 and 1984 (solid) and those used in this study (striped).

15 to 20 n mi (or 24 to 32 km) in diameter. In general, all of the distributions show a guassion, or semi-guassian distribution. This variable platform of aircraft reconnaissance, synoptic and satellite resources allows a multi-facet investigation of the typhoons outer winds.

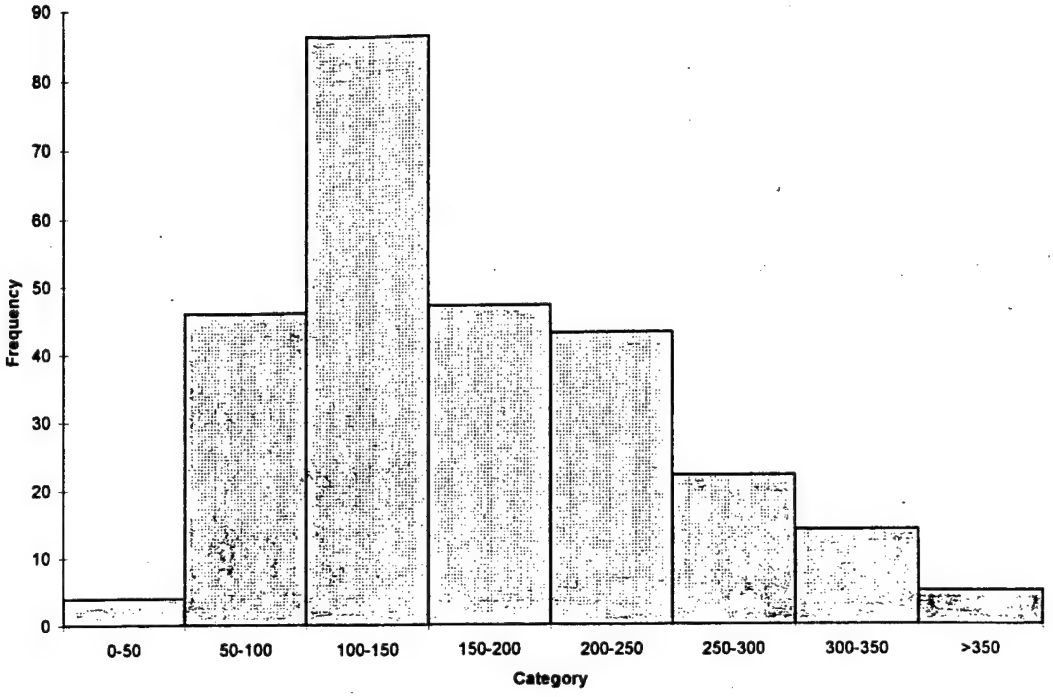


Figure 2.5: Distribution of R30 for 1980-1984 in n mi: All cyclones.

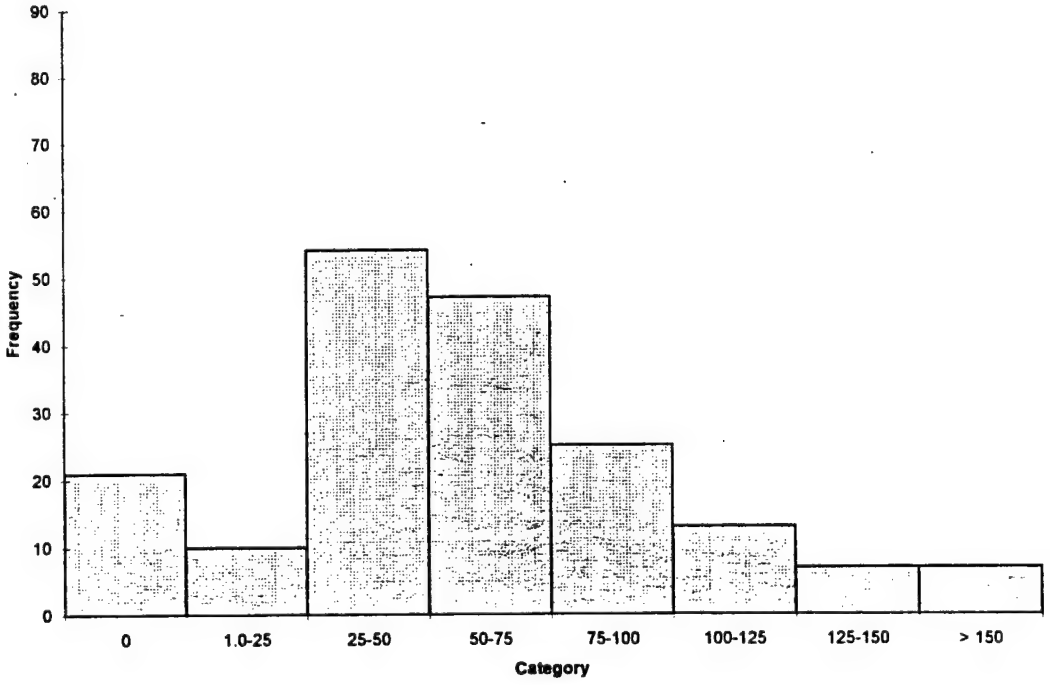


Figure 2.6: Distribution of R50 for 1980-1984 in n mi: All cyclones.

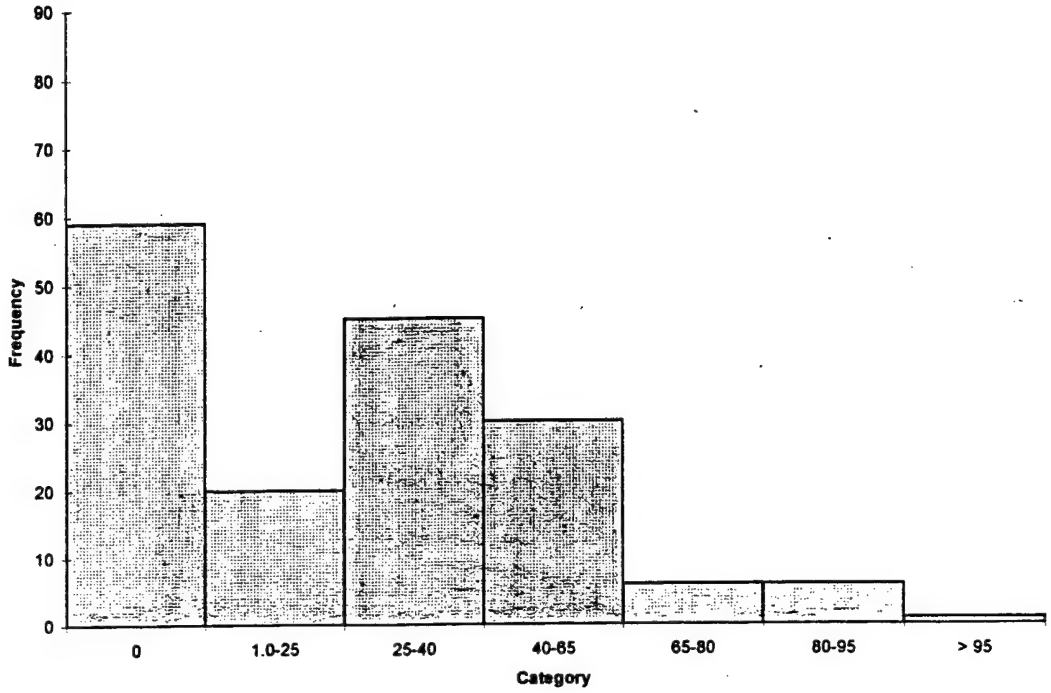


Figure 2.7: Distribution of R65 for 1980-1984 in n mi: All cyclones.

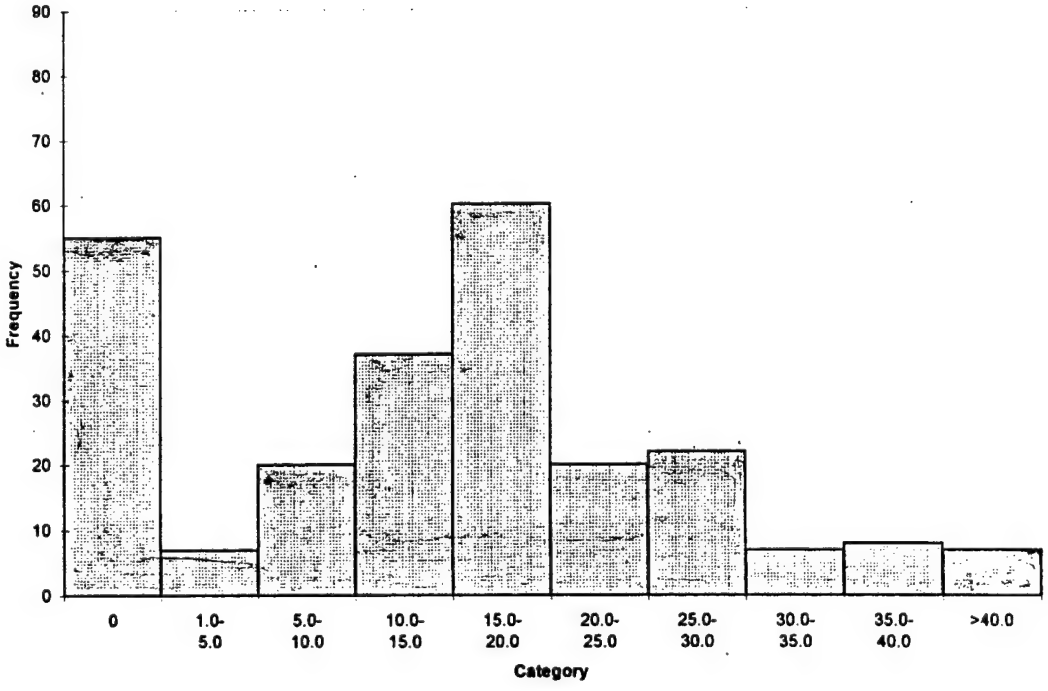


Figure 2.8: Distribution of aircraft measured eye size for 1980-1984 in n mi: All cyclones.

# Chapter 3

# OBSERVATIONS AND CLIMATOLOGY

## 3.1 Two Types of R30 Profiles

Once the data set was prepared and studied, time series of R30, R50, R65, ER04 and MSLP of individual tropical cyclones were produced. These parameters were studied to see how these parameters changed with pressure and time. Some examples of individual cyclone variations will now be given. Figures 3.1 shows Dinah 1984 whose R30 increased one day past Maximum Intensity (MI). Dinah's R50 grew until MI, then remained somewhat constant. Figure 3.2 shows Abby 1983, one of the larger typhoons in the data set. It shows that R30 and R50 continued to increase for at least five days after MI. R65 grew for four days past MI. This seems rather unusual (and causes one to ponder where the extra kinetic energy is coming from). There seemed to be a distinct class of cyclones whose outer winds, most often represented by R30, continued to increase while the cyclone center was filling. In all, there were 13 cyclones in this study exhibiting this characteristic. On average, R30 for delayed cyclones continued to grow for 2.2 days past MI. For five of these cyclones, R30 grew at least 2.5 days past MI. Of the nine cyclones where a growth tend in R50 past MI could be determined, eight of them showed continued growth for at least one day. Although a growth trend for R65 past MI could only be determined for five of these cyclones, four of these showed increasing growth for at least one day past MI. Eight out of thirteen of these cyclones showed secondary pressure minimums after MI. Of the eight cyclones with these secondary pressure minimums, five of them showed a growth in R30 for at least two days past MI. Seven of the delayed cyclones which spent most of their life cycle west of 140°E, showed increases in R30 and R50 for 2.6 days past MI. Six of the delayed cyclones which formed and remained east of 140°E showed increases in R30 for

1.6 days past MI. The trend in R50 for the more eastward cyclones was usually not determinable. This may mean that the cyclones more deeply embedded in the monsoon flow are able to increase their outer winds for a longer time past MI. The delayed cyclones east of 140° longitude tend to travel north and northeastward. This may suggest that they are interacting more often with mid-latitude troughs and may be gaining energy from these troughs.

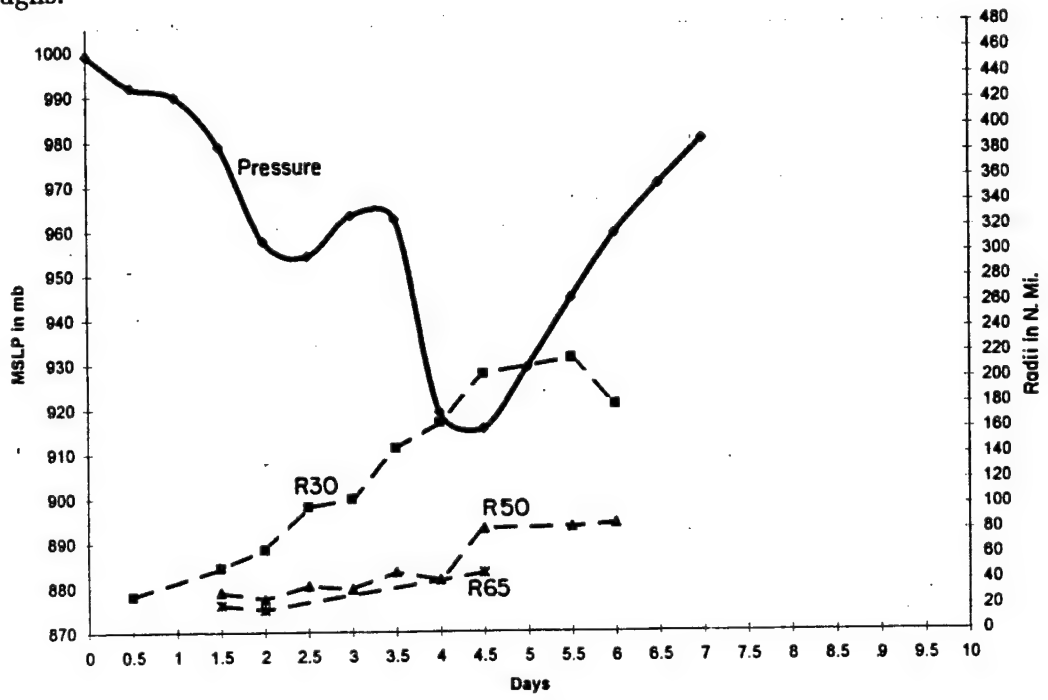


Figure 3.1: The time evolution of R30, R50, R65 and central pressure (MSLP) for Dinah 1984.

However, there was another set of cyclones whose R30 trend seems to follow the trend in the central pressure. Figure 3.3 shows Irma 1981 whose peak R30 value is reached one day before MI. After MI, R30 started to decrease. However, R50 and R65 showed continued growth for at least one day past MI. Figure 3.4 shows Orchid 1983 whose peak R30 value is reached 2.5 days before MI, and then begins to decrease. But R50 and R65 continued to grow until the time of maximum intensity. In all, there were eight cyclones whose R30 exhibited this characteristic. These are termed simultaneous cyclones. Of the eight simultaneous cyclones where a growth trend in R50 could be determined, three of them showed continued growth at least one day past MI. In addition, only two of the cyclones

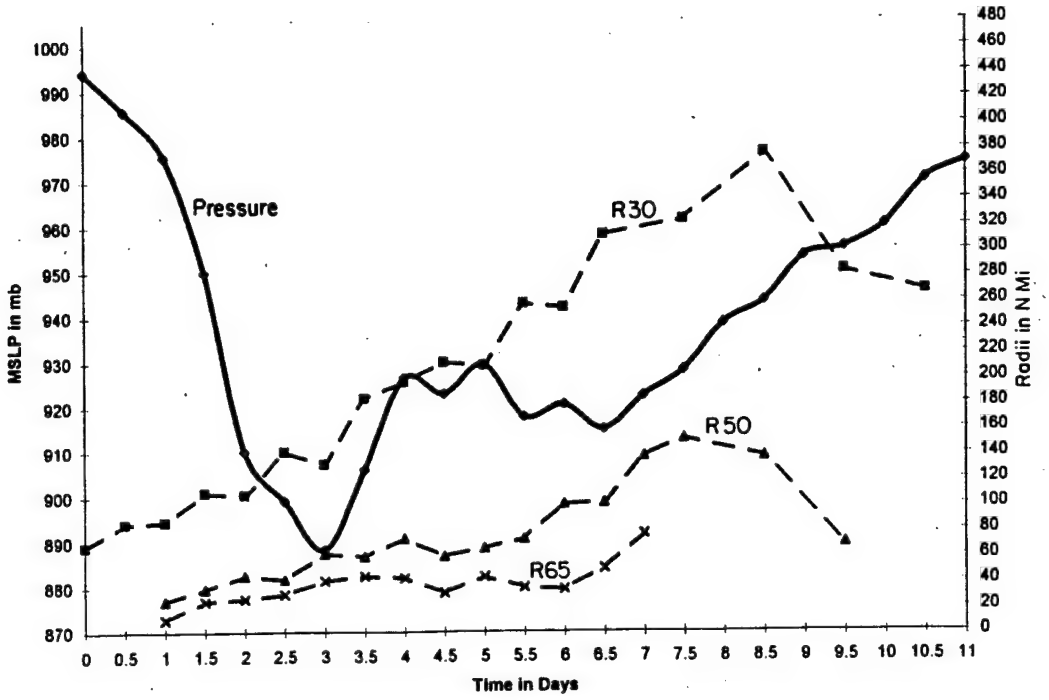


Figure 3.2: The time evolution of R30, R50, R65 and central pressure (MSLP) for Abby 1983.

showed secondary pressure minimums after MI. Only two of the simultaneous cyclones showed growth trends of R65 past MI. Due to the lack of data here, no characteristic trend in R65 could be determined.

This is not the first time these different outer wind classes were found in cyclones. It has been known that cyclones typically expand in size for a period of time as they fill (Weatherford 1988b 1989). Weatherford (1989) created time series of the cyclones outer core strength and central pressure. These time series indicated general classes of cyclones. Those with Outer-Core Strength (or OCS) which continued to increase past MI or decreased at or shortly before MI. Shoemaker (1989) noted this and defined cyclones that continued to increase in size past MI as "delayed" cyclones. Cyclones that reached maximum R30 at or shortly before MI he defined as "simultaneous" cyclones. This study has retained Shoemaker's definition but with slight modifications. All cyclones whose R30 continues to increase at least one day past MI were defined as "delayed." Cyclones whose maximum R30 was reached before, at or less than a day after MI were defined as "simultaneous".

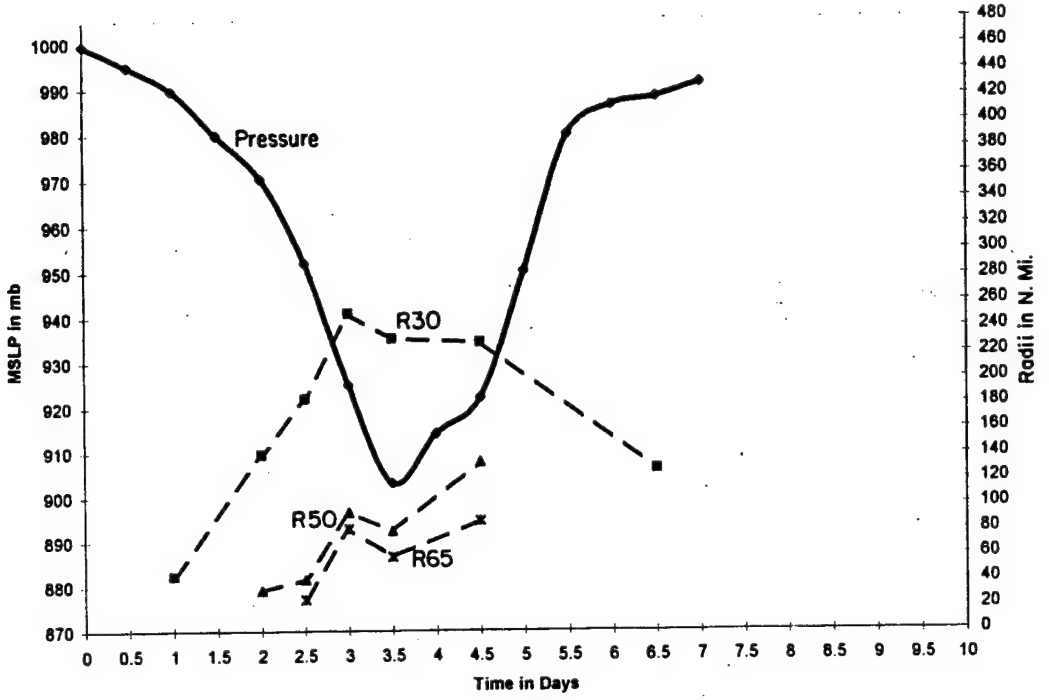


Figure 3.3: The time evolution of R30, R50, R65 and central pressure (MSLP) for Irma 1981.

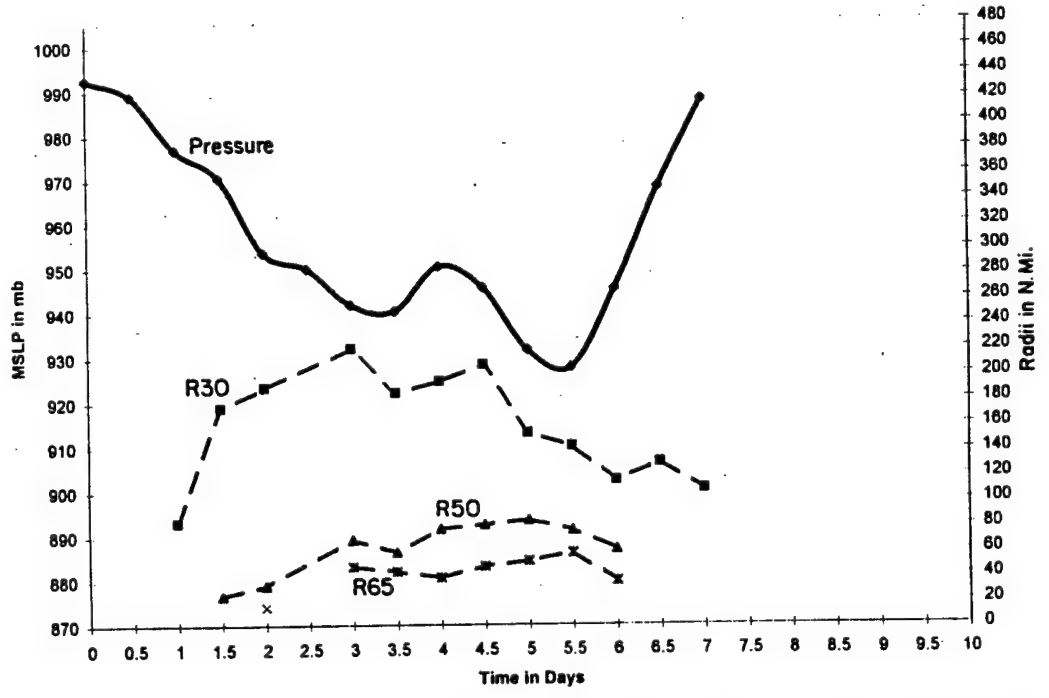


Figure 3.4: The time evolution of R30, R50, R65 and central pressure (MSLP) for Orchid 1983.

There were some curious aspects of each of these classifications. For instance, each delayed cyclone was not the same. R30 for delayed cyclones did not decrease at the same time after MI. Sometimes a cyclone's R30 would increase one day past MI, other times five days past MI. Simultaneous cyclones were not the same either. Some simultaneous cyclone's R30 would start decreasing two days prior to MI while others would start to decrease right at MI.

### 3.2 Very Large Typhoons, or Gyres

There was also a class of cyclones similar to simultaneous ones with regard to their trend in R30. These cyclones usually formed or moved into (early in its life cycle) a broad monsoon trough. They attained very large sizes early in their life cycle. On average, these cyclones had R30 values $\geq$ 190 n mi (305 km) only one and a half days after reaching a tropical storm intensity, while their central pressures were higher than 970 mb. These cyclones were defined as gyres. It must be stressed that gyre cyclones are not the same as monsoon gyres. A monsoon gyre is a very large low-level cyclonic vortex in the Northwest Pacific which may or may not have tropical cyclones embedded within it (JTWC 1993a,b; Hall et al. 1993). Neither should gyre cyclones be confused with Brand's (1972) definition of giant typhoons. Giant typhoons were defined as typhoons whose average outer closed isobar was greater than 10° in radius. The gyre cyclone definition is based upon the life cycle of R30 and the central pressure. Figure 3.5 shows and example of a gyre cyclone. Holly (1984) had a maximum R30 of 390 n mi (630 km) early in its life cycle, yet the central pressure was only 977 mb. Note the life cycle of the central pressure. The cyclone never becomes very intense with only a slow pressure drop to maximum intensity and a slow rise afterwards. We believe this is a consequence of the gyre cyclone's large inertial stability which acts to prohibit inner-core spinup. R30 never increased past MI for these cyclones. Additionally, they showed very slow growth trends in R30. None of the gyre cyclones showed secondary pressure minimums after MI.

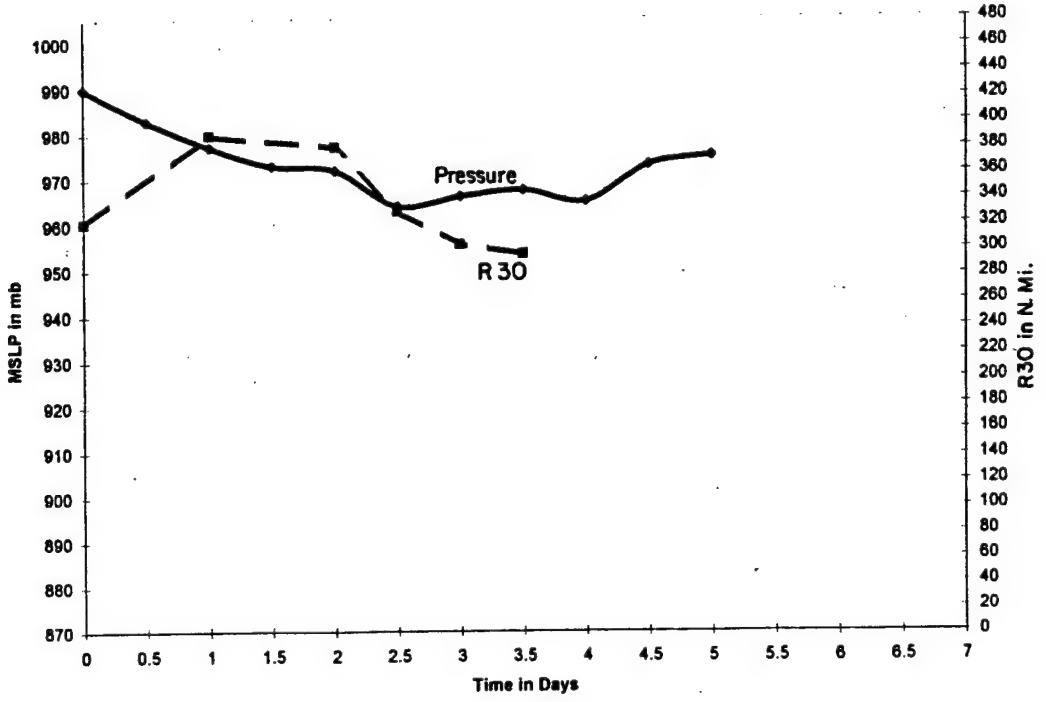


Figure 3.5: The time evolution of R30 and central pressure (MSLP) for Holly 1984.

### 3.3 ER04 and R30 Evolution With Time

Time series of individual cyclone's ER04 and R30 were also created. Figure 3.6 shows Cary 1984 whose maximum R30 occurs four days after MI. From day zero to day two a steady growth in R30 can be seen. However, from day 2.5 to 4 there is very little change in growth; the growth of the cyclone has been interrupted. From day 3.5 to 5.5, a slow growth rate has resumed even though the central pressure is rising. Note that ER04 follows the growth well, even picking up on the interruptions. Figure 3.7 shows Doyle 1984 whose maximum R30 occurs on day 1.5, then stays close to the same value the rest of the period. Here again, an interruption of outer wind growth has taken place, like that of Cary 1984. But in this case, growth did not resume despite the rising MSLP. ER04 does not follow the growth rate well initially but does better during the cyclone's more mature stages. Figure 3.8 shows Dinah 1984 whose R30 increases in a remarkably linear fashion until a day after MI. Note how well ER04 does in following the R30 growth rate. It appears that individual cyclones can have periods of relatively steady and slow increases in R30, as well as periods of little or no change. It was also noted that for a majority of the data, ER04 was well

related to the trend in R30. These observations will prove to be useful for estimating and predicting the tropical cyclone's outer wind profile as discussed in Chapters 5 and 6.

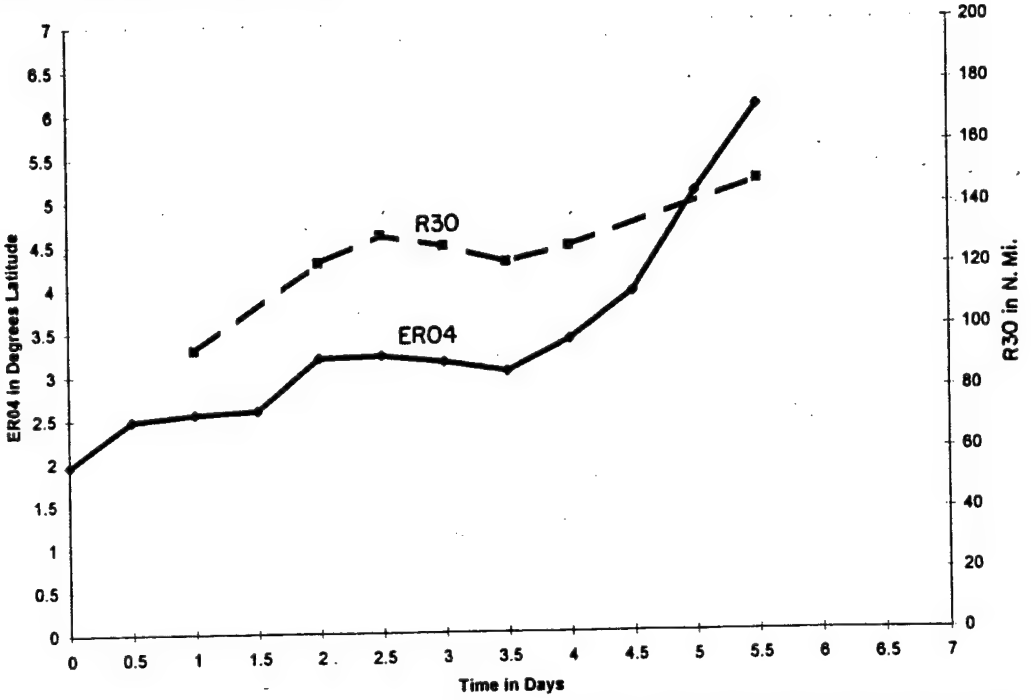


Figure 3.6: The time evolution of R30 and synoptic size (ER04) for Cary 1984.

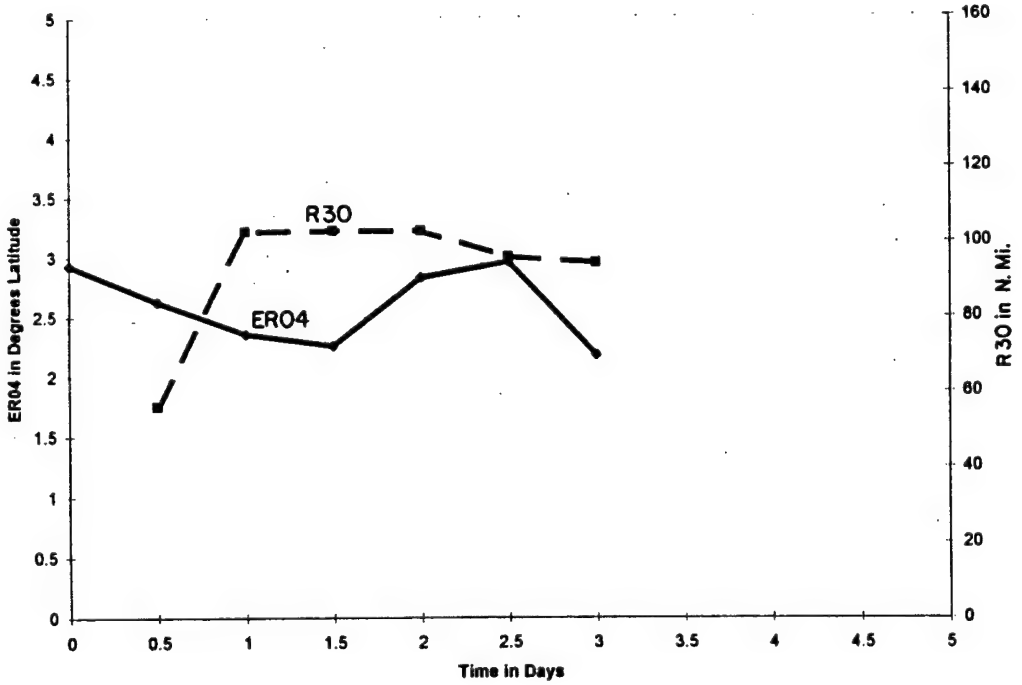


Figure 3.7: The time evolution of R30 and synoptic size (ER04) for Doyle 1984.

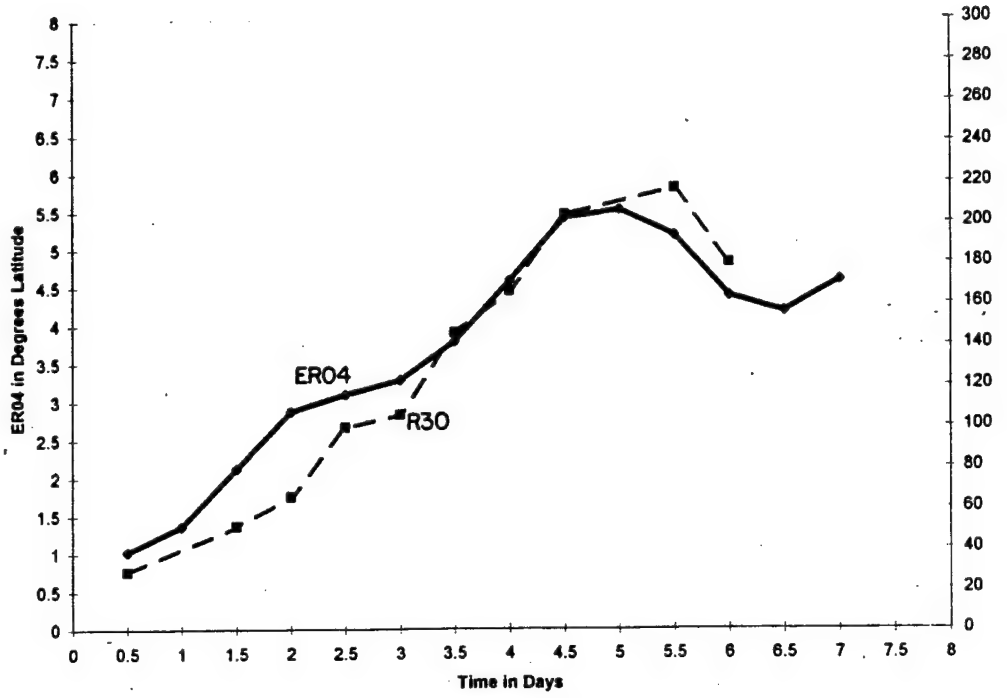


Figure 3.8: The time evolution of R30 and synoptic size (ER04) for Dinah 1984.

## 3.4 Seasonal, Motion, Size and Intensity Climatology of Simultaneous, Delayed and Gyre Cyclones

Of the 26 cyclones that were not interrupted by land near MI,[1] 50 percent were delayed, 31 percent simultaneous and 19 percent were gyres. For stratification purposes, cyclones were also divided into seasonal and late season categories. October fifteenth appears to be the best seasonal dividing date. From this study of typhoons between 1980–1984, forty occurred before 15 October and eighteen after 15 October. Table 3.1 showed that two thirds of the seasonal cyclones were delayed, while approximately the same amount of late season cyclones were simultaneous. Most of the gyre cyclones were in the early season category.

This shows that delayed and gyre cyclones are more likely to be seasonal, while simultaneous storms are more likely to occur late in the season. Figures 3.9 and 3.10

[1]The reason for excluding storms that strike land near MI is there was no way to tell if it would be simultaneous or delayed. However, gyres could be distinguished well before MI. One gyre did strike land just after MI and is the only exception to the non-landfall category.

Table 3.1: Percentage of early season (before 15 October) cyclones and late season (after 15 October) cyclones that were delayed, simultaneous or gyres.

| Cyclone Type | Seasonal | | Late Season | |
|---|---|---|---|---|
| | Number of Cyclones | Percent | Number of Cyclones | Percent |
| Delayed | 9 | 64 | 4 | 33 |
| Simultaneous | 1 | 7 | 7 | 58 |
| Gyres | 4 | 29 | 1 | 8 |
| Total | 14 | 100 | 12 | ~ 100 |

show the geographic locations of seasonal and late season cyclones respectively at MI. Note that seasonal cyclones reached MI generally further north than late season cyclones. Late season cyclones are clustered right around 17°N. This is not surprising. Early in the season, warm sea surface temperatures and the monsoon trough extends further to the north than in the fall and winter. What is noteworthy is the sparcity of simultaneous cyclones before 15 October. This implied that the change in the seasons, and thus the changing synoptic conditions has a strong seasonal component.

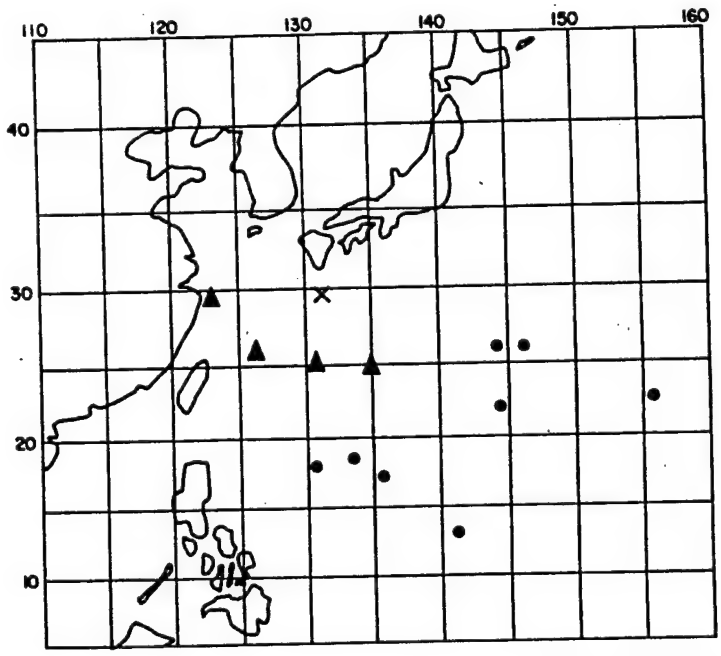


Figure 3.9: The position of seasonal (before 15 October) simultaneous (X), delayed (•), and gyre (△) cyclones at maximum intensity.

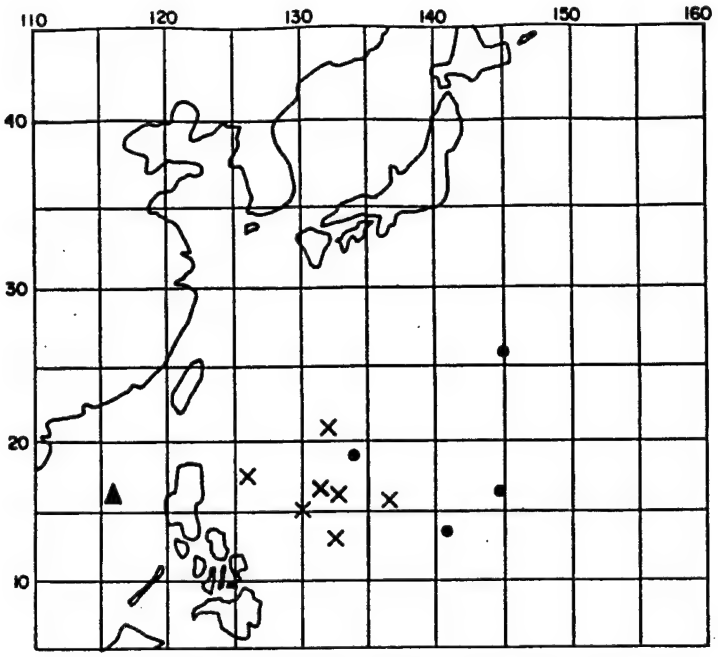


Figure 3.10: The position of late season (after 15 October) simultaneous (X), delayed (•), and gyre (△) cyclones at maximum intensity.

We also found that the different cyclone types have a relationship to their motion. The northward movement of cyclone motion was calculated for delayed, simultaneous and gyre cyclones in degrees latitude per day. The largest distance in degrees latitude was divided by the time it took to cover the distance. For example, Abby 83 moved 24.8° northward in 11 days, thus averaging 2.25° latitude poleward per day. Cyclones that were moving 2° or more northward per day were placed in the northerly category "N". Cyclones that were averaging less than 2° exhibiting more of a westerly or a very slow meandering motion in the westerly category "W".

Table 3.2: Percentage of north (N), and westward or slow moving (W) cyclones that were delayed, simultaneous, or gyres.

| | % N Movers: (17 storms) | % W Movers: (9 storms) | Ratio of Number of Storms North/West |
|---|---|---|---|
| Delayed | 59% | 33% | 3.33 |
| Simultaneous | 18% | 56% | 0.6 |
| Gyres | 23% | 11% | 3.9 |
| Total | 100% | 100% | 1.9 |

Table 3.2 shows that simultaneous cyclones were generally moving westward, or moving very slowly and meandering. The average movement northward of the simultaneous cyclone was $1.69°d^{-1}$. Gyre cyclones have a distinct tendency to move northward. The average movement northward of the gyres was $2.5°d^{-1}$. Delayed cyclones were more likely to be gaining latitude faster than their simultaneous cousins. The average movement northward for the delayed cyclone was $2.92°d^{-1}$, which is 1.7 times more than simultaneous cyclones. The five most northward moving delayed cyclones average change of latitude was $4.44°d^{-1}$. The five most westward simultaneous cyclones had an average change in latitude of $0.72°d^{-1}$ which is six times less than the five most northward delayed cyclones. Only 17 percent of northward moving cyclones were simultaneous, but 62% of the more westerly moving cyclones were simultaneous. These observations are a reflection of the synoptic conditions which govern the motion of tropical cyclones, and perhaps affect the outer wind profile.

Next, the largest and smallest cyclones in the data set were examined with regards to their cyclone type, intensity, and center location at the time maximum R30 was reached. Table 3.3 shows that three of the largest cyclones were gyres. This was expected since they are on average larger than the other cyclone types. There was no preference for simultaneous or delayed cyclones to be in the largest or smallest category. This means that just because a cyclone is delayed does not mean it will be very large. Also, just because a cyclone is simultaneous does not mean it will be very small.

Table 3.3: The number of delayed, simultaneous, and gyre cyclones in the largest and smallest categories.

| Cyclone Category | Eight Largest | Eight Smallest |
|---|---|---|
| Gyres | 3 | 0 |
| Simultaneous | 2 | 4 |
| Delayed | 3 | 4 |

Table 3.4 shows the number of minimal, intermediate, and super typhoons that are in the largest and smallest categories. Mostly supertyphoons and gyres made up the largest cyclones. Most minimal and intermediate typhoons made up the smallest cyclones but

this is not a strong relationship. As noted by Merrill (1980) and Weatherford (1985), only a weak relationship between cyclone size and central pressure. Finally, the position of the cyclone, the month of occurrence, and the maximum R30 obtained are shown in Figs. 3.11 and 3.12. Most of the largest cyclones are west of 135° longitude, and occurred before 15 October generally north of 23° latitude. The smaller cyclones are more scattered about, and occurred after 15 October at a latitude south of 23°.

Table 3.4: The number of minimal, intermediate and supertyphoons in the largest and smallest categories.

| Cyclone Category | Eight Largest | Eight Smallest |
|---|---|---|
| Minimal Typhoon (980 to 950 mb) | 3 | 3 |
| Intermediate Typhoon (920 to 950 mb) | 1 | 4 |
| Supertyphoons (< 920 mb) | 4 | 1 |

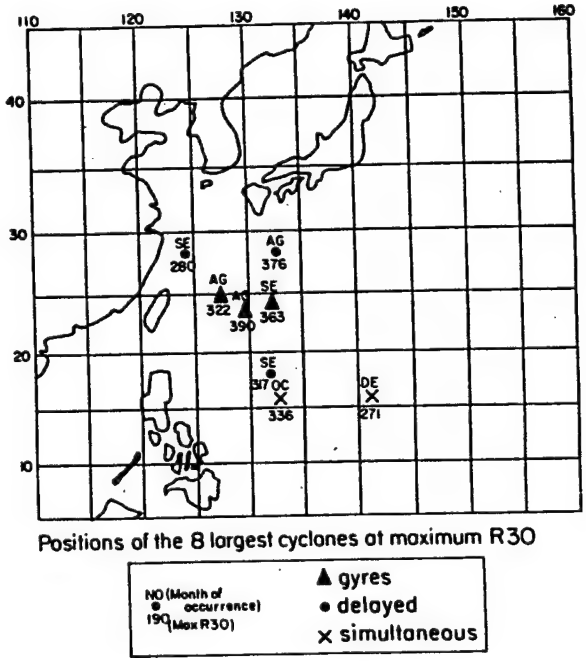


Figure 3.11: The positions of the eight largest cyclones at maximum R30. Gyres are denoted by (△), simultaneous by (X), and delayed by (•). The maximum R30 is below the cyclone symbol, and the month maximum R30 occurred is above.

In summary, there are three classes of cyclones observed in the data set. Delayed cyclones generally show increases in their outer wind radii for at least one day past MI. Delayed cyclones that spend much of their time west of 140° longitude show increases in

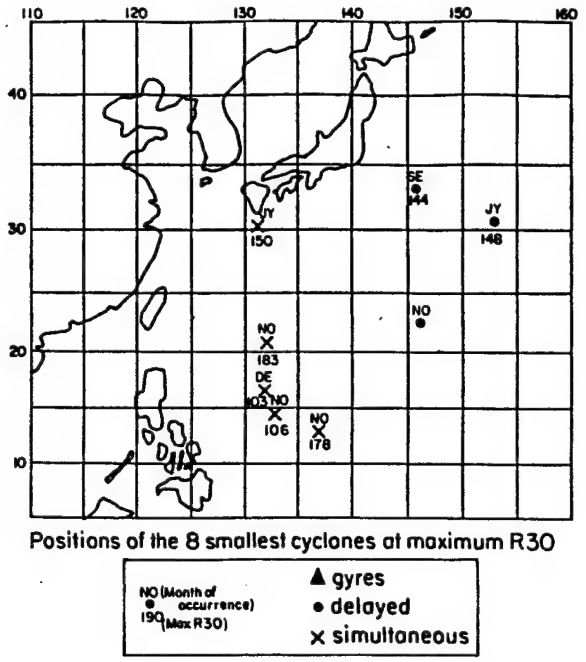


Figure 3.12: The positions of the eight smallest cyclones at maximum R30. Simultaneous are denoted by (X) and delayed by (•). The maximum R30 is below the cyclone symbol, and the month maximum R30 occurred is above.

their outer wind radii for longer periods of time than delayed cyclones that stay further east. Simultaneous cyclones generally show decreases in their outer wind radii prior to or at MI. Gyres are larger than delayed and simultaneous cyclones throughout their entire life cycle. Observations also showed that individual cyclones could show periods of steady, slow or even no increases in their outer wind radii. The size of the cyclone on a surface synoptic map as measured by ER04 tended to follow the trend in R30 which will prove to be useful for forecasting the outer wind profile discussed in Chapters 5 and 6. Delayed and gyre cyclones were more likely to occur before 15 October, while simultaneous ones were more likely after 15 October. Delayed and gyre cyclones tended to have a more northerly component in their motion, while simultaneous cyclones traveled more westward or more slowly. Although gyre cyclones are always large, delayed and simultaneous cyclones can be both large and small. The larger cyclones tended to be further west in comparison to smaller cyclones. Composites of these different cyclone characteristics are investigated in the next chapter.

# Chapter 4

# COMPOSITE STUDIES OF DELAYED AND SIMULTANEOUS CYCLONES

## 4.1 Composites of Pressure, Eye Size, and the Outer Wind Profile

Composite life cycles were developed for delayed, simultaneous, and gyre cyclones which did not interact significantly with land near MI. This composite life cycle would begin approximately when the cyclone first became a tropical storm, go through MI, and end during the later stages of the life cycle. The beginning of the composite life cycle for the entire non-landfall data set averaged around 995 mb, and ended near 980 mb. For delayed cyclones, the average beginning and ending were 996 and 975 mb respectively. For simultaneous cyclones, the average beginning and ending were 994 and 982 mb respectively. For gyre cyclones, it was 995 and 977 mb, respectively.

Once the life cycle was defined, there needed to be a way to normalize the cyclone's life cycle. This is because individual cyclones did not last the same amount of time in the composite life cycle. Abby 1983 spent 11 days in the composite life cycle but Orchid only spent 7 days. One way to do this is to create a time variable that would normalize the amount of time each cyclone spent in the composited life cycle. This was defined as the number of days that have elapsed since the beginning of the life cycle divided by the total number of days in the entire cycle. For example, Abby 1983 had 11 days in it's composited life cycle, so the fifth day of her life would represent the midpoint or the 46% point of the life cycle. After this was accomplished for all cyclones, averages were made of R30, R50, R65, minimum central pressure, ER04, aircraft measured eye size, center track latitude and longitude for roughly the 5, 25, 45, 60, 75, and 95 percent points in the life cycle. In order for a composite average to be calculated, there had to be at least 50% of

all observations available. For example, if there were 26 cyclones in the sample but only 12 observations were available, then an average was not calculated.

### 4.1.1 All Storms

The first composite is composed of all 26 cyclones. The average minimum pressure (941 mb) was reached at the 61% point of the life cycle. R30 generally increased until MI was reached, then started a slow decrease. R50 and R65 also increased up to MI but continued to expand past MI (albeit at a slower rate) to at least the 77% complete point of the life cycle. Figure 4.1b shows that the eye size remains fairly constant with size until near minimum pressure when there was a small contraction. After minimum pressure, the eye size starts to increase until about the 77% of the way through the cyclone's life cycle. After this point, there were not enough eye measurements to make a composite (that is, the eye typically disappears). It is usual to see the expansion of the eye continue for a slightly longer time than the expansion of R30. Figure 4.1c showed that the cyclone size parameter, or ER04, correlated very well with R30.

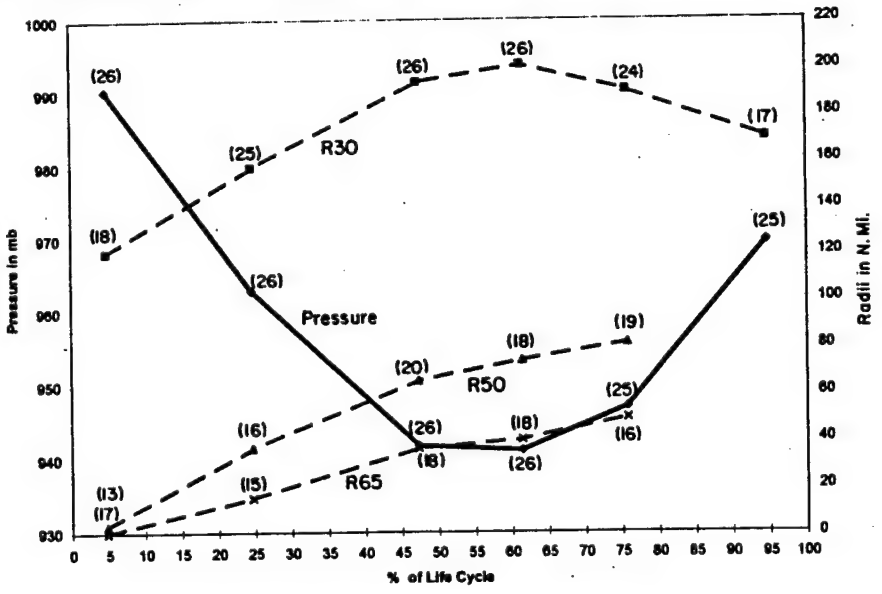


Figure 4.1: (a) Composite of the outer wind profile and MSLP for 26 non-landfall cyclones versus life cycle. Numbers in parenthesis denote number of observations.

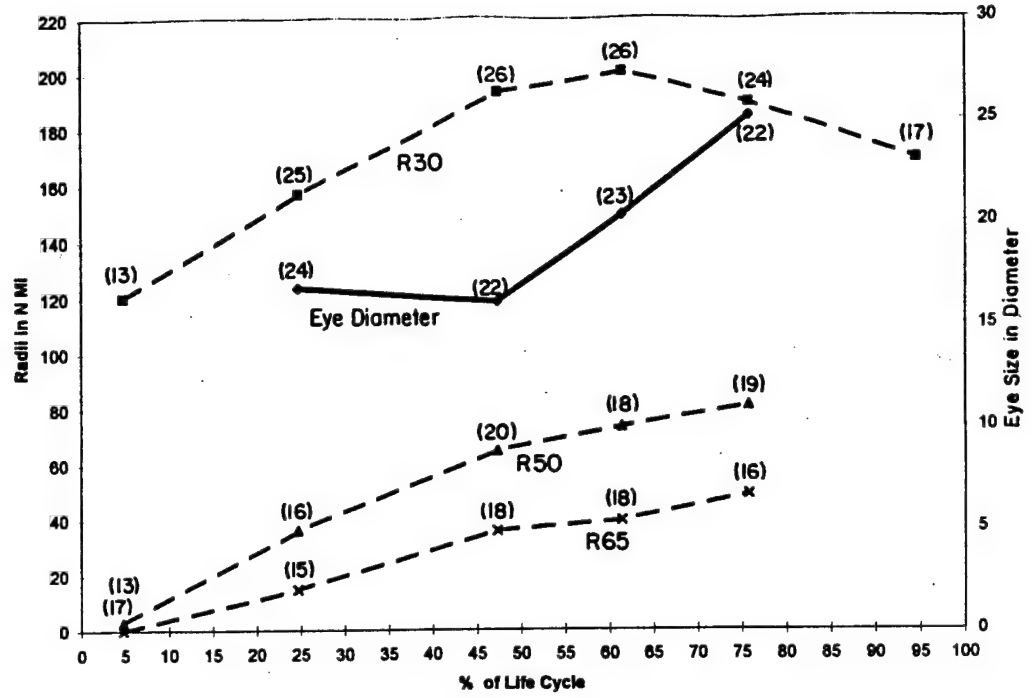


Figure 4.1: (b)Composite of the outer wind profile and eye size for 26 non-landfall cyclones versus life cycle. Numbers is parenthesis denote number of observations.

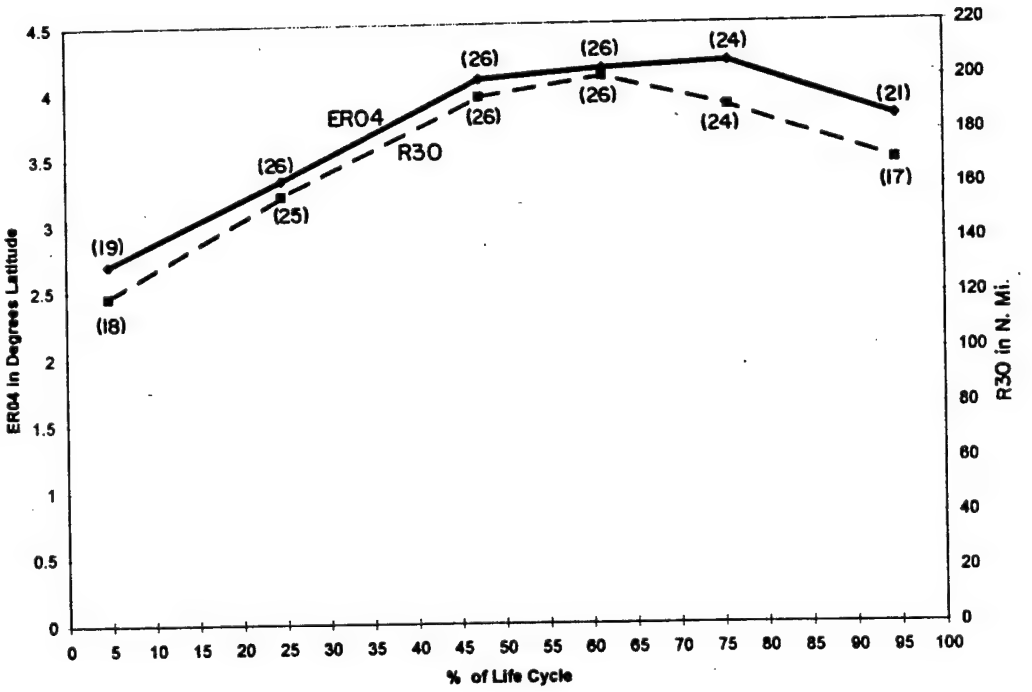


Figure 4.1: (c) Composite of R30 and ER04 for 26 non-landfall cyclones versus life cycle. Numbers is parenthesis denote number of observations.

### 4.1.2 Simultaneous Cyclones

The size of R30 (Fig. 4.2a) during the life cycle of simultaneous cyclones is smaller compared to the composite of all the cyclones. The maximum R30 for simultaneous cyclones, approximately 175 n mi (282 km) and occurs close to MI. R50 and R65 essentially show no growth just after MI. Figure 4.2b shows the eye size life cycle of simultaneous cyclones. Generally, the eye size appears early in the life cycle and is somewhat constant to about the 83% point of the cyclone's life cycle. R30 starts to decrease about the 50% point in the cyclone's life cycle. Weatherford (1989) found that, on average, the eye size typically expands while the storm is filling. She also found that the OCS of the cyclone typically increases until the eye disappears. This however is not observed in simultaneous cyclones, and it may be a clue to why the outer wind profile contracts during the filling stages. Figure 4.2c shows that R30 and ER04 have a close relationship. The average minimum pressure (933 mb) was reached at the 48% complete point of the life cycle.

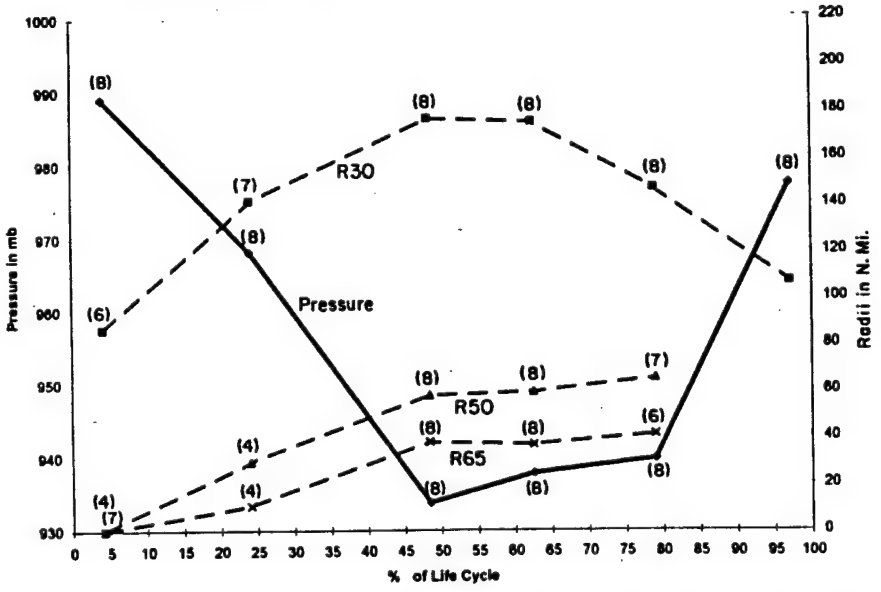


Figure 4.2: (a) Composite of the outer wind profile and MSLP vs. the life cycle for eight simultaneous cyclones. Numbers in parenthesis denote number of observations.

### 4.1.3 Gyre Cyclones

Figure 4.3a, and b shows the composites of five gyres. R30 for gyres (Fig. 4.3a) is largest close to MI with a maximum of about 260 n mi (419 km). Note that R30 at the

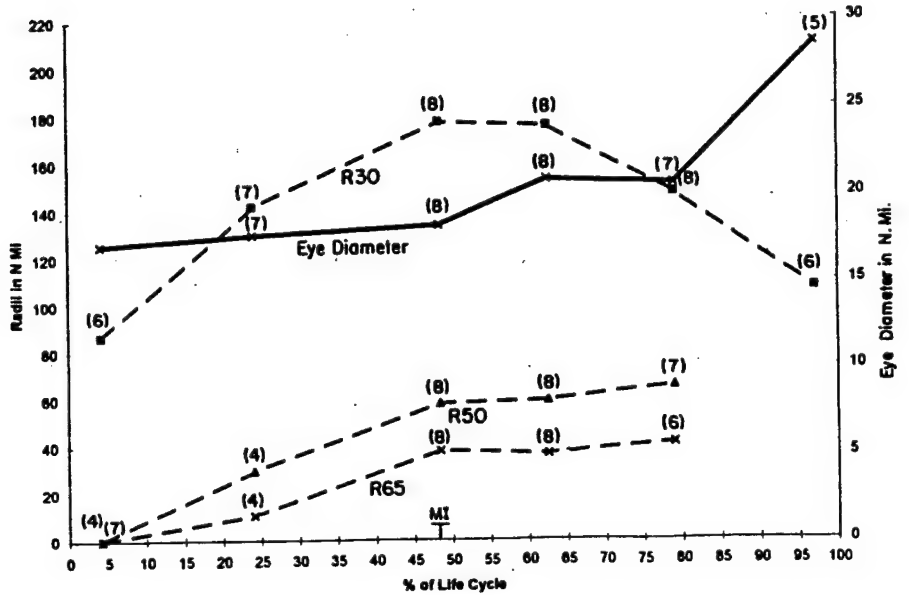


Figure 4.2: (b) Composite of the outer wind profile and eye size vs. the life cycle for eight simultaneous cyclones. Numbers in parenthesis denote number of observations.

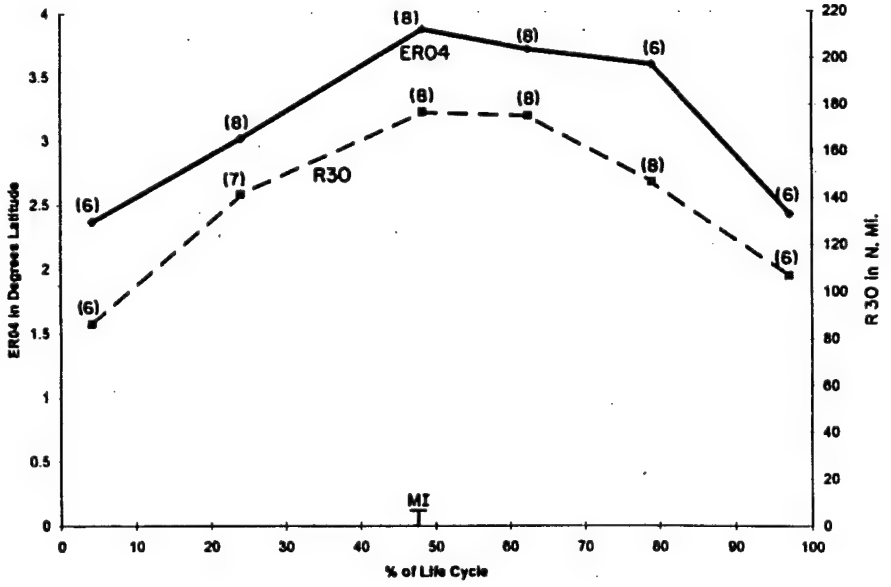


Figure 4.2: (c) Composite of R30 and ER04 vs. the life cycle for eight simultaneous cyclones. Numbers in parenthesis denote number of observations.

beginning of the life cycle is close to 4 times larger than the simultaneous cyclones. In fact, these cyclones, in terms of the depth of their central pressure, and their very large size appear to be quite different from the other two classes of storm types. Composites of R50 and R65 for gyres were not available due to lack of data. Figure 4.3b shows that the ER04 continues to be very well related to R30.

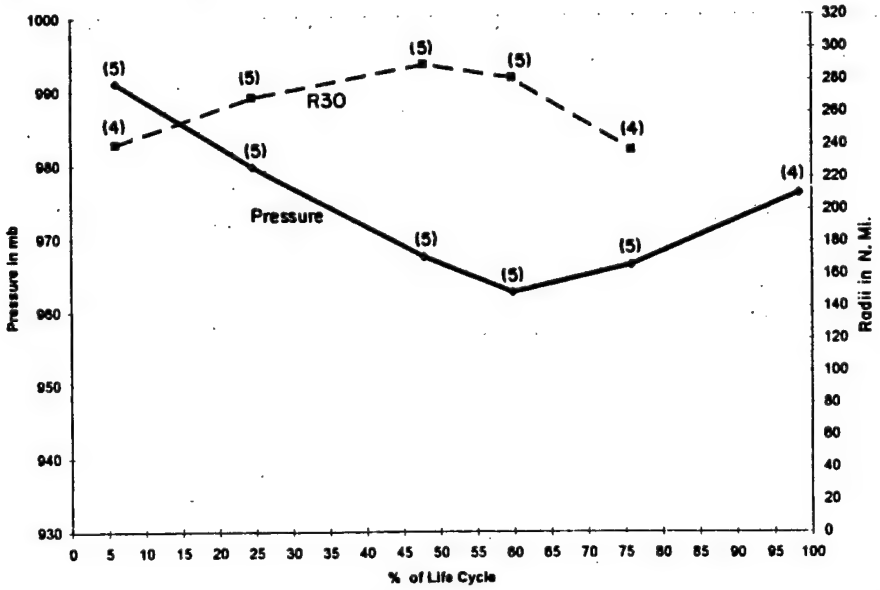


Figure 4.3: (a) Composite of R30 and MSLP vs. life cycle for five gyres. Numbers in parenthesis denote number of observations.

### 4.1.4 Delayed Cyclones

Figure 4.4a shows the composite of 13 delayed cyclones. Note that R30 showed an approximately linear growth up to the 90% point of the cyclone's life cycle. R50 and R65 increased to at least the 75% point of the cyclone's life cycle. The average minimum pressure (936 mb) was reached at the 61% point of the cyclone's life cycle. So on average, MI occurs a little later for delayed cyclones as compared to simultaneous cyclones. Figure 4.4b shows that the eye decreases in size shortly before MI is reached. It then increases to the 75% point of the cyclone's life cycle, and then typically disappears. By the time the eye has disappeared, the increase in R30 has almost stopped which is expected. Also, the eye does not appear to be as persistent late in the life cycle as it is in simultaneous cyclones. Finally, Fig. 4.4c shows that R30 and ER04 correlate extremely well. This

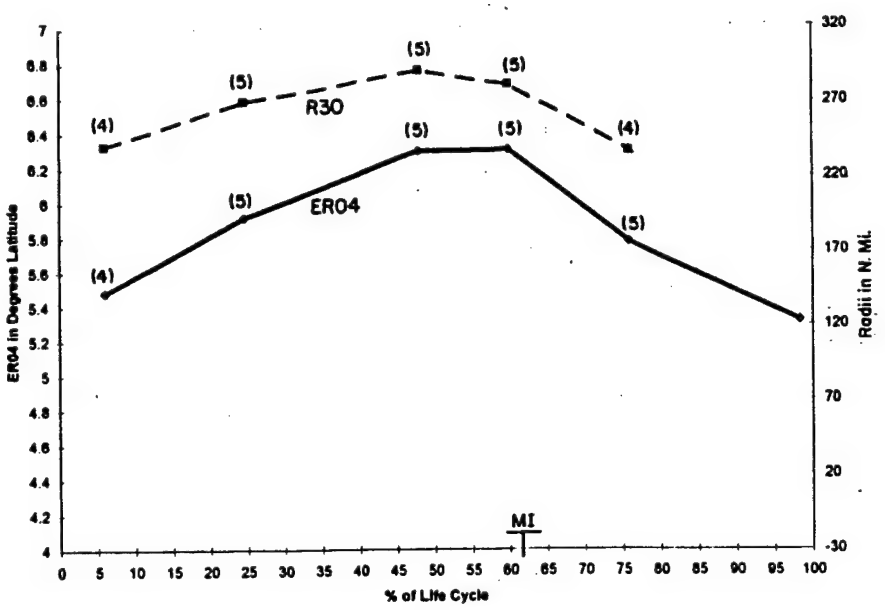


Figure 4.3: (b)Composite of R30 and ER04 vs. life cycle for five gyres. Numbers in parenthesis denote number of observations.

normalized ER04 synoptic size variable is an important way of estimating the outer wind strength.

### 4.1.5 Direct Comparisons

To make direct comparisons of R30, R50, and R65 of each cyclone type they were plotted side by side. The R30 for gyres (Fig. 4.5) were much larger than either delayed or simultaneous cyclones. They exhibit a slow growth and decay throughout the life cycle. The delayed and simultaneous R30 profiles are very similar up until the time of MI. At that point, R30 decreases for simultaneous cyclones, while in delayed cyclones it continues to increase. Figure 4.6 shows a comparison of the central pressure with time for the three cyclone gyres. It showed that the inner core of simultaneous and delayed cyclones are not that different. This may imply that some mechanism is acting close to MI which suppresses the outer wind profile of simultaneous cyclones. This mechanism may be related to the near constant eye size of simultaneous cyclones. Gyre cyclones however do not get anywhere near as intense. They deepen and fill very slowly. Figure 4.7 shows profiles of ER04 for each cyclone type which are very similar to the R30 profiles shown in Fig. 4.5.

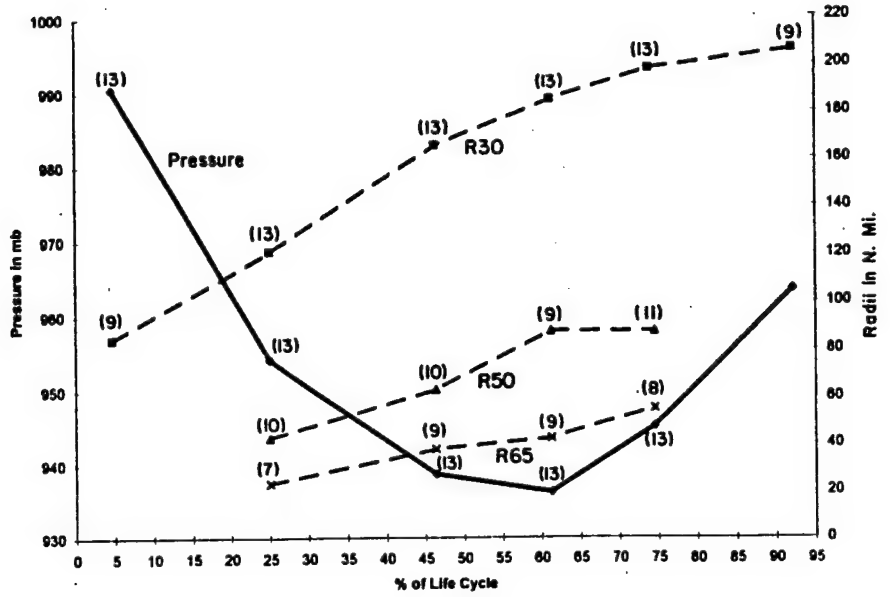


Figure 4.4: (a) Composite of the outer wind profile and MSLP vs. life cycle for 13 delayed cyclones. Numbers in parenthesis denote number of observations.

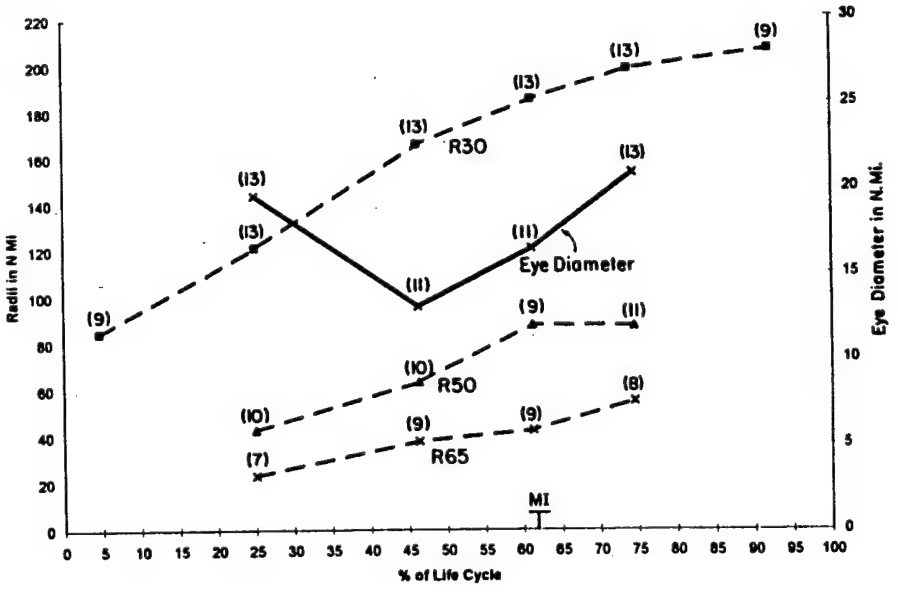


Figure 4.4: (b) Composite of the outer wind profile and eye size vs. life cycle for 13 delayed cyclones. Numbers in parenthesis denote number of observations.

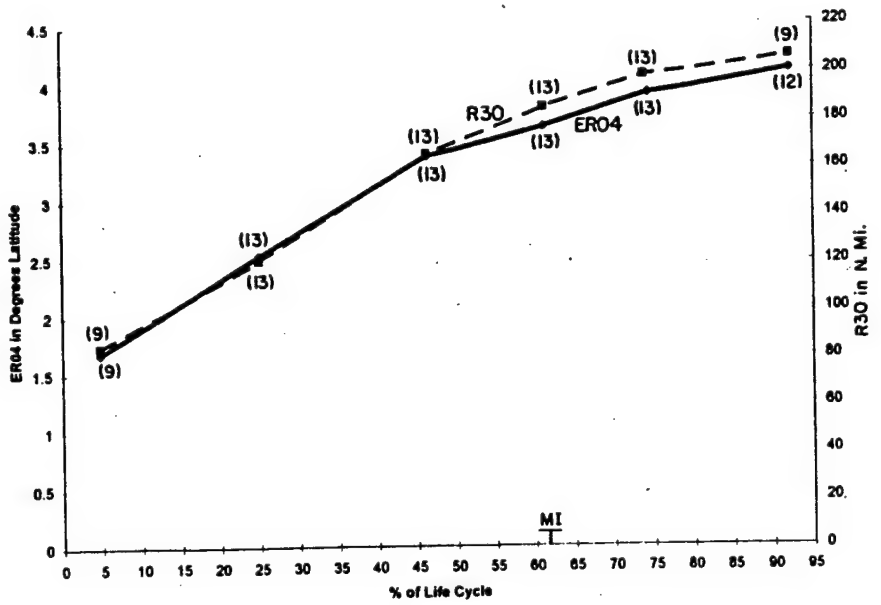


Figure 4.4: (c) Composite of R30 and ER04 vs. life cycle for 13 delayed cyclones. Numbers in parenthesis denote number of observations.

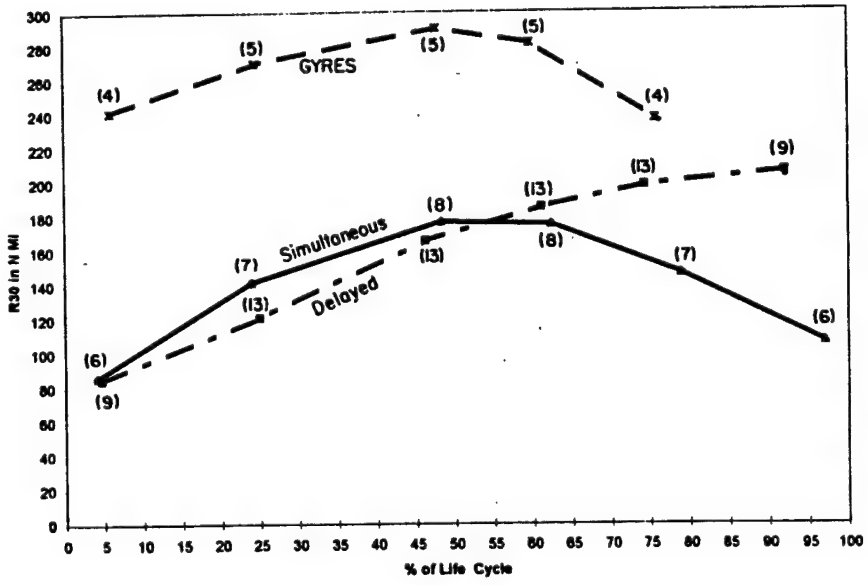


Figure 4.5: Comparison of R30 versus life cycle for delayed, simultaneous and gyre cyclones. Numbers in parenthesis denote number of observations.

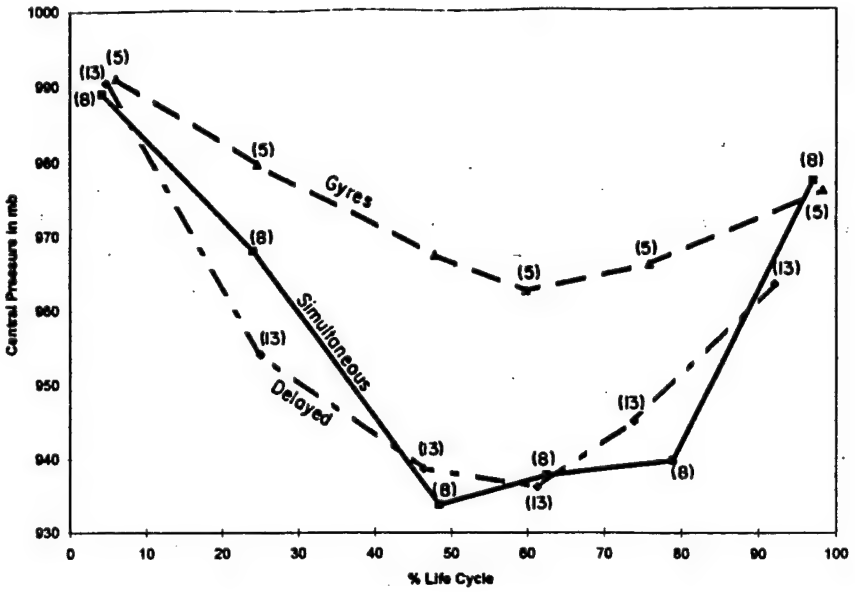


Figure 4.6: (a) Comparison of central pressure (MSLP) versus life cycle for delayed, simultaneous and gyre cyclones. Numbers in parenthesis denote number of observations.

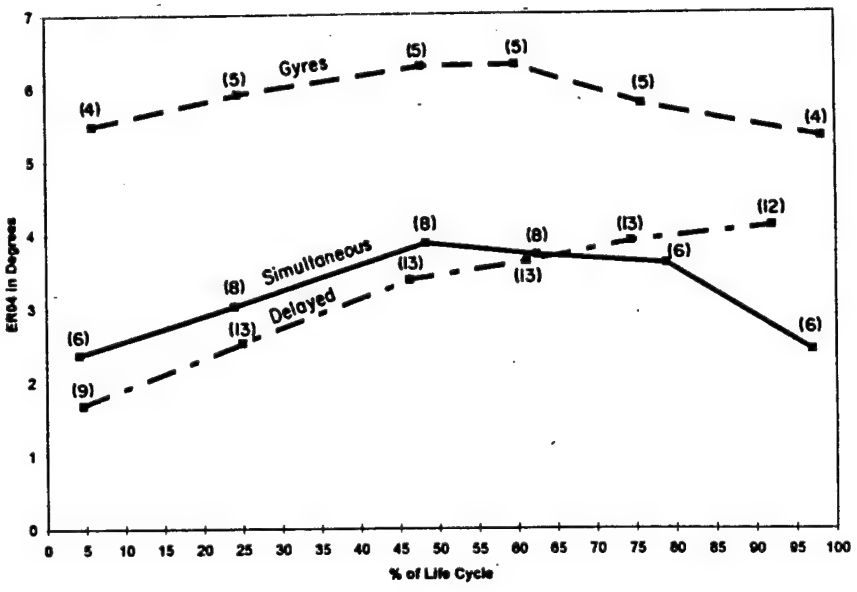


Figure 4.7: Comparison of ER04 versus life cycle for delayed, simultaneous and gyre cyclones. Numbers in parenthesis denote number of observations.

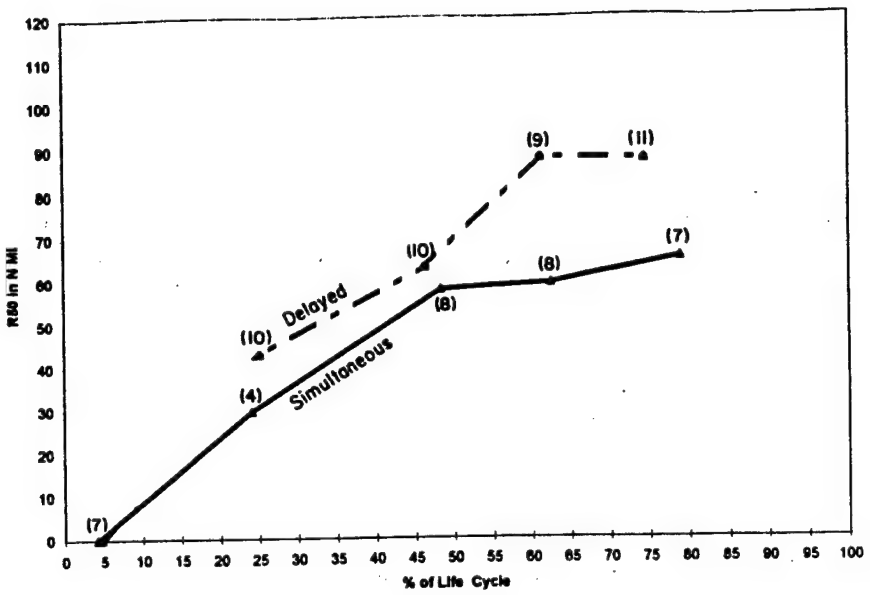


Figure 4.8: R50 versus life cycle. Numbers in parenthesis denote number of observations.

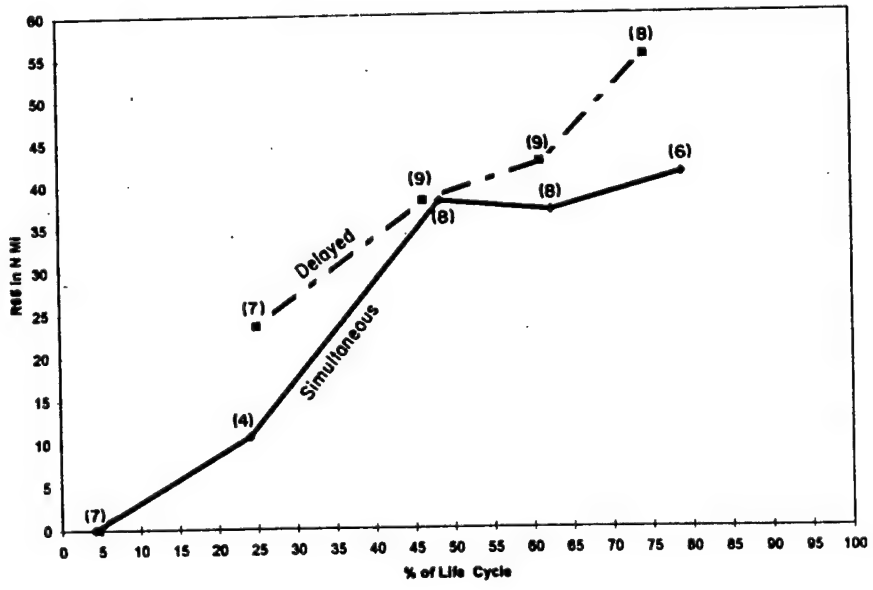


Figure 4.9: R65 versus life cycle. Numbers in parenthesis denote number of observations.

R50 (Fig. 4.8) for both delayed and simultaneous cyclones were very similar until close to the halfway point in the life cycle. At this point, R50 for delayed cyclones continued to increase for a little longer while R50 for simultaneous cyclones flattened out. R65 for delayed cyclones continued to grow a little longer than simultaneous cyclones (Fig. 4.9). Note that the closer you get to the inner core, the less you are able to distinguish any differences in the wind profile between delayed and simultaneous cyclones.

## 4.2 Composites of Cyclone Center Latitude and Longitude

Plots of each cyclone type's latitude and longitude versus it's life cycle were also generated (Figs. 4.10 and 4.11). When viewing center track latitude, delayed cyclones are initially further north by about two degrees than simultaneous cyclones. By the middle of the life cycle, this difference had increased to 3 degrees. At the end of the life cycle, delayed cyclones are about 8 degrees further north than simultaneous cyclones. Gyres tended to behave more like delayed cyclones in terms of latitude gain during the life cycle but are initially located a little farther north. Throughout their life cycle, gyres were about five degrees further north than simultaneous cyclones, and about two to three degrees further north than delayed cyclones. The author believes that these observations are related to the synoptic conditions governing the cyclone motion. Gyres appear to be gaining latitude at the same rate as simultaneous cyclones but are located further north due to the northward placement of the monsoon trough. Delayed cyclones can be seen to gain latitude at a faster rate than simultaneous and gyre cyclones indicating the presence of a south-north upper-level steering flow.

This steering flow may indirectly cause the eyes of delayed cyclones to expand after MI. The 'inertial stability' or the resistance of the air to horizontal displacement is given by:

$$IS = [(\zeta_r + f)(\tfrac{2V_t}{r} + f)]^{1/2}$$

where 'IS' is the cyclone's inertial stability in $s^{-2}$, $\zeta_r$, *and* $\frac{2V_t}{r}$ are measures of the cyclone's vorticity, and f is the Coriolis parameter. As delayed cyclones move far enough northward,

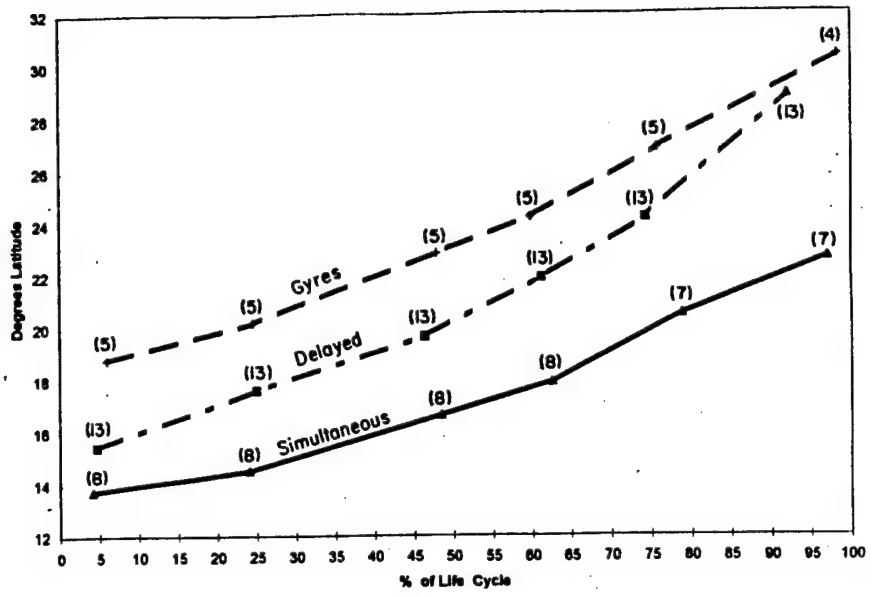


Figure 4.10: Cyclone latitude versus life cycle for delayed, simultaneous and gyre cyclones. Numbers in parenthesis denote number of observations.

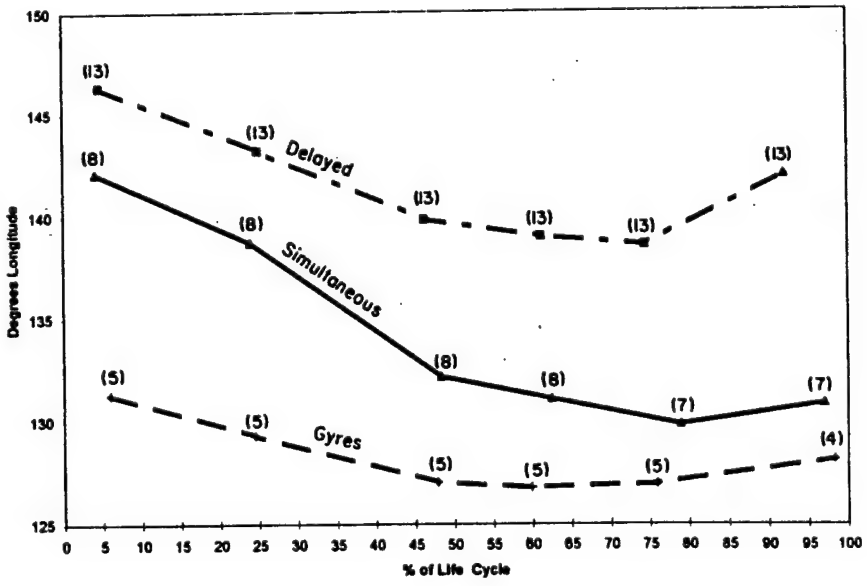


Figure 4.11: Cyclone longitude versus life cycle for delayed, simultaneous and gyre cyclones. Numbers in parenthesis denote number of observations.

f gets larger. A point is reached where the air cannot reach the center of the cyclone due to the increase of inertial stability. this may help cause the eye to expand as the cyclone moves northward. This may intensify the outer core winds since momentum is advected through the outer core towards the expanding eye.

Simultaneous cyclones have a more westward component of motion. Therefore, their IS does not reach the point where air can reach the cyclone center until late in the life cycle when it is higher in latitude. This would explain the relatively constant eye size for these cyclones until late in the life cycle. It also explains simultaneous cyclones having a slightly larger R30, and therefore a stronger OCS than delayed cyclones prior to MI. The eye size for simultaneous cyclones is not contracting while delayed eyes are prior to MI.

Large differences could also be seen when viewing each cyclone type center track longitude. Initially, delayed cyclones were further east than simultaneous cyclones by about 4 degrees. This difference increases to about 7 degrees halfway through the life cycle. At the end of their life cycle, delayed cyclones are almost 11 degrees further east than their simultaneous cousins. This shows that delayed cyclones tend to have a westward component of motion until the 45 percent point of their life cycle. At this point, predominantly northward and eventually northeast motion develops. Simultaneous cyclones appear to be moving westward at a faster rate than delayed or gyre cyclones. Gyre cyclones were much more different than the other two cyclone types. They tended to change very little in longitude. They also started ten degrees further east than simultaneous storms. This means that they generally travel more northward, and are climatologically associated with a strong monsoon trough. It appears that specific synoptic patterns are affecting the latitude and longitude tracks of simultaneous, delayed and gyre cyclones. Figure 4.12 is a map with the center coordinates and R30 shown at each stage of the composite life cycle for delayed, simultaneous and gyre cyclones. Gyre cyclones can plainly be seen further west than either simultaneous and delayed cyclones. Simultaneous cyclones don't track as far northward as delayed or gyre cyclones. Delayed cyclones are further east than simultaneous cyclones. However, there is considerable scatter to the composite track of

delayed cyclones. This is due to one group of cyclones remaining significantly east of 140° longitude, and one group remaining west of it.

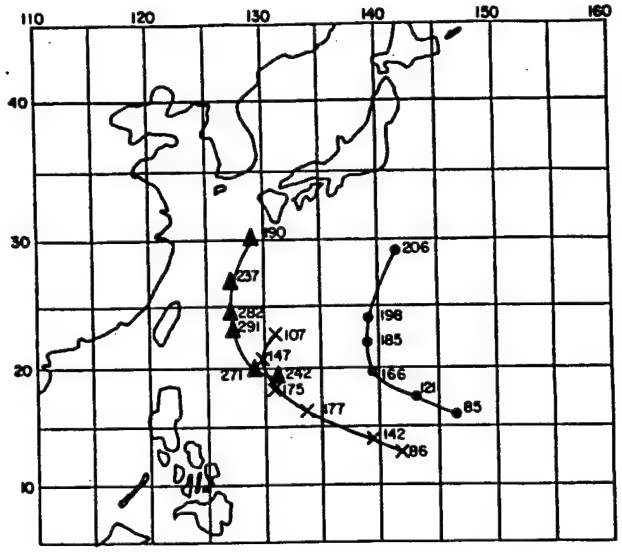


Figure 4.12: Center coordinates and R30 at each point of the life cycle of delayed (•), simultaneous (X) and gyre (△) cyclones.

So synoptic patterns give insight as to why a cyclone becomes delayed, simultaneous or gyre-like.

## 4.3 Composites of Synoptic Surface Pressure Patterns

An effort was made to quantify surface synoptic pressure patterns by creating a composite pattern for each cyclone type. Since the surface synoptic maps available did not extend much south of 10°N, it was decided to measure the surface pressure from WSW to ESE of the cyclone center. Using these surface maps, measurements of pressure were made at roughly 220, 435, 650, 870, 1090, 1300, and 1520 n mi from the center (approximately 4, 8, 12, 16, 20, 24 and 28°) of the cyclone along the 245°, 290°, 315°, 360°, 045°, 070° and 115° directional radials. These measurements were made from two days prior to two days after MI. This is the critical point in the cyclone's life cycle that

determines whether it will be delayed or simultaneous. Using this data, composites of the surface pressure patterns were created.

Figures 4.13–4.21 show the results of these composited surface pressure maps.

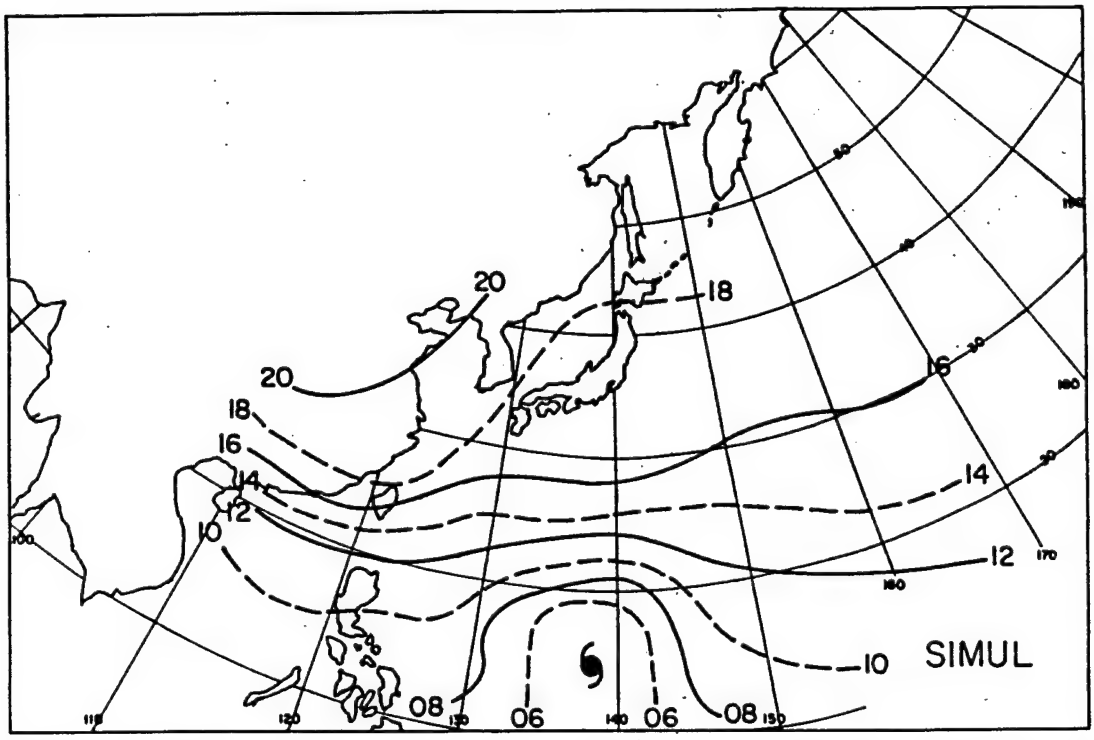


Figure 4.13: Surface synoptic pressure pattern for simultaneous cyclones two days prior to maximum intensity (MI).

Simultaneous cyclones show an area of moderately strong high pressure established WNW to ENE of their center at two days prior to MI. The center of the high appeared to be over the Asian continent indicating that the associated air mass was cooler and drier. The pressure have increased as the center of the high has moved directly north of the cyclone center by MI. By two days after MI, a stronger area of high pressure is moving off the Asian continent into the Pacific. This high pressure center is located northwest of the cyclone center. A weakness has developed in the surface ridging north-northeast of the cyclone center which may account for the more northwestward movement of the cyclone. Note, that throughout the time period, the pressure gradient is very tight NW through NE of simultaneous cyclones. This would seem to argue for a stronger OCS throughout

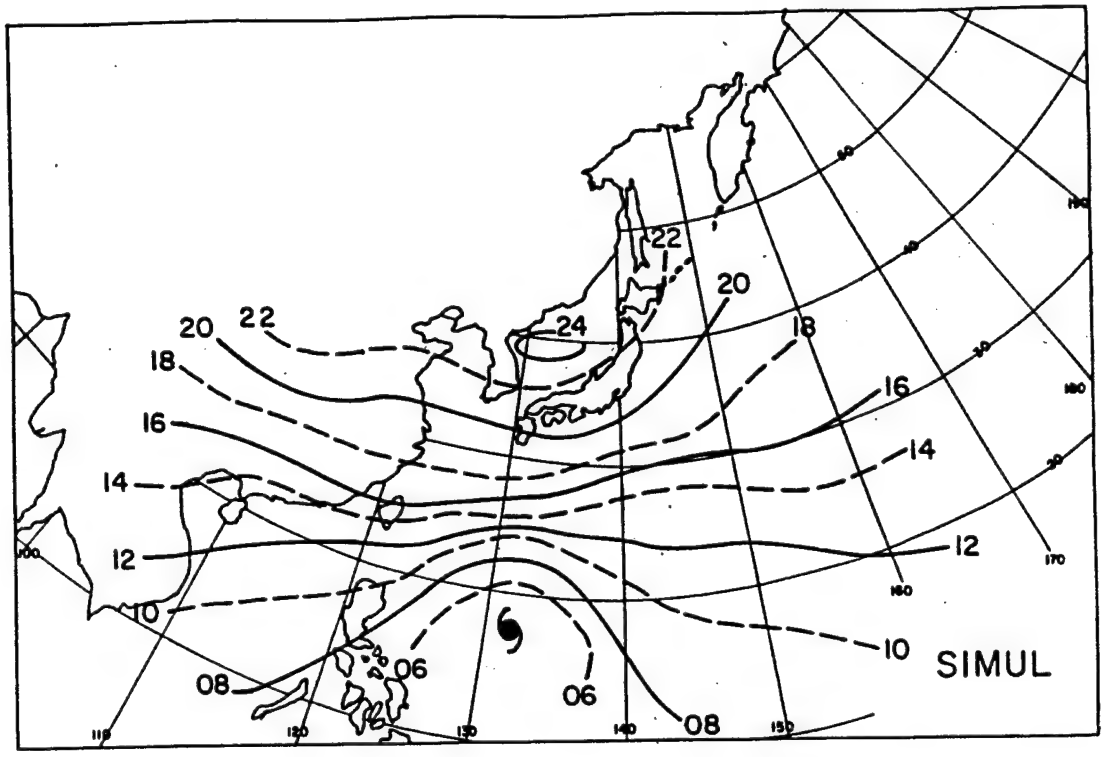


Figure 4.14: Surface synoptic pressure pattern for simultaneous cyclones at maximum intensity (MI). Cyclone's position two days earlier is annotated.

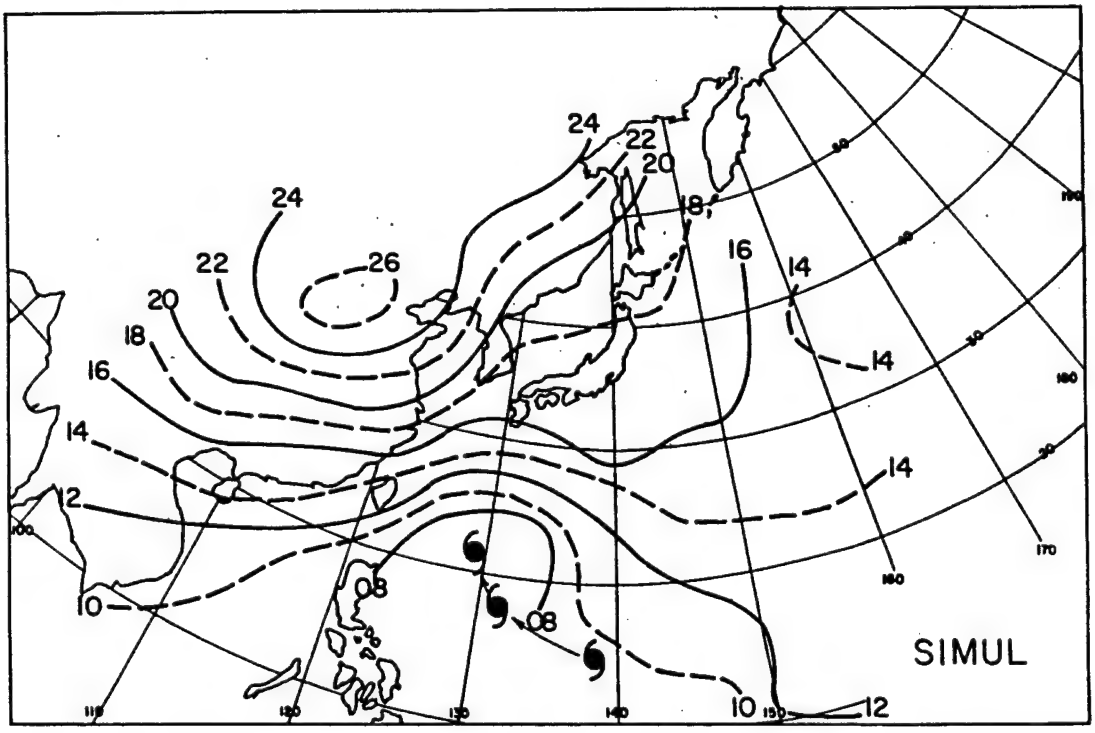


Figure 4.15: Surface synoptic pressure pattern for simultaneous cyclones two days after maximum intensity (MI). Cyclone's position two and four days earlier are annotated.

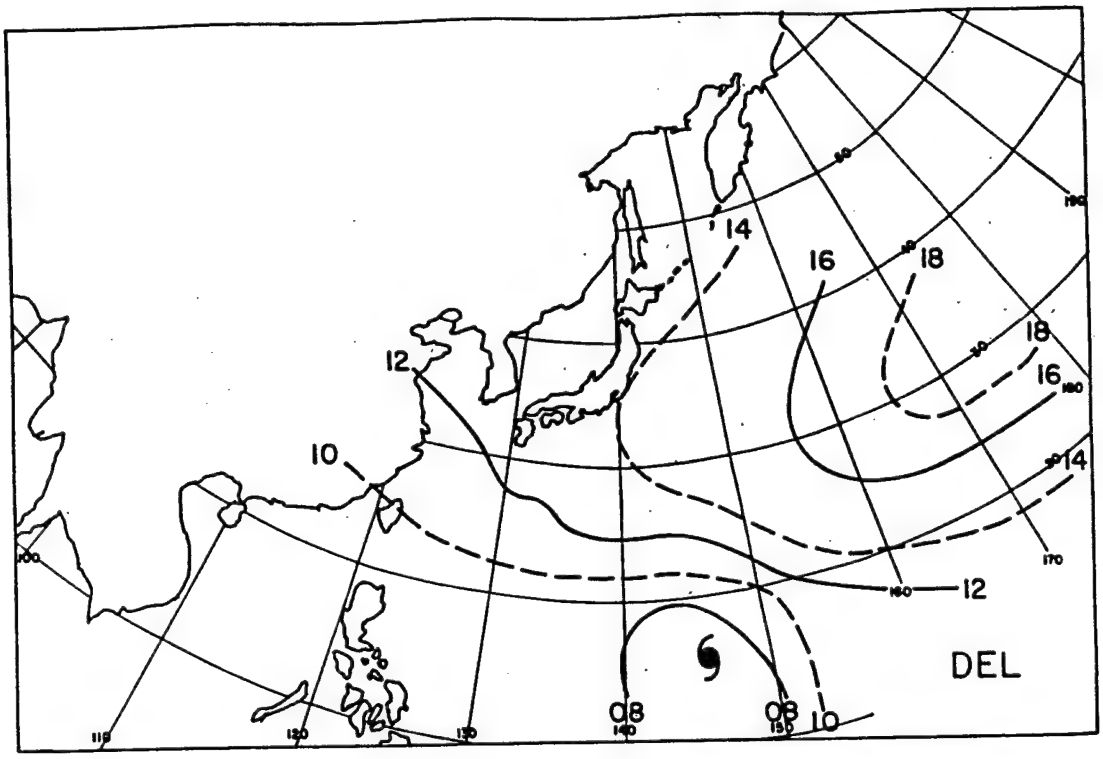


Figure 4.16: Surface synoptic pressure pattern for delayed cyclones two days prior to maximum intensity (MI).

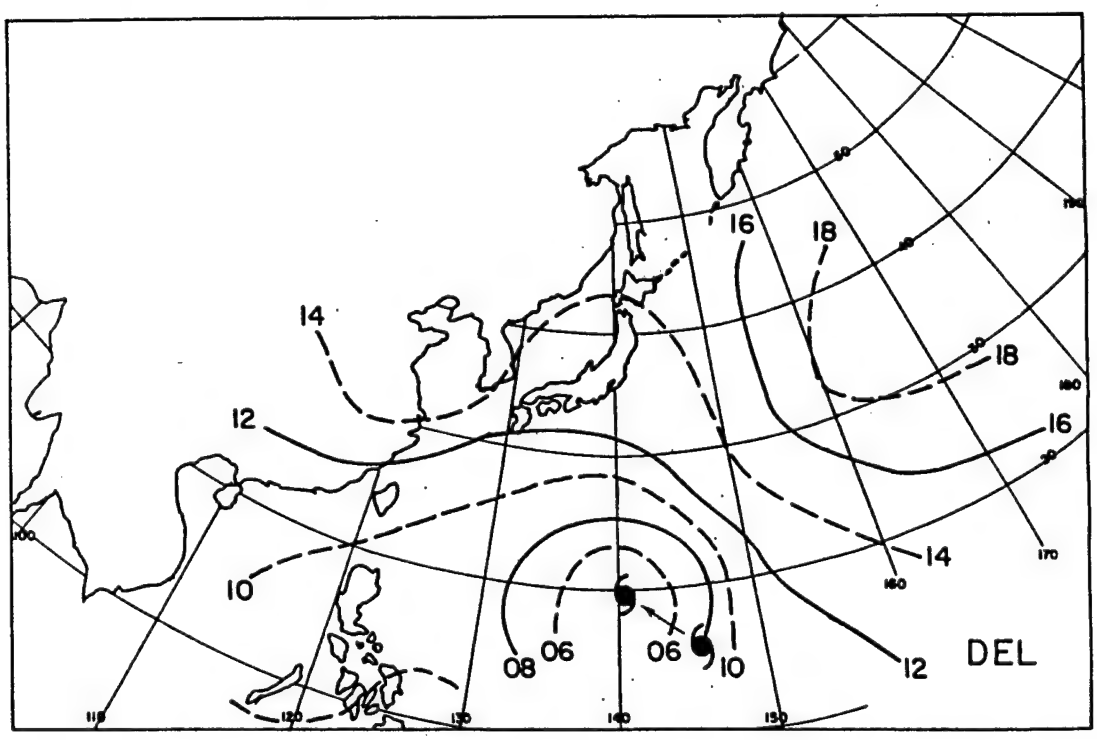


Figure 4.17: Surface synoptic pressure pattern for delayed cyclones at maximum intensity (MI). Cyclone's position two days earlier is annotated.

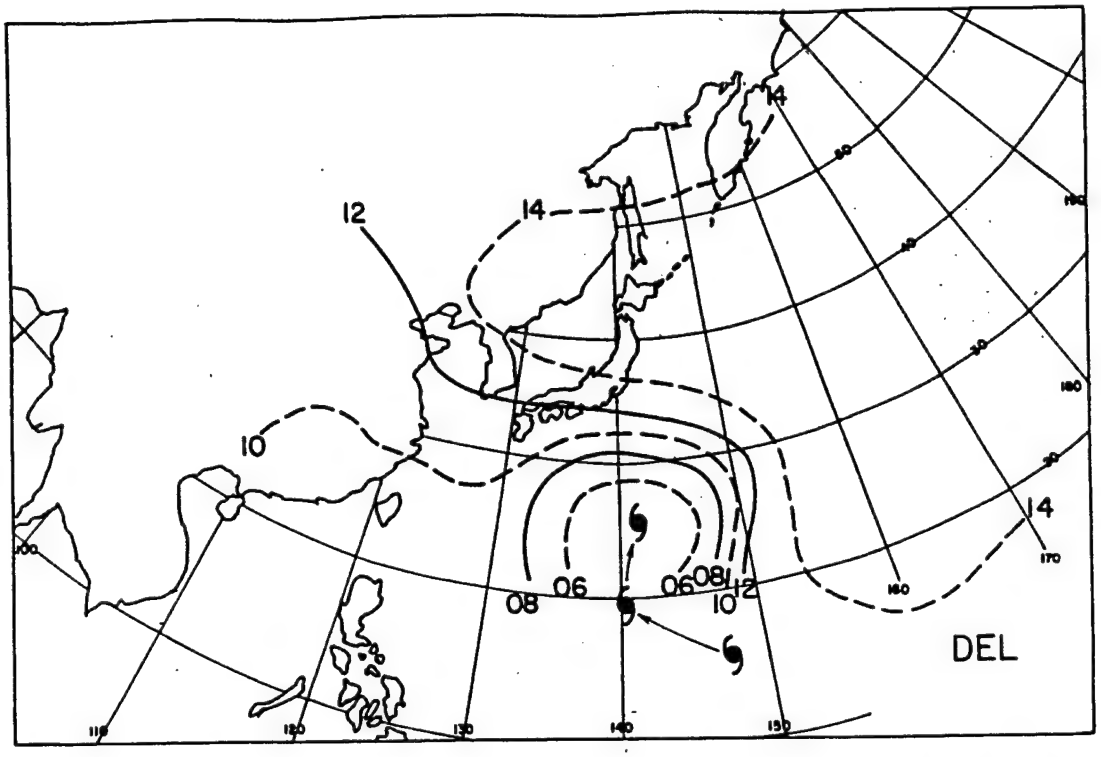


Figure 4.18: Surface synoptic pressure pattern for delayed cyclones two days after maximum intensity (MI). Cyclone's position two and four days earlier are annotated.

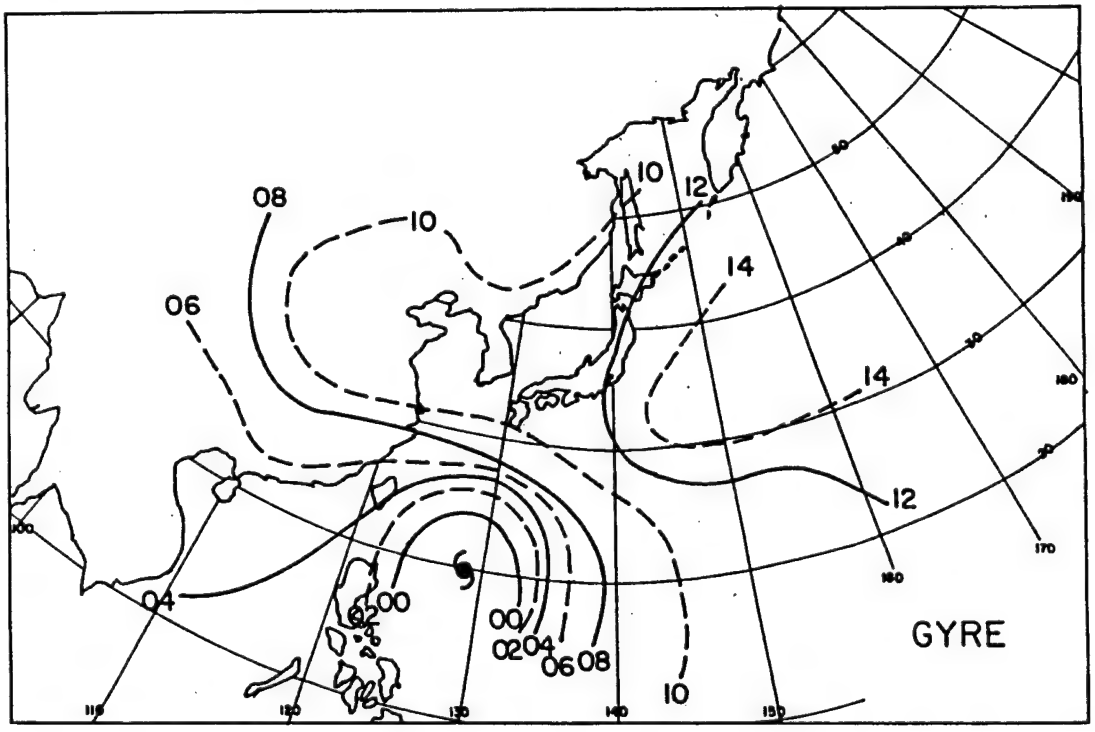


Figure 4.19: Surface synoptic pressure pattern for gyre cyclones two days prior to maximum intensity (MI).

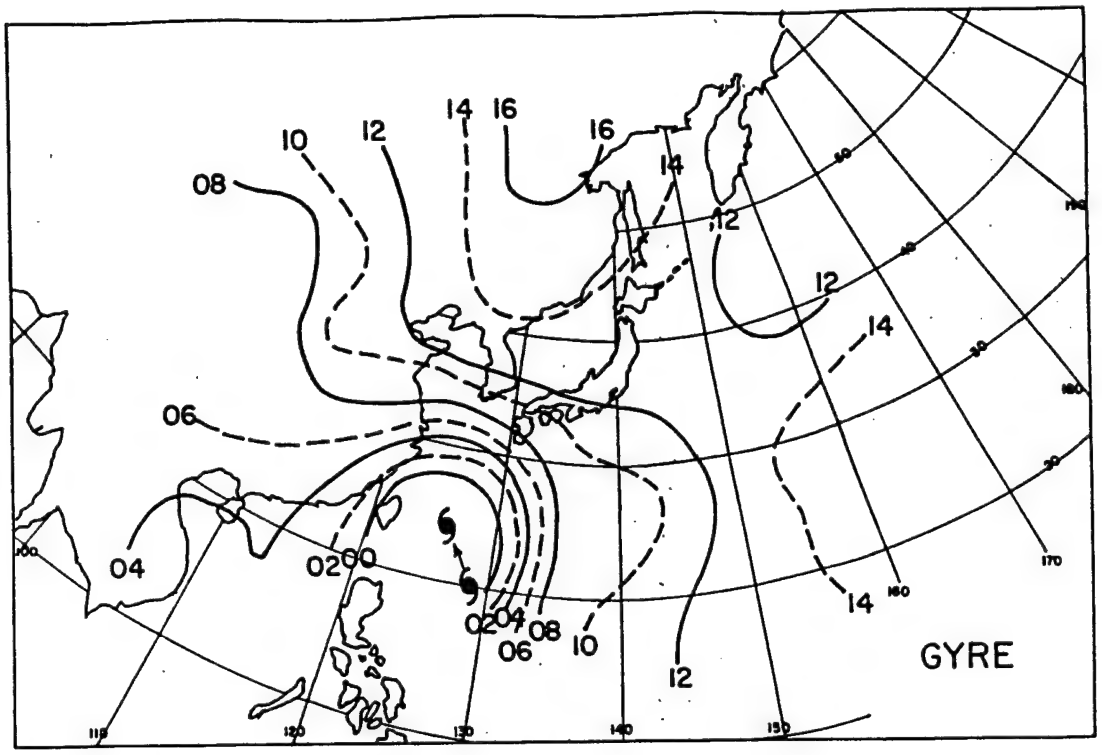


Figure 4.20: Surface synoptic pressure pattern for gyre cyclones at maximum intensity (MI). Cyclone's position two days earlier is annotated.

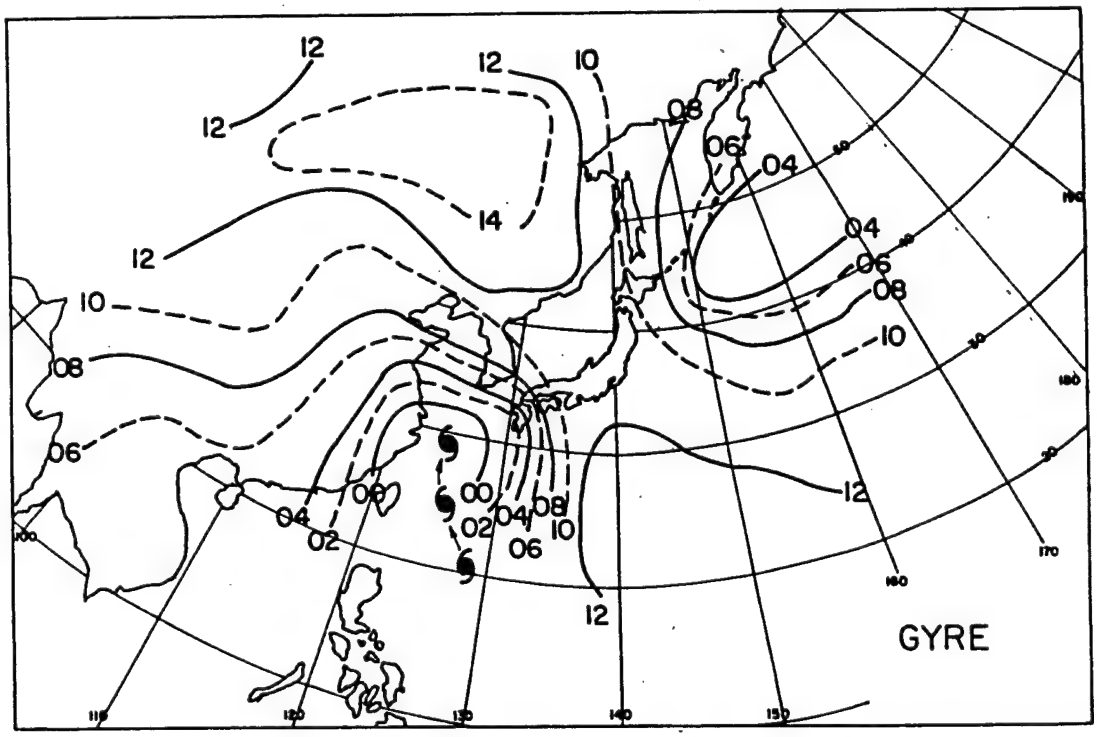


Figure 4.21: Surface synoptic pressure pattern for gyre cyclones two days after maximum intensity (MI). Cyclone's position two and four days earlier are annotated.

the time period. However, this is not observed. Overall, the synoptic pattern observed would be expected in the latter part of the typhoon season.

Composite maps for delayed cyclones show a completely different synoptic pattern. From two days prior to MI, the subtropical high is plainly visible. The pressures north of the cyclone are not anywhere near as high compared to simultaneous cyclones. This allows for the cyclones more northwesterly motion track up to MI. By MI, a clear weakness has developed in the surface pressure pattern. By two days after MI, delayed cyclones have now turned to a more northerly track. Weak high pressure could be seen moving north of the cyclone center. On average, high pressure northwest of the delayed cyclone is much weaker than simultaneous cyclones yet stronger northeast and east-northeast of the center. The synoptic patterns for gyre cyclones are similar to delayed cyclones with some exceptions. Gyre cyclones are associated with a broader monsoon trough. The area south of the 1008 mb isobar for gyres is much greater than delayed cyclones throughout the time period. The pressure over southeast Asia are significantly lower for gyres than delayed cyclones. The subtropical high appears weaker for gyres than delayed cyclones. Finally, a broad low pressure area develops northeast of gyre cyclones two days after MI.

All of these observations reinforce the results found in Chapter 3; that most delayed and gyre cyclones occur in the summer and early fall while simultaneous cyclones occur middle to late fall. During summer and early fall, there is a subtropical high located over the central Pacific. This would cause higher pressures northeast and east-northeast of cyclone centers that are in the vicinity. The subtropical high and transient mid latitude weather systems are probably related to the delayed cyclones more northwest to north motion track. Typically, high pressure is weaker over the Asian continent during this time of year due to the dominance of the monsoon low that forms over the Himalayas. During the latter parts of fall, cooler and drier high pressure systems form more often over the Asian continent. This could cause a strong ridge of high pressure to be prevalent NW to N of tropical cyclones in the vicinity. From Figs. 4.1c, 4.2c, 4.3b and 4.4c it is apparent that ER04 is positively correlated with R30. that is, as ER04 increases then R30 increases

and vice versa. This means that if a cyclone moves into a region of higher pressure, it's synoptic size, and therefore R30 will become smaller. Similarly, if a cyclone moves into a region of lower pressure, it's synoptic size and R30 will grow larger. This is additional evidence that the synoptic pressure pattern influences the outer wind profile of tropical cyclones.

Synoptic pressure differences tended to be the greatest from WNW to ENE of the different cyclone types. Therefore, a pressure index was created to see if any skill existed in differentiating between simultaneous, delayed and gyre cyclones. Firs the pressure was averaged from 8 to 16 degrees along the WNW, NW, N, NE and ENE radials from the cyclone center. The index is defined as:

$$PI = (WNW + NW + N - NE - ENE - 1000)$$

where WNW, NW, N, NE, ENE refers to the average pressure from 8 to 16 degrees along these radial directions. The constant '1000' refers to the amount of pressure in millibars to be subtracted from the difference of the average pressures. Figures 4.22–4.26 show the average pressure patterns and PI values of simultaneous, delayed and gyre cyclones two days prior and after two days MI.

Tables 4.1–4.3 show both instantaneous and 24 hr averages of PI for each cyclone type. Table 4.4 shows the difference between simultaneous minus delayed PI values with the largest values occurring at MI and one day afterward. Two days prior to MI, noticeable differences occur between simultaneous and delayed cyclone types. In general, instantaneous PI values $\geq 12$ were associated with simultaneous cyclones; values $\leq 8$ were associated with delayed cyclones. This shows that some forecast skill exists to at least differentiate between simultaneous and delayed cyclone types using synoptic pressure analyses. On the other hand, this index did not show much difference between delayed and gyre cyclones. However, gyres are distinguishable from other cyclones due to their extremely large ER04 and R30 values very early in their life cycle.

Simultaneous and delayed cyclones differ only in the change of their outer core wind profile and their eye size with time. With respect to the wind profile, the closer one gets

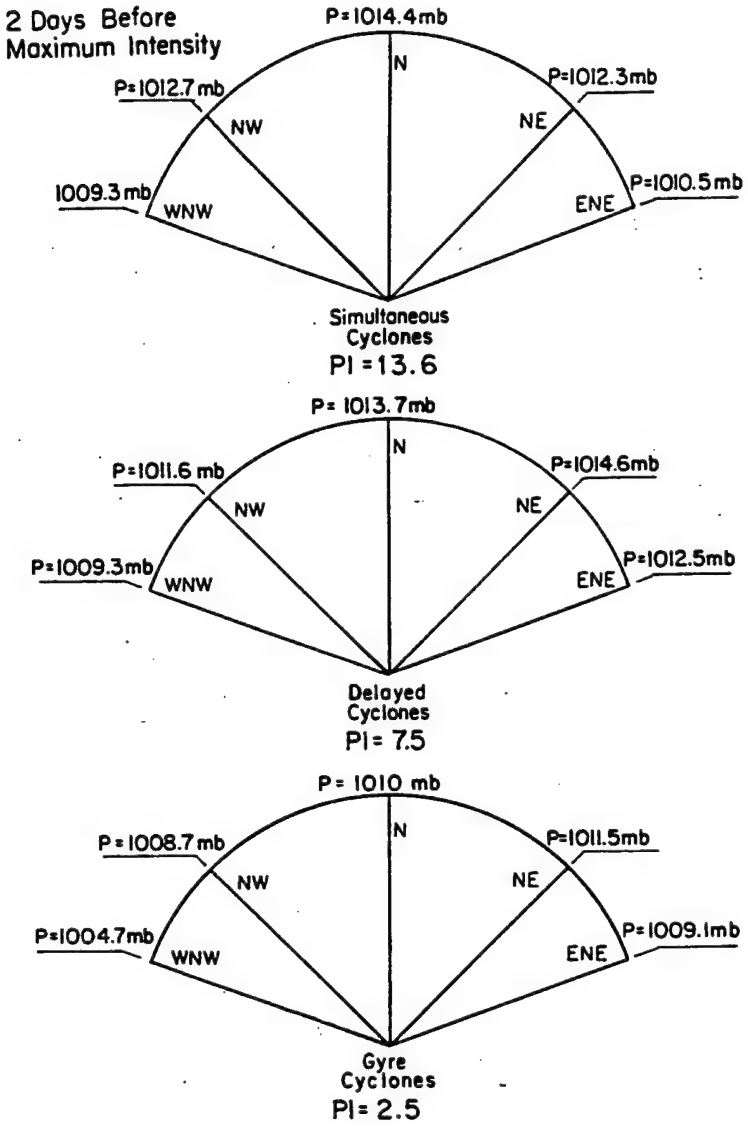


Figure 4.22: The surface pressure averaged from 8 to 16° in the directions WNW, NW, N, NE, and ENE of the center of simultaneous and delayed cyclones 2 days before maximum intensity (MI).

Table 4.1: PI results for composite surface pressure field of simultaneous cyclones.

| Days Till MI | Instantaneous PI | 24hr Avg PI |
|---|---|---|
| −2 | 13.6 | |
| −1 | 17.5 | 15.6 |
| 0 | 21.3 | 19.4 |
| 1 | 24.9 | 23.1 |
| 2 | 18.6 | 21.8 |

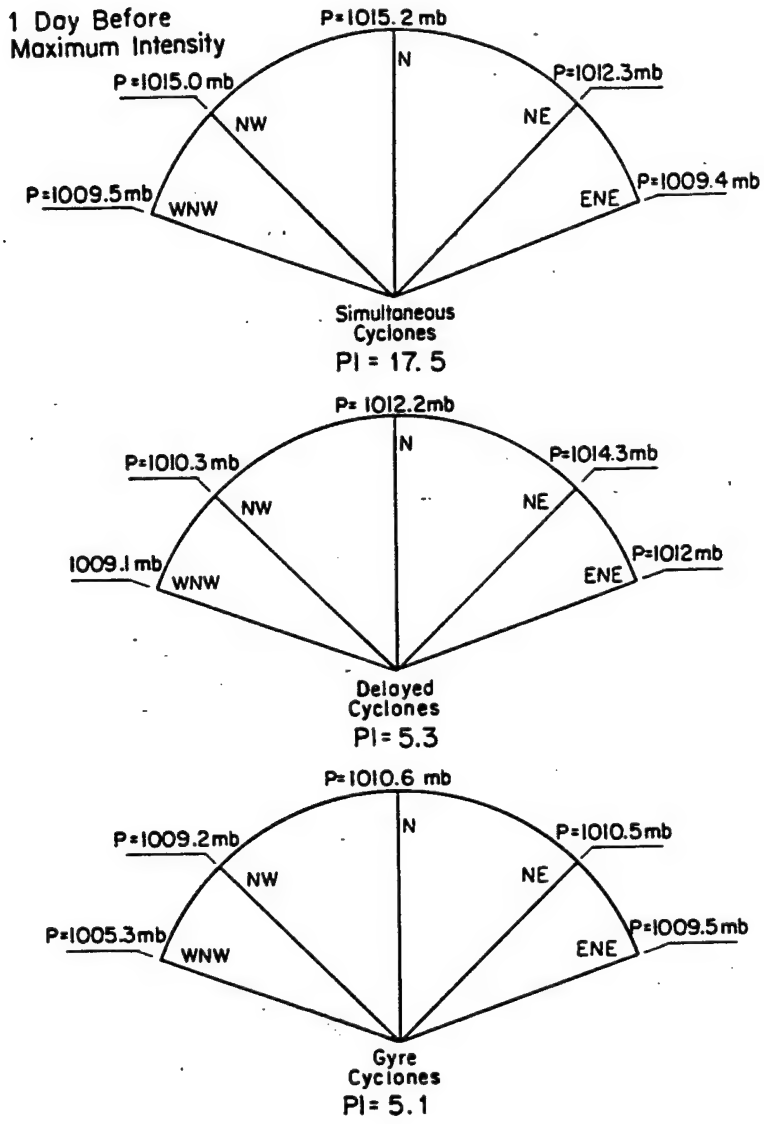


Figure 4.23: Same as Fig. 4.22 except one day before MI.

Table 4.2: PI results for composite pressure field of delayed cyclones.

| Days Until MI | Instantaneous PI | 24hr Avg PI |
|---|---|---|
| −2 | 7.5 | |
| −1 | 5.3 | 6.4 |
| 0 | 4.4 | 4.9 |
| 1 | 7.7 | 6.1 |
| 2 | 6.9 | 7.3 |

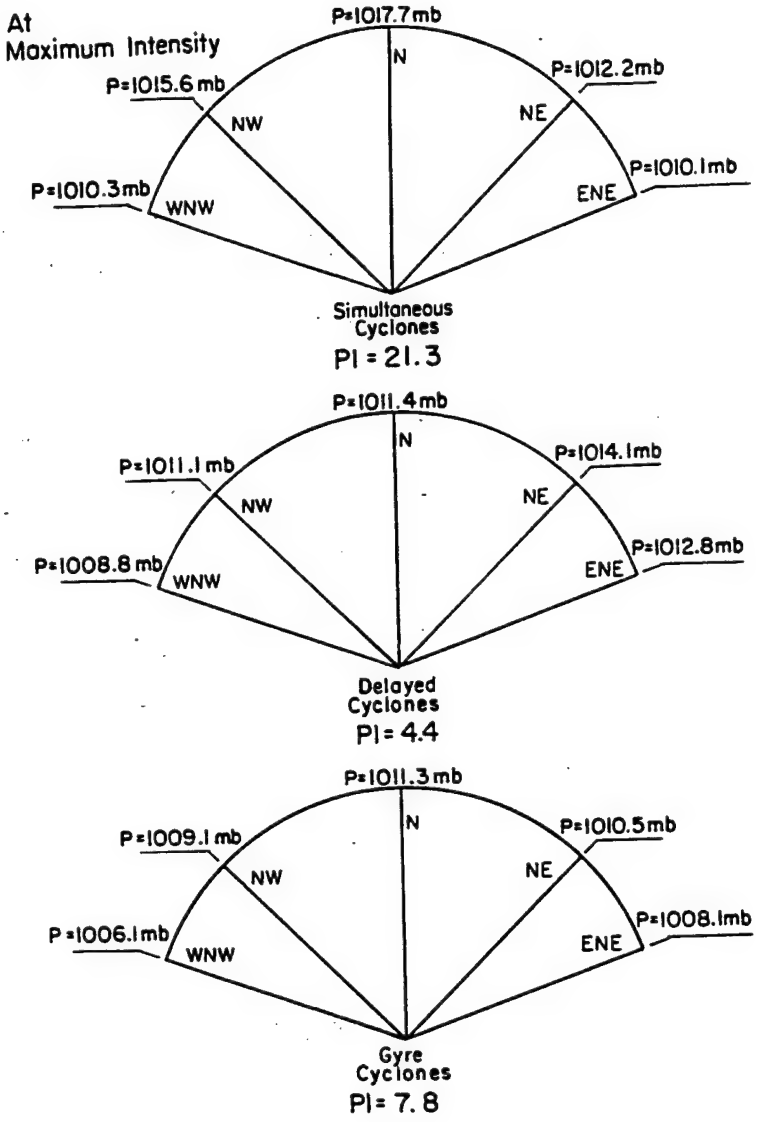


Figure 4.24: Same as Fig. 4.22 except at MI.

Table 4.3: PI results for composite pressure field of gyre cyclones.

| Days Until MI | Instantaneous PI | 24hr Avg PI |
|---|---|---|
| –2 | 2.5 | |
| –1 | 5.1 | 3.8 |
| 0 | 7.8 | 6.4 |
| 1 | 5.9 | 6.9 |
| 2 | 5.3 | 5.6 |

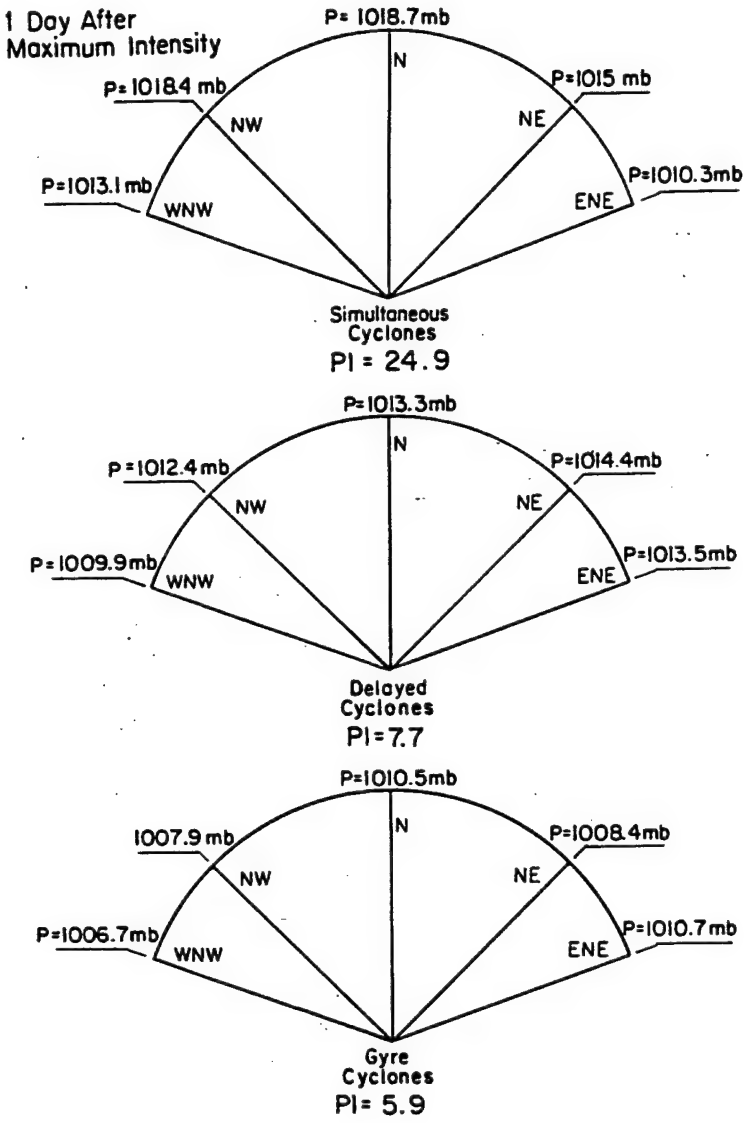


Figure 4.25: Same as Fig. 4.22 except one day after MI.

Table 4.4: Δ PI results for composite pressure field for simultaneous minus delayed cyclones.

| Days Until MI | Δ PI | 24hr Avg Δ PI |
|---|---|---|
| −2 | 6.1 | |
| −1 | 12.2 | 9.2 |
| 0 | 16.9 | 14.5 |
| 1 | 17.2 | 17.0 |
| 2 | 11.7 | 14.5 |

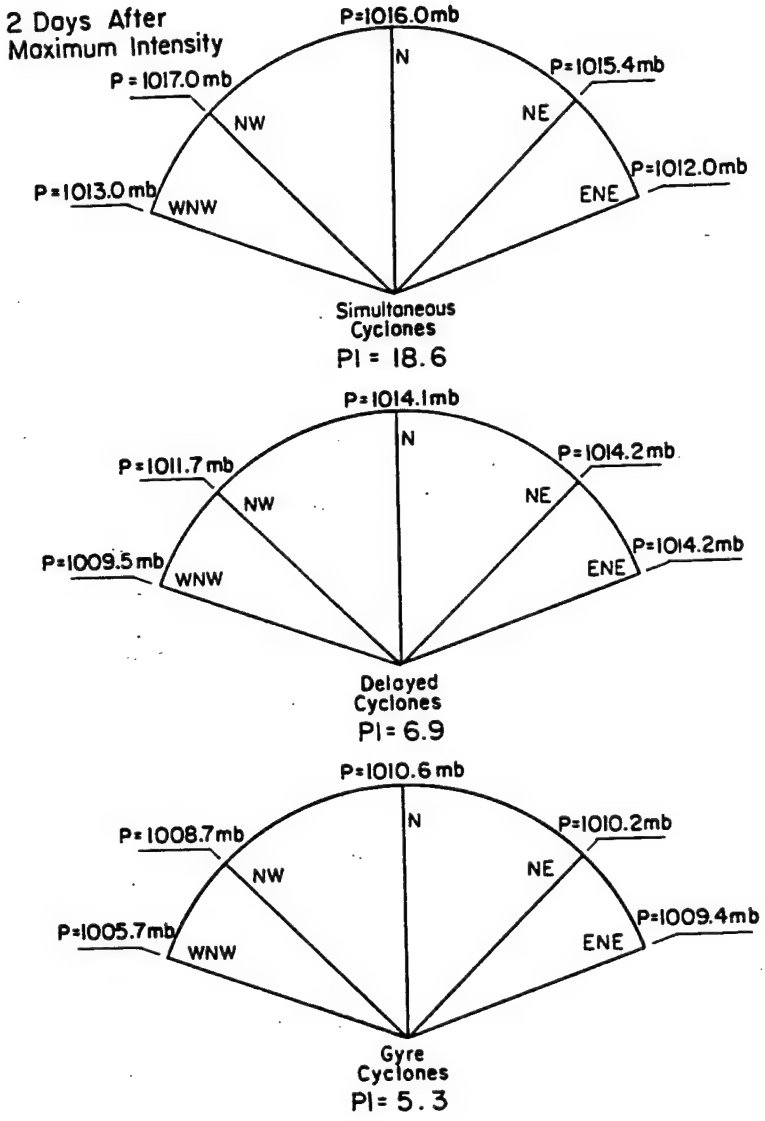


Figure 4.26: Same as Fig. 4.22 except two days after MI.

toward the inner core, the less one is able to differentiate between the two. Also, the change in their central pressure with respect to time are similar for both cyclone types. In general, the synoptic size of a cyclone will grow smaller/larger as it enters a region of higher/lower environmental surface pressure. Also, in terms of synoptic motion tracks, delayed storms move much further north and east than simultaneous cyclones (see Fig. 4.17). These characteristics reflect a possible synoptic mechanism that causes one or the other cyclone type. However, there remain differences in the life cycle of eye size for simultaneous and delayed cyclones. There appeared to be some bad eye data for gyres so a composite was not attempted. This would suggest that the change in the size of the eye plays a role in determining the tropical cyclones outer wind profile. For instance, as the eye expands in the filling stages of delayed cyclones, momentum is advected toward the eyewall. This acts to strengthen the outer core (Weatherford 1989). However, the eye essentially remains constant for much of their life cycle of simultaneous cyclones. Therefore, the OCS of simultaneous cyclones weaken.

Gyre cyclones, on the other hand, appear to be fundamentally different than any other cyclone. Gyres are large from the very onset of tropical storm status and remain so throughout their life. Their central pressure never drops very low compared to simultaneous and delayed cyclones. These cyclones tended to form further north and west than both simultaneous and delayed cyclones and generally traveled northward (see Fig. 4.7).

Synoptic pressure patterns were composited and distinct synoptic features could be found for simultaneous, delayed and gyre cyclones. An index was created that showed there may be some ability to predict whether a cyclone will become simultaneous or delayed. In Chapter 5, statistical relations are studied and tested and equations developed to estimate the cyclone's outer wind radii.

# Chapter 5

# STATISTICAL RELATIONS BETWEEN THE OUTER WIND PROFILE AND VARIOUS PARAMETERS

## 5.1 Statistical Relations For Four Year Data Set

Statistical relations estimating R30, R50, and R65 can be derived from the variety of available data sets. The variables chosen for testing are central pressure, the 12 hr change in central pressure (dp/dt), ER04, latitude, longitude, and eye size as measured by aircraft reconnaissance. The central pressure (MSLP), synoptic size (ER04) and the 12hr central pressure charge (dp/dt) all help to determine the pressure gradient of the cyclone. These variables can't recreate the distribution of the pressure gradient because this requires both pressure and pressure change observations throughout the inner and outer core of the cyclone. This knowledge is not available to the forecaster; however, these variables should be correlated to the extent of the gale force winds. Latitude and longitude were also chosen for testing since chapters 3 and 4 showed that the track of the cyclone seemed to be related (presumably though interaction with the synoptic environment) to the extent of gale force winds (R30). Shoemaker (1989) observed that R30 was well related to R50 with a correlation factor of 0.82. In light of this, tests for R30 vs R50, and R50 vs R65 were run as well. From Chapters 3 and 4 it was found that gyre cyclones were fundamentally different than simultaneous and gyre cyclones. They begin their life cycle at a large size (as measured by ER04 and R30) and tend to remain large throughout their life cycle. Gyres typically are not very intense. The question is should these cyclones be placed in a data set of their own? Figure 5.1 is a graph of R30 versus central pressure for all cyclones. Note the very large scatter throughout the plot and that $R^2$ is only 15 percent. Figure 5.2 is a graph of R30 versus central pressure with gyre cyclones excluded. The

scatter is reduced significantly for the higher central pressures and $R^2$ is now 40 percent. Removing the gyres from the data set meant removing only 14 percent of the observations. However, the variance explained is more than doubled. Therefore, correlation tests were run separately for simultaneous/delayed cyclones and gyre cyclones. Table 5.1 summarizes the correlation tests between R30 and these variables.

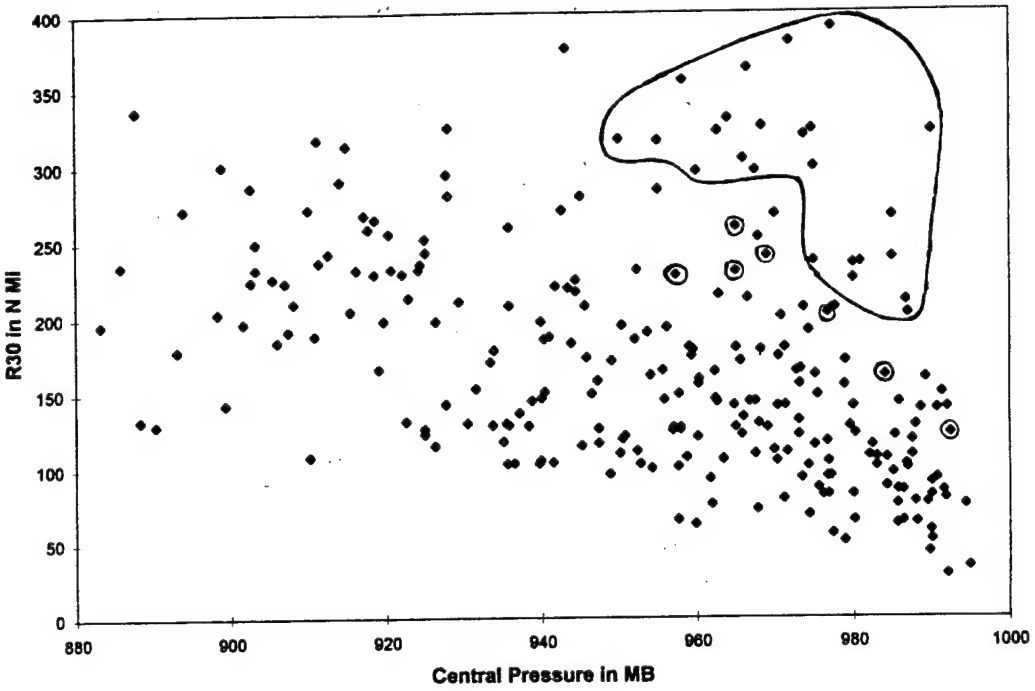


Figure 5.1: R30 versus MSLP for all cyclone classes. There are 258 observations and the variance explained is 15 percent. Gyre observations are circled in black.

Table 5.1: Correlation test, the number of observations, correlation coefficient and variance explained for the data set. Gyre observations are not included.

| Test w/o Gyres | No. Obs | R*100 | $R^2$*100 |
|---|---|---|---|
| R30 vs MSLP | 223 | 63% | 40% |
| R30 vs dP/dt | 230 | 04% | 00% |
| R30 vs ER04 | 223 | 69% | 47% |
| R30 vs Lat. | 223 | 33% | 11% |
| R30 vs Lon. | 223 | 26% | 09% |
| R30 vs Eye size | 215 | 05% | 00% |
| R50 vs R30 | 163 | 77% | 59% |
| R65 vs R50 | 120 | 92% | 84% |

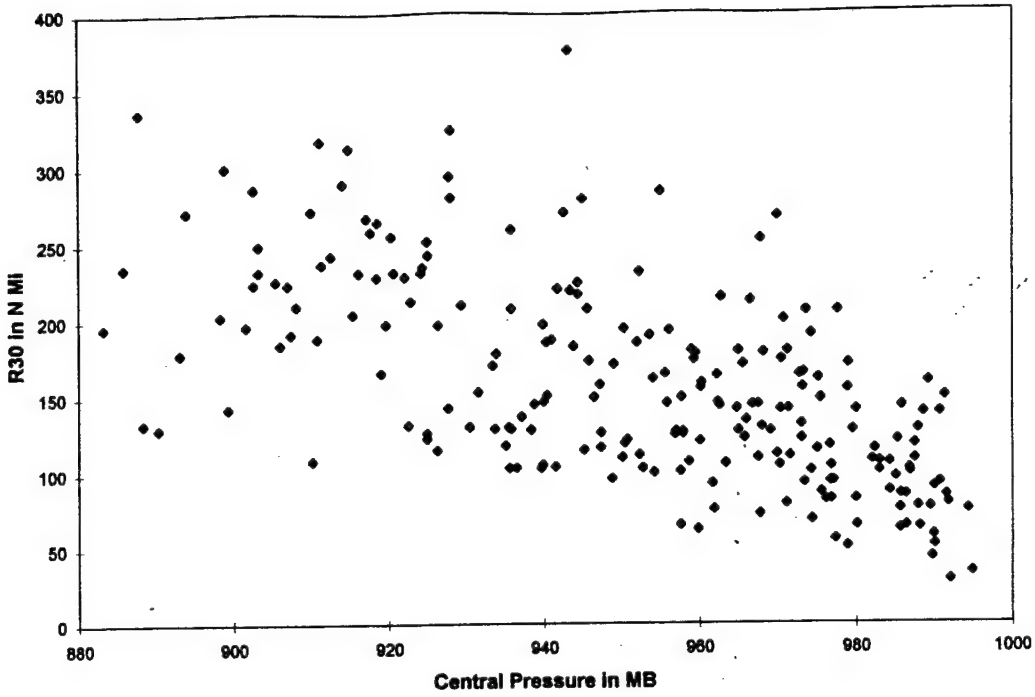


Figure 5.2: R30 versus MSLP excluding observations from gyre cyclones. There are 223 observations and the variance explained is 40 percent.

Central pressure (MSLP) and ER04 are both good variables for R30. This means that with the exclusion of gyres a better relationship exists between R30 and central pressure. Latitude and longitude are weakly predictive variables. Also R30 and R50 appeared to be well related to R50 and R65 respectively. The 12 hr central pressure change (dp/dt) showed very little correlation with R30. Evidently central pressure changes do not affect the size of the storm.

It is interesting to note that eye size alone was not related to R30. But when eye size and MSLP are combined a relationship with R30 is obtained. Weatherford (1985) found that given a particular eye size and MSLP, a good estimate of R30 can be obtained. With slight changes to Weatherford's definitions for small, medium and large eye categories, the author was able to duplicate her results. These are shown in Table 5.2. Generally, the larger the eye the stronger the relationship between R30 and MSLP.

These results were obtained using aircraft measured eye sizes. Of all the cases in which satellite and aircraft data were available, 38% of the time the eye was not visible with

Table 5.2: Number of observations, correlation and variance results for R30 versus MSLP for a given eye size category. Gyre cyclones are not included.

| Size Category | No. Obs | R*100 | $R^2$*100 |
|---|---|---|---|
| R30 versus MSLP for No Eyes | 36 | 60% | 34% |
| R30 versus MSLP for 0 n mi < Eye Sizes ≤ 15 n mi | 62 | 64% | 40% |
| R30 versus MSLP for 15 n mi < Eye Sizes ≤ 30 n mi | 101 | 74% | 55% |
| R30 versus MSLP for Eye Sizes > 30 n mi | 14 | 93% | 85% |

satellite data. This presents a data availability problem. Also, the size of the satellite observed eye may not match the aircraft measured one. Convection and cloud cover may obstruct part of the eye which may make it appear smaller than it really is. In light of these problems, this study focuses on other ways of determining R30.

Table 5.3 shows that ER04 also does well in estimating R30 for gyre cyclones. Once again, MSLP and ER04 were highly correlated with R30. Latitude, longitude and the 12 hr central pressure change (dp/dt) may also be useful for predicting R30. Note that dp/dt was more correlated to R30 for gyre cyclones than simultaneous or delayed cyclones. The parameters most promising for estimating R30 were correlated to each other to see the extent to which each variable was related to each other.

Table 5.3: Same as Table 5.1 except gyre cyclones only.

| Test Gyres | No. Obs | R*100 | $R^2$*100 |
|---|---|---|---|
| R30 vs MSLP | 35 | 59% | 33% |
| R30 vs dP/dt | 35 | 39% | 13% |
| R30 vs ER04 | 35 | 84% | 69% |
| R30 vs Lat. | 35 | 42% | 15% |
| R30 vs Lon. | 35 | 26% | 09% |

Table 5.4 shows that ER04 and Latitude were somewhat related with 23% of the variance explained. Figure 5.1 shows a scatter plot of ER04 vs Latitude. Generally, as a typhoon moves further north the larger the ER04. This is just what composite analysis revealed in Merrill, 1980. MSLP and ER04 were related, but not enough to exclude using them together in a statistical equation.

For gyre cyclones (see Table 5.5), MSLP and ER04 are better related. Therefore, these variables will not be used together in a regression equation. However, Table 5.5 shows

Table 5.4: Correlation tests between different variables for the simultaneous/delayed data sets.

| Test | No. of Cases | R*100 | $R^2$*100 |
|---|---|---|---|
| MSLP vs ER04 | 223 | 39% | 15% |
| MSLP vs Lat. | 223 | 8% | 00% |
| MSLP vs Lon. | 223 | 30% | 09% |
| ER04 vs Lat. | 223 | 48% | 23% |
| ER04 vs Lon. | 223 | 15% | 02% |
| Lat. vs Lon. | 223 | 07% | 00% |

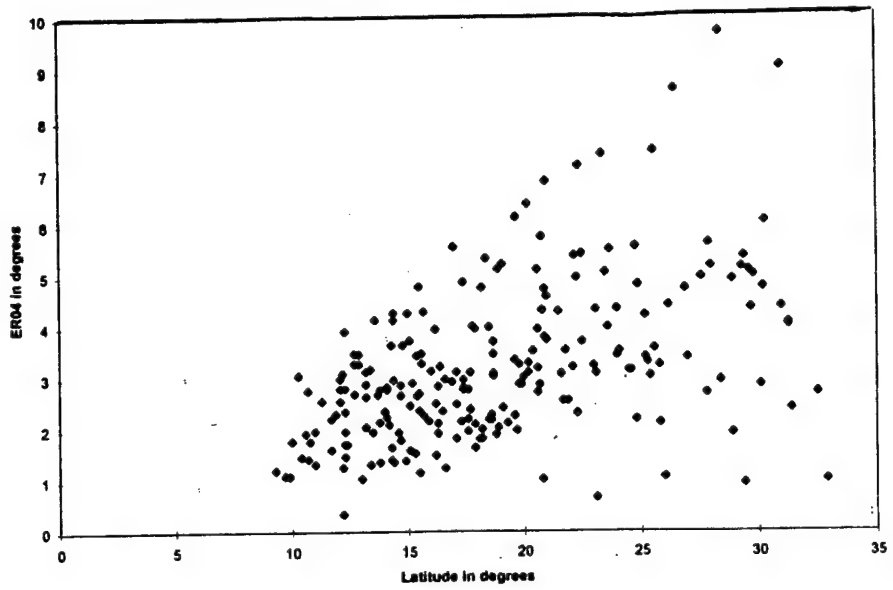


Figure 5.3: ER04 versus latitude for all cyclone types.

that the 12 hour pressure change and ER04 may be useful as variables in a statistical equation together. Since there are only 35 gyre cyclone observations, a multiple regression equation was not attempted because it may not be meaningful. Therefore, only ER04 will be used to predict R30 for gyre cyclones.

Table 5.5: Same as Table 5.4 except for gyre cyclones only.

| Tests with Gyres | No. of Cases | R*100 | $R^2$*100 |
|---|---|---|---|
| MSLP vs ER04 | 56 | 58% | 32% |
| MSLP vs dP/dt. | 56 | 04% | 00% |
| ER04 vs dP/dt | 56 | 10% | 00% |

## 5.2 Statistical Relations Using Satellite Data Set

Correlation tests were also run for satellite data and outer wind observations during the years 1983-1984. It is important to note that this data set did not include gyres, and is half the size of the previous simultaneous/delayed data set. Shoemaker (1989) found that the satellite parameters with pixel counts $\leq -25°C$ for a running mean of the past 24 to 72 hrs had the highest correlation to R30. The author decided to re-test these satellite parameters for past running means of 24 to 48 hrs. Table 5.6 lists the satellite parameters and the abbreviations used. Table 5.7 shows the results.

Table 5.6: Satellite parameters tested and their accompanying abbreviations.

| Satellite Parameter | Abbreviation |
|---|---|
| Pixel count of clouds $\leq -25°C$, that extend 0-6° from the cyclone center, 24 hr prior running mean | 06@2524 |
| Pixel count of clouds $\leq -25°C$, that extend 2-6° from the cyclone center, 24 hr prior running mean | 26@2524 |
| Pixel count of clouds $\leq -25°C$, that extend 0-4° from the cyclone center, 24 hr prior running mean | 04@2524 |
| Pixel count of clouds $\leq -25°C$, that extend 2-4° from the cyclone center, 24 hr prior running mean | 24@2524 |
| Pixel count of clouds $\leq -25°C$, that extend 0-6° from the cyclone center, 48 hr prior running mean | 06@2548 |
| Pixel count of clouds $\leq -25°C$, that extend 2-6° from the cyclone center, 48 hr prior running mean | 26@2548 |
| Pixel count of clouds $\leq -25°C$, that extend 0-4° from the cyclone center, 48 hr prior running mean | 04@2548 |
| Pixel count of clouds $\leq -25°C$, that extend 2-4° from the cyclone center, 48 hr prior running mean | 24@2548 |

As expected, ER04 and MSLP had the strongest correlation with R30. The 48 hr prior running mean of the percent area coverage of -25°C or colder cloud cover at 0-4, 0-6, 2-4, and 2-6° from the center of the typhoon were the next best variables for determining R30. The variance explained by some of these parameters was about half that found by Shoemaker 1989. One reason for this is Shoemaker used a nonlinear correlation test, while the author used a linear one. Also, the author used more information (synoptic and aircraft data) to determine R30 for each cyclone. With the exception of ER04 and MSLP

Table 5.7: Correlation tests of R30 vs various physical parameters for simultaneous/delayed cyclones in 1983–1984; no gyres are included.

| Test | No. Obs | R*100 | $R^2$*100 |
|---|---|---|---|
| R30 vs MSLP | 127 | 66% | 43% |
| R30 vs ER04 | 117 | 76% | 57% |
| R30 vs Latitude | 127 | 42% | 17% |
| R30 vs Longitude | 127 | 23% | 05% |
| R30 vs 0-6@2524 | 127 | 41% | 16% |
| R30 vs 2-4@2524 | 127 | 37% | 13% |
| R30 vs 0-4@2524 | 127 | 34% | 11% |
| R30 vs 2-6@2524 | 127 | 42% | 17% |
| R30 vs 0-6@2548 | 117 | 50% | 25% |
| R30 vs 2-4@2548 | 117 | 46% | 21% |
| R30 vs 0-4@2548 | 117 | 45% | 20% |
| R30 vs 2-6@2548 | 117 | 50% | 25% |

(which were tested earlier), the best variables were correlated against each other (Table 5.8).

Table 5.8: Correlation tests between the best potential variables for R30 in Table 5.6 using simultaneous/delayed cyclones in 1983–1984; no gyres are included.

| Test with Sat Data | No. Obs | R*100 | $R^2$*100 |
|---|---|---|---|
| MSLP vs 04@2548 | 117 | 55% | 29% |
| MSLP vs 24@2548 | 117 | 33% | 10% |
| MSLP vs 06@2548 | 117 | 51% | 25% |
| MSLP vs 26@2548 | 117 | 48% | 22% |
| ER04 vs 04@2548 | 117 | 09% | 00% |
| ER04 vs 24@2548 | 117 | 12% | 00% |
| ER04 vs 06@2548 | 117 | 24% | 05% |
| ER04 vs 26@2548 | 117 | 27% | 06% |
| 06@2548 vs 26@2548 | 117 | 99% | 99% |
| 06@2548 vs 04@2548 | 117 | 92% | 84% |
| 06@2548 vs 24@2548 | 117 | 94% | 89% |
| 26@2548 vs 04@2548 | 117 | 88% | 78% |
| 26@2548 vs 24@2548 | 117 | 92% | 84% |
| 04@2548 vs 24@2548 | 117 | 99% | 98% |

Table 5.8 shows that only one of the satellite variables should be combined with MSLP and ER04 in a statistical equation. It must be noted that the areal coverage of pixel counts from 0-6 and 0-4 should not be used in a statistical equation with MSLP. The correlation coefficients are just too high ( $>$ 50%). The relationship of MSLP and

the area of cloud top temperatures colder than $-25°C$ was also noted by Shoemaker (1989) but is not well understood. ER04 was found to be very weakly related with the various satellite parameters. This was surprising. It was expected that there would be a stronger relationship. If upper level warming generated by the cyclone's outer and inner core convection lowers the pressure at the surface, then it would be reasonable to conclude that the outer closed isobar would be reasonably related to the extent of mid and upper level cloudiness. Perhaps the weak relationship is due to the definition of ER04 which is not always the cyclone's outer closed isobar. What's more likely is that the upper-level warming in the outer core is not strongly related to the amount of cloud cover with temperatures $\leq -25°C$.

## 5.3 Regression with multiple variables

The best variables from the above data sets were combined to produce statistical equations. For the four year data set of simultaneous and delayed cyclones, International Mathematics Statistics Library (IMSL 1987) was used to create multiple regression equations using the variables ER04, MSLP, latitude, and longitude. Results of the best two and three variable equations are given in Table 5.9.

Table 5.9: Multiple regression equation results for the four year simultaneous/delayed cyclone data set. Gyres were not included.

| Variables Used for R30 | No. of Observations | R | $R^2$ | P-values |
|---|---|---|---|---|
| MSLP, ER04 | 218 | 79% | 63% | 0.0, 0.0 |
| MSLP, ER04, LAT | 218 | 79% | 63% | 0.0, 0.0, 0.18 |
| MSLP, ER04, LON | 218 | 79% | 63% | 0.0, 0.0, 0.14 |

Each equation explains the same amount of variance. The advantage of the first equation is it has only two variables. A variable was considered useful for predicting if the P-Value was $< 0.2$. A 'P'-value is the probability that given the null hypothesis (in this case, the variable being tested equals zero) that a sample result will be at least as unlikely as that observed (Anderson et al. 1994). As can be seen from Table 5.9, the P-Values for latitude and longitude are close enough to 0.2 to remove them from consideration as variables.

Table 5.10: Multiple regression equation results for the two year/ satellite simultaneous/delayed cyclone data set.

| Variables Used for R30 | No. of Observations | R | $R^2$ | P-values |
|---|---|---|---|---|
| ER04, 04@2548 | 117 | 85% | 72% | 0.0, 0.0 |
| ER04, MSLP, 24@2548 | 117 | 87% | 75% | 0.0, 0.0, 0.0 |

For the two year satellite data set, satellite variables, ER04 and MSLP were combined to produce statistical equations. Results of the best two and three variable equations are given in Table 5.10. From Table 5.10, it is apparent that both equations can be used, but the difference in the variance is only 3%. This means that adding MSLP to ER04 and 24@2548 does not add significant skill for predicting R30. More importantly, it appears from Table 5.10 that MSLP can be replaced completely by the satellite parameter 04@-25. This means that an equation (to estimate R30) can be used without relying on MSLP, a variable that is only estimated from satellite analysis.

## 5.4 Best Regression Equations

The best regression results from the four-year data set for the simultaneous/delayed are from the following equations:

$$ER30_{sim/del} = A_1 * MSLP + A_2 * ER04 + A_3 \tag{5.1}$$

where $A_1 = -1.013$, $A_2 = 22.747$ and $A_3 = 1048.04$ and ER30 is in n mi.

$$ER30_{gyre} = B_1 * ER04 + B_2 \tag{5.2}$$

where $B_1 = 35.65$, $B_2 = 61.35$. MSLP is measured in mb, ER04 in degrees, and ER30 is in n mi. Equation 5.1 is strictly for delayed and simultaneous storms, while Eq. 5.2 is only for gyres. The best results for the two year satellite data set for simultaneous/delayed are:

$$ER30 = C_1 * ER04 + C_2 * 04@2548 - C_3 \tag{5.3}$$

where $C_1 = 28.22$, $C_2 = 1.73$ and $C_3 = -57.14$ with ER30 in n mi and

$$ER30 = D_1 * MSLP + D_2 * ER04 + D_3 * 24@2548 + D_4 \quad (5.4)$$

where $D_1 = -0.63$, $D_2 = 24.46$, $D_3 = 1.02$ and $D_4 = 606.88$ and ER30 is in n mi. Regression equations were also developed for R50 and R65. These equations however will use ER30 as a primary variable. The equations are

$$ER50 = E_1 * ER30 + E_2 \quad (5.5)$$

where $E_1 = 0.43$, $E_2 = -10.98$ and ER50 in n mi and

$$ER65 = F_1 * ER30 + F_2 \quad (5.6)$$

where $F_1 = 0.25$ and $F_2 = -6.17$ and ER65 is in n mi. The number of cases, correlation coefficient, variance explained, and standard deviation of the errors (SD) of Eqs. 5.1–5.6 are listed in Tables 5.11–5.13.

Table 5.11: Number of cases, correlation coefficient, variance and standard deviation of errors for Eqs. 5.1–5.4.

| Eq. for ER30 | No. of Cases | R | $R^2$ | SD in n mi |
|---|---|---|---|---|
| 5.1 | 218 | 79% | 63% | 40 |
| 5.2 | 35 | 83% | 69% | 42 |
| 5.3 | 117 | 85% | 72% | 37 |
| 5.4 | 117 | 87% | 75% | 34 |

Table 5.12: ER30 equation used to estimate ER50, number of cases, correlation coefficient, variance, and standard deviation of errors for Eq. 5.5.

| ER30 Eq. used to get ER50 | No. of Cases | R | $R^2$ | SD of error in n mi |
|---|---|---|---|---|
| 5.1 | 163 | 68% | 46% | 28 |
| 5.3 | 87 | 65% | 41% | 28 |
| 5.4 | 87 | 70% | 49% | 26 |

The reason why the variance explained is lower for estimating R50 and R65 using Eqs. 5.5–5.6 as compared to Table 5.1 is simple. Equations 5.5–5.6 are using estimated values for R30, not the observed values. Table 5.11 shows that Eq. 5.4 (which has 3 variables) does not increase the variance more than Eq. 5.3 (which has 2 variables) for estimating

Table 5.13: ER30 equation used to estimate ER65, number of cases, correlation coefficient, variance, and standard deviation of errors for Eq. 5.6.

| ER30 Eq. used to get ER65 | No. of Cases | R | $R^2$ | SD of error in n mi |
|---|---|---|---|---|
| 5.1 | 120 | 58% | 34% | 19 |
| 5.3 | 77 | 45% | 19% | 19 |
| 5.4 | 77 | 63% | 38% | 17 |

R30. However, if ER30 from Eq. 5.4 is used for estimating R50 much better results occur than ER30 from Eq. 5.3. Therefore, it appears there is an advantage in using Eq. 5.4 when estimating R50 and R65. In an effort to see if there could be a way to improve upon the estimations of R50 and R65, a mathematical relationship for the decay of the outer winds proposed by Depperman (1947), Hughes (1952), Riehl (1954, 1963) and Shea and Gray (1973) was tested. This relation is given by

$$V_t R^x = C$$

where C is a constant, and x is 0.5. To find ER50 and ER65 as a function of ER30 we obtain the following relationships:

$$ER50 = (30/50)2 * ER30 = 0.36 * ER30 \tag{5.7}$$

$$ER65 = \frac{30}{65}^2 * ER30 = 0.21 * ER30 \tag{5.8}$$

where ER30, ER50, and ER65 are in n mi. Using the estimated values of R30 (ER30), estimates for R50 and R65 were produced using Eqs. 5.5–5.8. The estimates for R30 using Eqs. 5.5 and 5.7 are graphed against each other and shown in Fig. 5.2. Likewise, the estimates for R65 using Eqs. 5.6 and 5.8 are graphed against each other and shown in Fig. 5.3. Both of these figures show that they are essentially a straight line. Careful inspection reveals that Eqs. 5.5, 5.7 and 5.6, 5.8 are essentially the same (note the small differences in slope). Essentially, Eqs. 5.5 and 5.6 are recapitulations of $V_t = K * R^{-x}$. For practical purposes, Eqs. 5.5 and 5.6 can be replaced by Eqs. 5.7 and 5.8 . This means that on average, the tropical cyclone's outer winds data set roughly follows a modified

Rankine vortex with x = 0.5. Since there is some skill in determining R50 and R65, then using $V_t * R^x = C$ should mean that the entire outer wind profile from R30 to R65 can be estimated with some confidence.

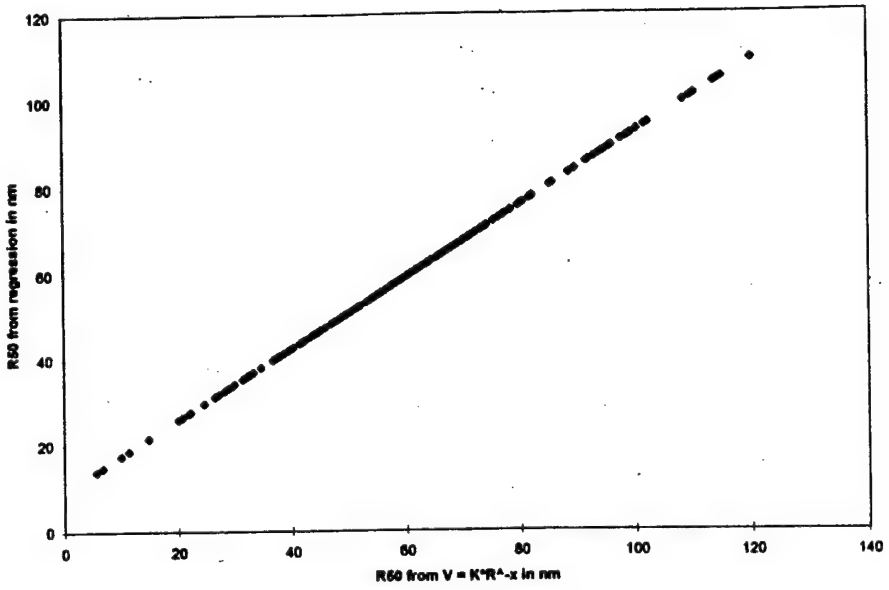


Figure 5.4: ER50 using regression formula versus ER50 derived from the modified Rankine Vortex relation.

## 5.5 Error Analysis

Error analysis were run on Eqs. 5.1–5.4 and 5.7–5.8. Specifically, the errors associated with these equations were calculated by subtracting the estimated value of R30, R50 and R65 from that which was observed. The error residuals were correlated against the observed size of the cyclone to see if there was any systematic bias due to the cyclone's size (see Tables 5.14–5.16).

In every test, a positive correlation was measured. This means when the cyclone is small the predicted R30 value is overestimated; when the cyclone is large, the predicted value is underestimated. The error residuals vs observed R30 showed weaker correlation coefficients as compared to R50 and R65 error residuals vs observed R50 and R65. This

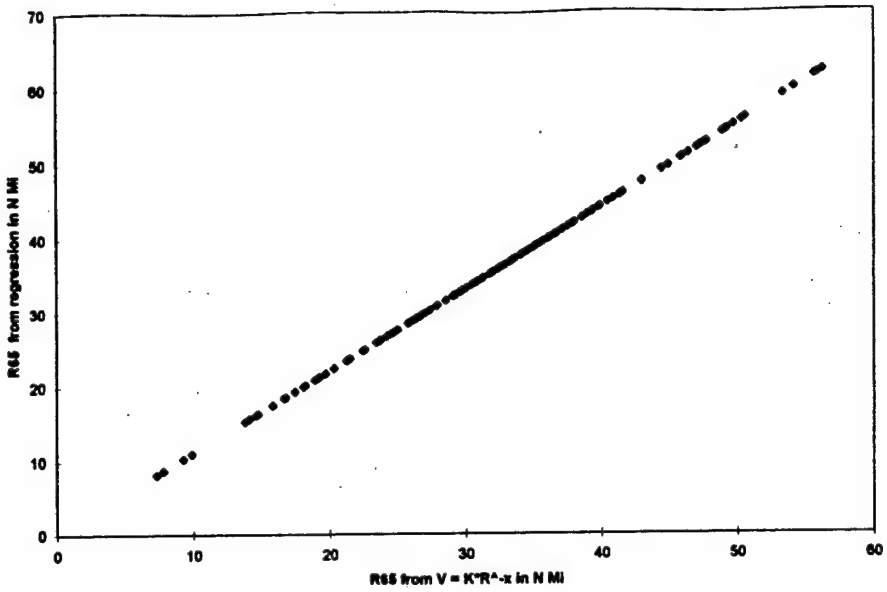


Figure 5.5: ER65 using regression formula versus ER65 derived from the modified Rankine Vortex relation.

Table 5.14: Error residuals from the estimated values of R30 using Eqs. 5.1–5.4 correlated against the observed values, the number of cases, correlation coefficients, and variances.

| Category | No. of Cases | R | $R^2$ |
|---|---|---|---|
| (R30 - Eq. 5.1) vs R30 | 218 | 61% | 36% |
| (R30 - Eq. 5.2) vs R30 | 35 | 55% | 28% |
| (R30 - Eq. 5.3) vs R30 | 117 | 52% | 27% |
| (R30 - Eq. 5.4) vs R30 | 117 | 48% | 23% |

means that ER50, and ER65 may be easier to correct resulting in more accurate values given the acquisition of a larger data set.

In summary, various physical parameters were correlated to R30. The physical parameters best related to R30, and not significantly related to each other were chosen for multiple regression analysis. The best equations developed from multiple regression analysis showed there is considerable skill in estimating R30, R50 and R65. The equations developed for predicting R50 and R65 were found to be a recapitulation of the mathematical relation $V_t * R^x = C$ where x = 0.5. This opens the way for estimating the entire outer radial wind profile from R30 to R65. In the next chapter, a technique is developed for forecasting 12–48 hours into the future of the outer wind profile.

Table 5.15: The error residual category (including ER50 as a function of Eqs. 5.1, 5.3 and 5.4), the number of cases, correlation coefficients, and variance explained of the error residuals versus the observed R50.

| Category | No. of Cases | R × 100 | $R^2$× 100 |
|---|---|---|---|
| R50-ER50 (Eq. 5.1) | 163 | 82% | 66% |
| R50-ER50 (Eq. 5.3) | 87 | 75% | 55% |
| R50-ER50 (Eq. 5.4) | 87 | 76% | 57% |

Table 5.16: The error residual category (including ER65 as a function of Eqs. 5.1, 5.2, and 5.3), the number of cases, correlation coefficients, and variance explained of the error residuals of R65 versus the observed R65.

| Category | No. of Cases | R × 100 | $R^2$× 100 |
|---|---|---|---|
| 5.1 | 120 | 74% | 54% |
| 5.2 | 77 | 81% | 65% |
| 5.3 | 77 | 79% | 61% |

# Chapter 6

# FORECASTING THE OUTER WIND PROFILE

## 6.1 Predicting 12–48 Hour Changes in the Outer Wind Radii

### 6.1.1 Average Changes in Delayed, Simultaneous and Gyre Cyclones

From our composite analyses in chapter 4, we can determine the average rate of change for R30, R50 and R65 for simultaneous, delayed and gyre cyclones. Using this information, it is possible to make estimates of the cyclone's future 12-48 hour size changes. Tables 6.1–6.3 shows the average rates of change of R30, R50 and R65 derived from the composite data for delayed, simultaneous, and gyre cyclones.

Table 6.1: The change in R30, R50 and R65 per day for delayed cyclones. MI approximately denotes when maximum intensity occurred.

| % Life Cycle Complete | $\Delta$ R30 in $nmi/d$ | $\Delta$ R50 in $nmi/d$ | $\Delta$ R65 in $nmi/d$ |
|---|---|---|---|
| 5 | NA | NA | NA |
| 25 | 29.7 | 34.9 | 19.1 |
| 47 | 31.4 | 14.2 | 10.2 |
| 61 MI | 20.7 | 26.5 | 4.5 |
| 75 | 16.2 | –1.0 | 15.7 |
| 95 | 7.0 | NA | NA |

Prior to MI, the average growth rates of both simultaneous and delayed cyclones are similar. At MI and after, delayed cyclones experienced a period of slow growth while simultaneous storms experienced negative growth. Gyre cyclones are similar to simultaneous cyclones although they increase in size at a slower rate before MI and decrease at a faster rate after MI. Figures 6.1 and 6.2 show that the rate of change of R30 for simultaneous and gyre cyclones are somewhat tied to their inner cores. That is, R30 decreases before significant pressure rises occur. Figure 6.3 shows the rate of change of R30 for delayed cyclones which never becomes negative within the composite life cycle.

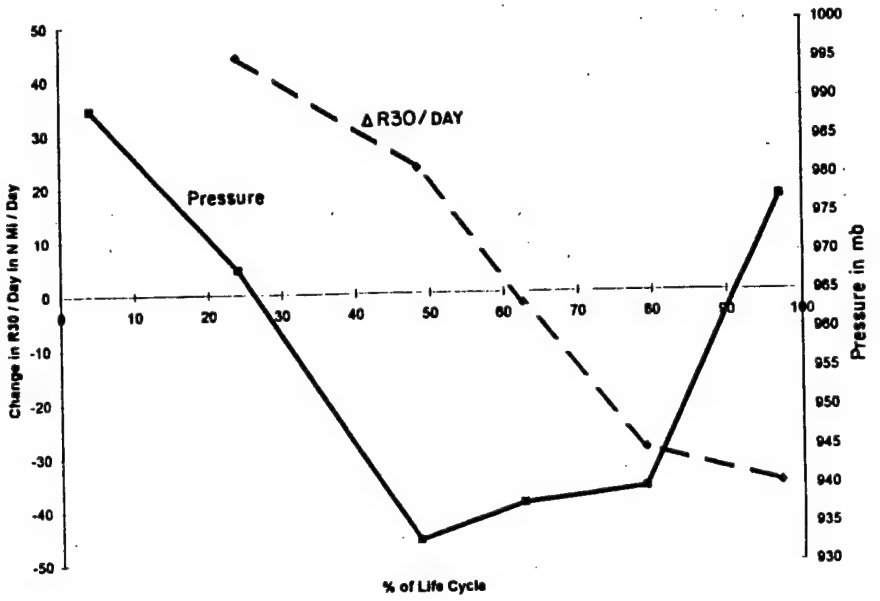


Figure 6.1: The change in R30 in $nmid^{-1}$ and central pressure (mb) versus cyclone life cycle for simultaneous cyclones.

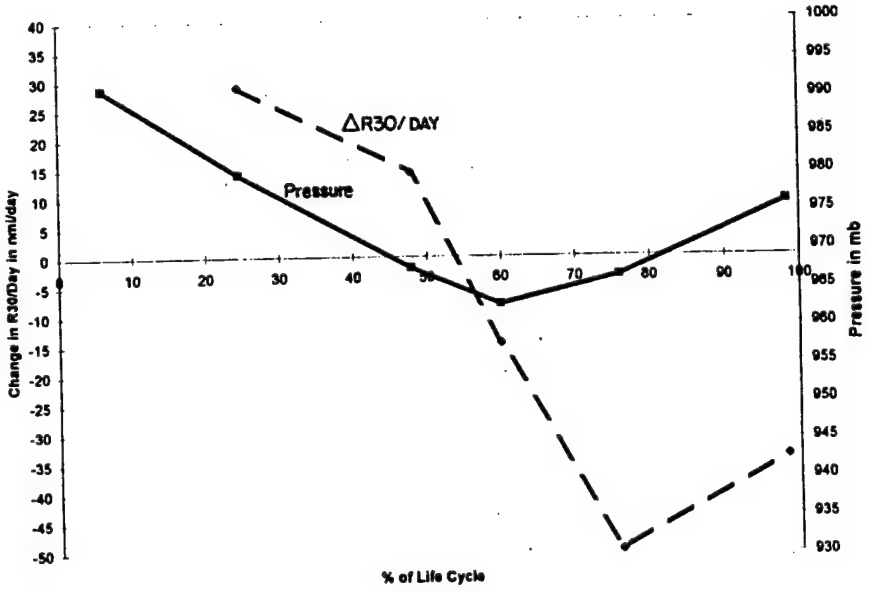


Figure 6.2: Same as Fig. 6.1 except for gyre cyclones.

Table 6.2: The change in R30, R50 and R65 per day for simultaneous cyclones. MI approximately denotes when maximum intensity occurred.

| % Life Cycle Complete | Δ R30 in $nmi/d$ | Δ R50 in $nmi/d$ | Δ R65 in $nmi/d$ |
|---|---|---|---|
| 5 | NA | NA | NA |
| 25 | 44.2 | 23.7 | 8.6 |
| 47 | 23.5 | 18.9 | 18.2 |
| 61 MI | −1.9 | 1.5 | −1.3 |
| 75 | −28.8 | 6.0 | 4.4 |
| 95 | −35.5 | NA | NA |

Table 6.3: The change in R30 per day for gyre cyclones. MI approximately denotes when maximum intensity occurred.

| % Life Cycle Complete | Δ R30 in $nmi/d$ |
|---|---|
| 5 | NA |
| 25 | 28.9 |
| 47 | 14.3 |
| 61 MI | −14.6 |
| 75 | −49.6 |

For both delayed and simultaneous cyclones, the rate of change of R50 and R65 are similar prior to MI. After MI, the observations become sparse, and it is difficult to determine meaningful trends. There weren't enough R50 and R65 measurements available to attempt a composite for gyre cyclones.

This presents some problems for deriving growth rates from which one can forecast future outer wind radii. First of all, the composite life cycle did not show a negative growth rate in R30 for delayed cyclones. Yet, at some point the cyclone will become smaller. Also, R50 and R65 did not show a clear decreasing trend for either cyclone type. This was due to the overall weakening of the winds close to the inner core late in the cyclone's life cycle. Therefore, a negative growth rate for R50 and R65 must occur at some point. The composite of simultaneous cyclones never showed a slow growth regime. However individual cyclones did show this, and was reflected in the size parameter ER04. This characteristic was discussed in Chapter 3. Additionally, individual cyclones of all types experienced periods where the outer wind radii showed no appreciable change in size. This was also discussed in Chapter 3 (see Figs. 3.6 and 3.7). Therefore, any forecast method should take into account periods when a cyclones size does not change.

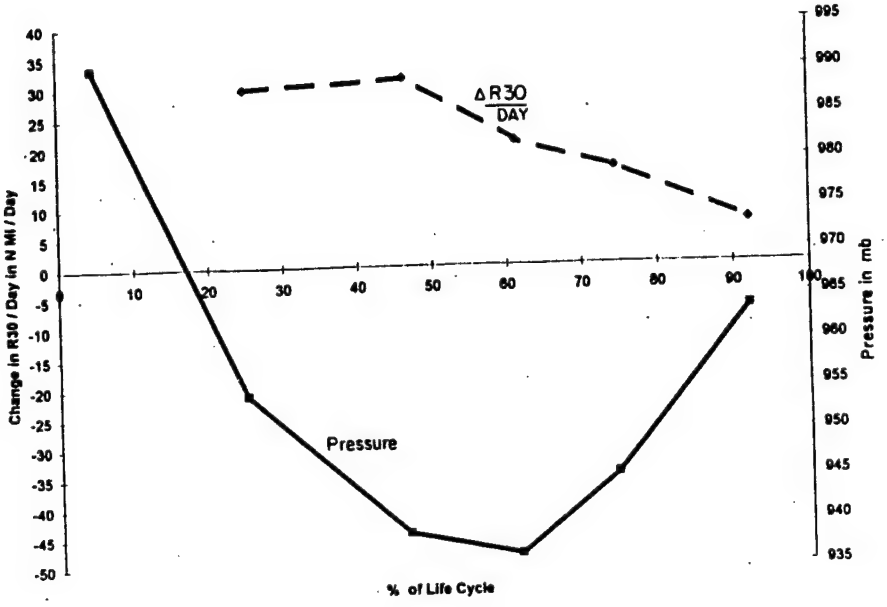


Figure 6.3: Same as Fig. 6.1 except for delayed cyclones.

To overcome the differences of individual storms from the composites, some general assumptions were made. Delayed and simultaneous cyclones are assumed to have the same initial growth rate. The Steady Growth Rate (STGR) is approximately the average of both cyclones growth rates prior to MI. Delayed cyclones are assumed to decrease at the same rate as simultaneous cyclones once a decreasing trend in ER04 (cyclone size on a synoptic map) is detected. The Negative Growth Rate (NGR) is approximately the average of the simultaneous cyclones growth rates at and after MI. For R50 and R65, it is assumed that the NGR is approximately two thirds of the value computed for R30 and R50 respectively. The Steady Growth Rate for Gyres (STGRG) is the average of the growth rate prior to MI. The Negative Growth Rate for Gyres (NGRG) is the average of the growth rate at and after MI. It will be assumed that simultaneous cyclones experience the same slow growth rate as delayed cyclones. The Slow Growth Rate (SGR) is approximately the average of the growth of delayed cyclones at and after MI. The SGR for R50 is assumed to be two-thirds the value of R30, and R65 two-thirds the value of R50. Tables 6.4 and 6.5 lists the 24 hr growth rates for R30, R50, and R65 of simultaneous, delayed and gyre cyclones. Table 6.6 shows the 36 hr and 48 hr growth rates for all cyclone types after an

interruption in its growth. To compute the 12, 36, and 48 hr growth rates multiply the 24 hr rate by 0.5, 1.5, and 2.0 respectively.

Table 6.4: Twenty-four hour forecasted growth rates for simultaneous/delayed cyclones.

| Category | Δ R30 in $nmi/d$ | Δ R50 in $nmi/d$ | Δ R65 in $nmi/d$ |
|---|---|---|---|
| Steady Growth Rate | +30 | +23 | +14 |
| Slow Growth Rate | +12 | +8 | +5 |
| Negative Growth Rate | −22 | −15 | −10 |

Table 6.5: Twenty-four hour forecast growth rates for gyre cyclones.

| Category | Δ R30 in $nmi/d$ |
|---|---|
| Steady Growth Rate | +22 |
| Negative Growth Rate | −32 |

Table 6.6: 36 and 48 hr growth rates for all cyclone types after an interruption to its growth has occurred.

| Outer Wind Radius | 36 hr Growth Rate Simultaneous/ Delayed Cyclones in n mi/day | 48 hr Growth Rate Simultaneous/ Delayed Cyclones in n mi/day | 36 hr Growth Rate Gyres Only in n mi/day | 48 hr Growth Rate Gyres Only in n mi/day |
|---|---|---|---|---|
| R30 | +6 | +12 | 5.5 | 11 |
| R50 | +4 | +8 | NA | NA |
| R65 | +3 | +6 | NA | NA |

The forecast scheme will use information from the trend in ER04 and central pressure to determine future outer wind radii. Although central pressure will not be explicitly available to the forecaster, an estimate can be made using the Dvorak intensity estimation scheme (Dvorak 1984). The following forecasting rules apply to all cyclones for all times.

1. Simultaneous, delayed and gyre cyclones will start out at their respective steady growth rates as shown in Tables 6.4 and 6.5.

2. If two consecutive ER04 values don't show a positive growth trend then hold the 12-24 hr R30, R50 and R65 growth rates at zero. Use the growth rates prescribed in Table 6.6 for the 36 and 48 hr forecast

3. If two consecutive ER04 values show a decreasing trend and MI has not been reached, then hold the 12 and 24 hr growth rates for R30, R50 and R65 at zero. Use the growth rates prescribed in Table 6.6 for the 36 and 48hr forecast until MI has been reached

4. If MI has been reached and two consecutive ER04 values show a decreasing trend then use a negative growth rate.

5. If MI has been reached, and ER04 continues to show an increasing trend then use the slow growth rate.

6. If at any time after a negative growth rate or an interruption to the growth of the cyclone's synoptic size has occurred, and two consecutively increasing ER04 values are measured then resume the slow growth rate.

Rules 1)–6) were tested on the simultaneous/ delayed cyclone and gyre cyclone data sets using Eqs. 5.1–5.4 and Tables 5.7–5.8. The results of these tests are shown in Tables 6.7–6.9.

Table 6.7: Number of cases and variance explained ($R^2$) for 12–48 hr predicted values of R30, R50, and R65 vs actual observed values 12-48 hours later for four years of simultaneous and delayed cyclones. No satellite data was available for this test. For this test Eqs. 5.1, 5.7 and 5.8 were used.

| PRxx | Cases | 12 hr fcst $R^2$ | Cases | 24 hr fcst $R^2$ | Cases | 36 hr fcst $R^2$ | Cases | 48 hr fcst $R^2$ |
|---|---|---|---|---|---|---|---|---|
| PR30 | 212 | 57% | 194 | 49% | 168 | 37% | 144 | 24% |
| PR50 | 175 | 45% | 162 | 40% | 148 | 34% | 130 | 29% |
| PR65 | 143 | 23% | 134 | 16% | 111 | 12% | 99 | 09% |

As can be seen, there is considerable skill in forecasting R30 to at least 24hrs in advance. Forecasted R50 values were not as good, but useful to at least 24 hours out. Overall, R65 didn't show significant forecasting skill

Table 6.8: Number of cases and variance explained ($R^2$) for 12-48 hr predicted values of R30 vs actual observed values 12-48hrs later for four years of gyre cyclones. For this test Eq. 5.2 was used.

| PRxx | Cases | 12 hr fcst $R^2$ | Cases | 24 hr fcst $R^2$ | Cases | 36 hr fcst $R^2$ | Cases | 48 hr fcst $R^2$ |
|---|---|---|---|---|---|---|---|---|
| PR30 | 34 | 60% | 31 | 60% | 27 | 58% | 24 | 32% |

Table 6.9: Number of cases and variance explained ($R^2$) for 12-48 hr predicted values of R30, R50, and R65 vs actual observed values 12-48hrs later for two years of simultaneous and delayed cyclones with satellite data. For this test Eqs. 5.4, 5.7 and 5.8 were used.

| PRxx | Cases | 12 hr fcst $R^2$ | Cases | 24 hr fcst $R^2$ | Cases | 36 hr fcst $R^2$ | Cases | 48 hr fcst $R^2$ |
|---|---|---|---|---|---|---|---|---|
| PR30 | 111 | 68% | 102 | 59% | 90 | 50% | 79 | 43% |
| PR50 | 93 | 44% | 85 | 32% | 82 | 28% | 72 | 23% |
| PR65 | 81 | 19% | 73 | 16% | 61 | 06% | 51 | 06% |

### 6.1.2 PI Index

A pressure index (PI) was created using the synoptic surface data from chapter 4 to differentiate between simultaneous and delayed cyclones. It was found that for the composite pressure patterns, instantaneous values $\geq 12$ corresponded to simultaneous types, and values $\leq 9$ corresponded to delayed types. Current and 24 hr averages were calculated for all cyclone types. However the 24 hr average is preferred since it will eliminate short term fluctuations in the pressure field. Therefore a cyclone was considered simultaneous if the 24 hr PI value satisfied any of the following conditions:

- PI was at or above 12 two days prior to MI, and remains at or above this value at least two days after MI
- PI climbs rapidly to 12 before MI, and continues to increase for at least two days after MI.

A cyclone was considered delayed if the 24 hr value of PI satisfied any of the following conditions:

- PI was at or below 9 prior to MI, and remains at or below this value at least two days after MI
- PI drops to 9 or below before MI, and continues to decrease for at least two days after MI.

No determination could be made for the cyclone if PI values were between 9 and 12, or if any of the rules above failed.

Table 6.10 shows that about the same amount of success was found for both simultaneous and delayed cyclones. However, the technique had trouble predicting delayed cyclones in the later part of the typhoon season. Also, the technique is good only if you have a good idea when MI will occur. Nonetheless, if one can tell if a typhoon has reached MI, there is some reasonable skill in determining if it will become simultaneous or delayed. This may be useful to military and civilian agencies for planning purposes. Since the PI index depends on a prior knowledge of when MI will occur no tests were attempted to use it in the forecast scheme.

Table 6.10: PI index prediction results.

| Category | Total # of Storms | Not Determined | # Correctly Predicted | % Correctly Predicted |
|---|---|---|---|---|
| Simultaneous Storms | 8 | 0 | 6 | 75.0% |
| Delayed Storms | 13 | 1 | 9 | 69.0% |
| Simultaneous + Delayed | 21 | 1 | 15 | 71.4% |

## 6.2 Correcting Outer Wind Radius Estimates For Motion Asymmetry

In Chapter 5, Eqs. 5.1–5.4, 5.7 and 5.8 were derived to estimate the current R30, R50, and R65. This estimate produces a vortex averaged value which can be corrected for the storm's motion ( Frank and Gray, 1980). Figure 6.4 shows how a cyclone's tangential winds should be increased on its right hand side and decreased on its left hand side due to its motion. The amount a cyclone's winds may be increased or decreased by it's motion vector is given by:

$$V_{t\ new} = V_t + |V_{motion}| * COS\theta \tag{6.1}$$

where $V_{t\ new}$ is the value for the tangential wind once the motion vector $V_{motion}$ has been added in. The angle $\theta$ is measured counterclockwise from a line drawn perpendicular to the motion vector. But this gives the change in the tangential wind speed but not the change in the radius of a given wind speed due to the motion vector. To convert the change in tangential wind speed to a change in R30 and R50 the author determined the ratio between the net distance between R30 and R50, and the difference in the wind speed:

$$(R30 - R50)/20 \tag{6.2}$$

where R30 and R50 are in n mi and the constant '20' is the decrease in the wind speed between the two kind of radii. This gives units of n mi/kt or the distance one travels per one knot decrease in wind speed. Using this ratio, one can adjust R30 and R50 by the following equations:

$$R30_n = R30 + (R30 - R50)/20 * |V_{motion}| * COS\theta \tag{6.3}$$

$$R50_n = R50 + (R50 - R65)/20 * |V_{motion}| * COS\theta \tag{6.4}$$

where $R30_n$ and $R50_n$ represent the motion vector adjusted R30 and R50. Eight different cyclone times were picked out to see this method of including outer wind asymmetries due to cyclone motion was similar to what was analyzed (see Figs. 6.5–6.12). In some cases Eqs. 6.3 and 6.4 did a good job in depicting motion asymmetries in the cyclone. However, it was obvious that distinct asymmetries not associated with cyclone motion also existed. A qualitative check revealed that a number of the more asymmetric cases were related to an asymmetric distribution of the height gradient at 700 mb. Hawkins and Black (1983) also noted distinct asymmetries associated with tropical cyclones that were not related to the cyclone's motion. McElroy (1996) also found distinct wind asymmetries associated

with the environmental flow through the cyclone. Additional research is needed to see if corrections for these non-motion asymmetries can be made.

In summary, a forecasting technique was developed for forecasting the change in the outer wind radii from 12–48 hrs into the future. The technique showed considerable skill for predicting R30 out to at least 36 hrs, and R50 to 24 hrs out. A technique for subtracting out the cyclones motion in order to obtain the outer wind asymmetries due to cyclone motion was developed. This technique was compared with actual cyclone asymmetries with some positive results. However asymmetries not due to cyclone motion will require further research.

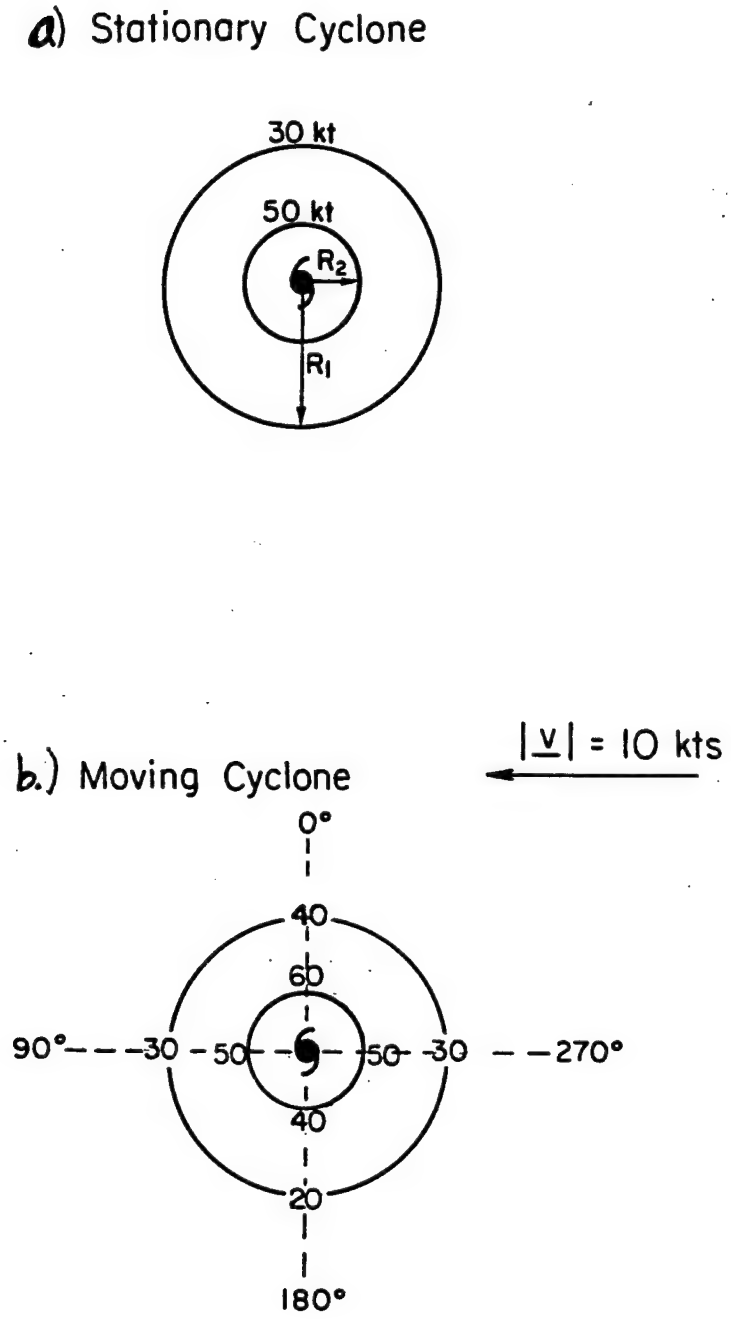


Figure 6.4: How the cyclones motion vector can change the tangential winds; a) stationary cyclones, b) cyclone moving west at 10 knots (5 $ms^{-1}$.

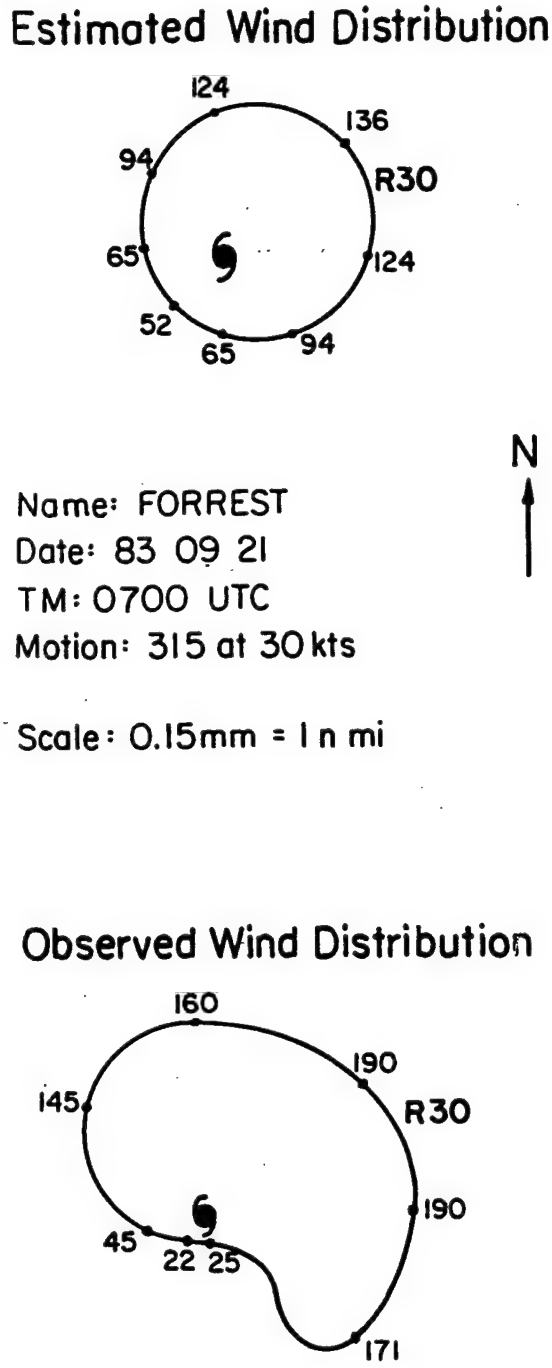


Figure 6.5: a) Cyclone tangential wind asymmetry as predicted by Eqs. 6.3 and 6.4, b) observed tangential wind asymmetry.

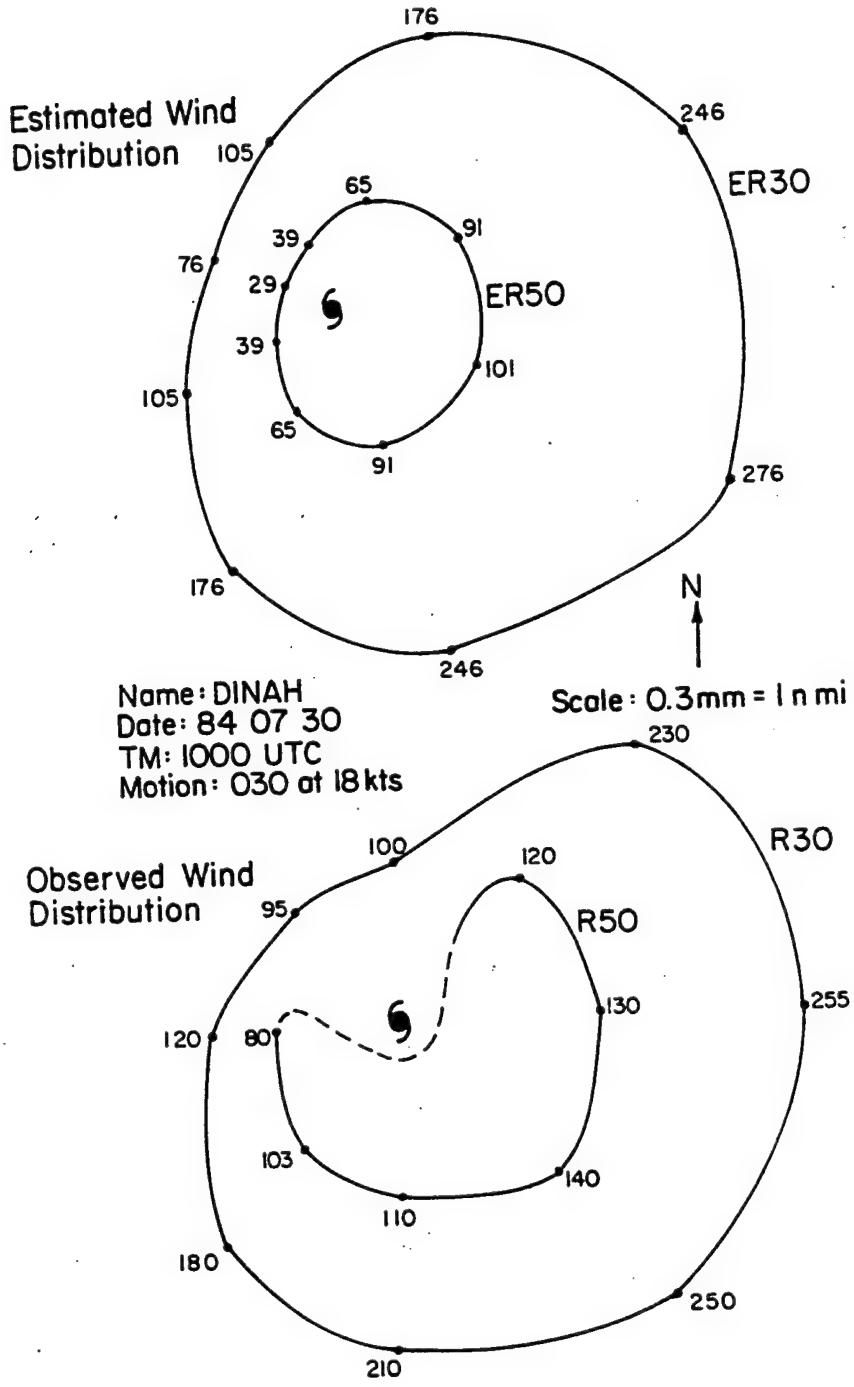


Figure 6.6: Same as Fig. 6.5.

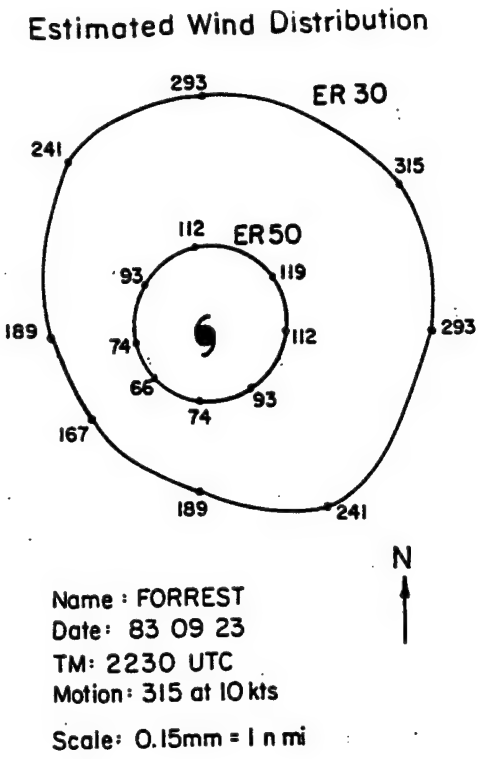


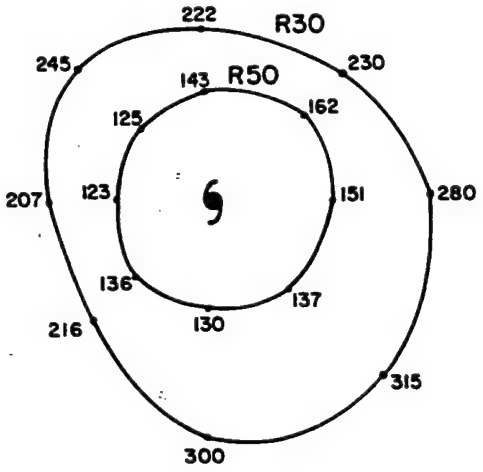


Figure 6.7: Same as Fig. 6.5.

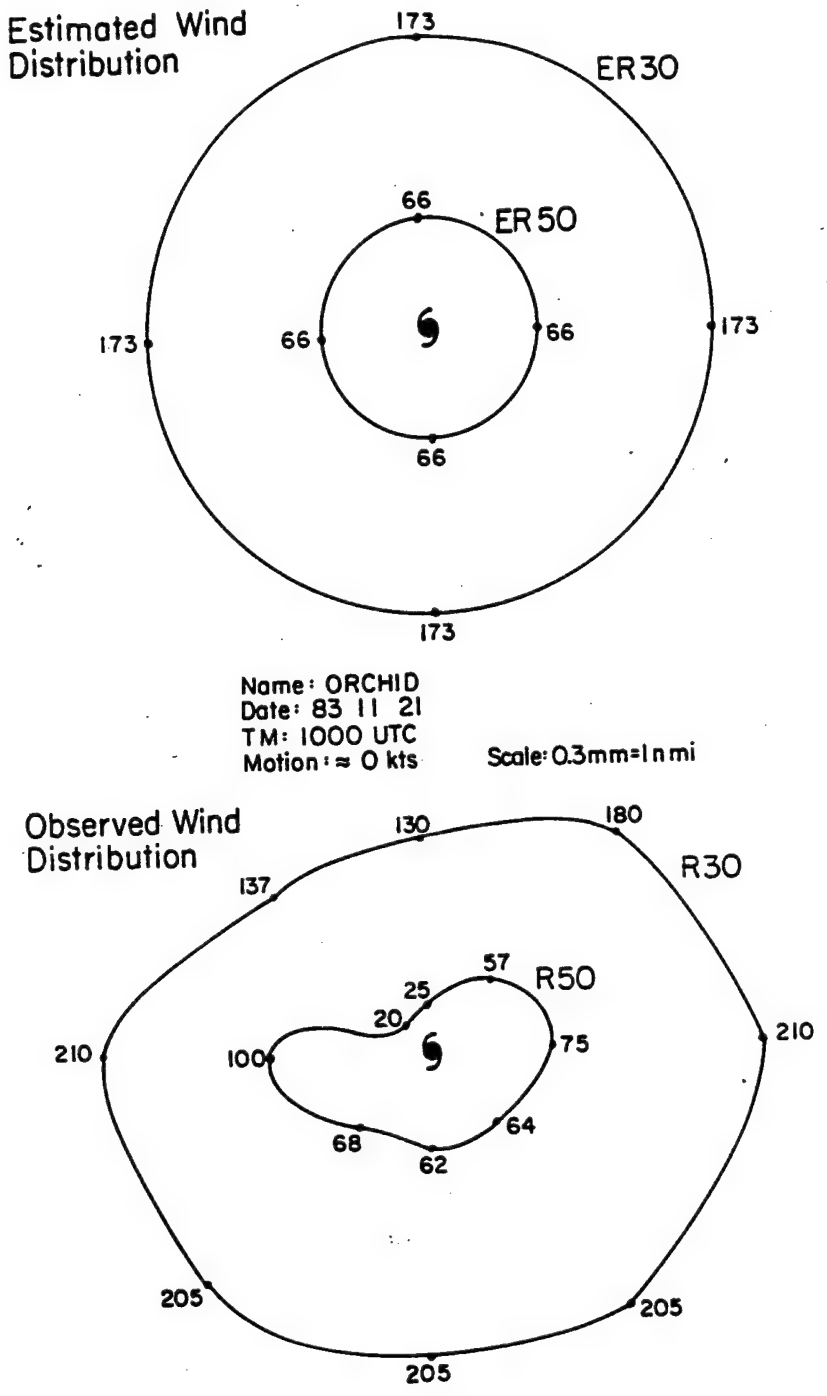


Figure 6.8: Same as Fig. 6.5.

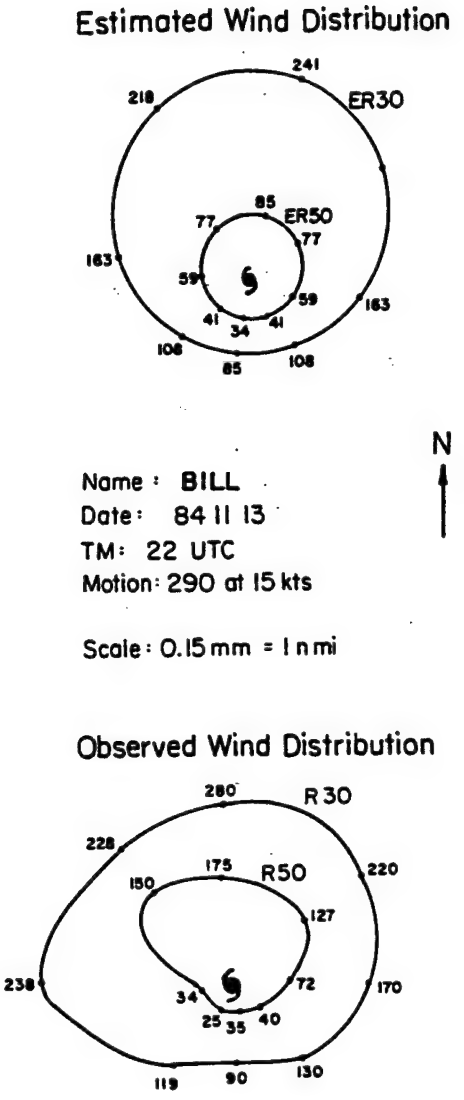


Figure 6.9: Same as Fig. 6.5.

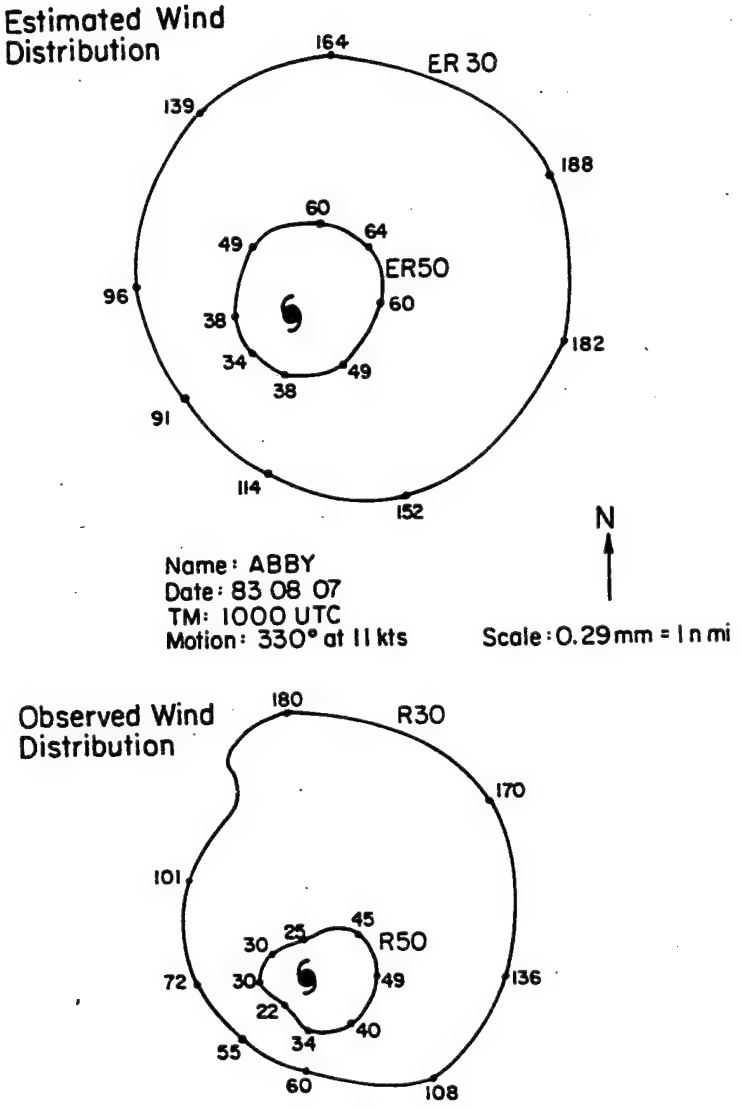


Figure 6.10: Same as Fig. 6.5.

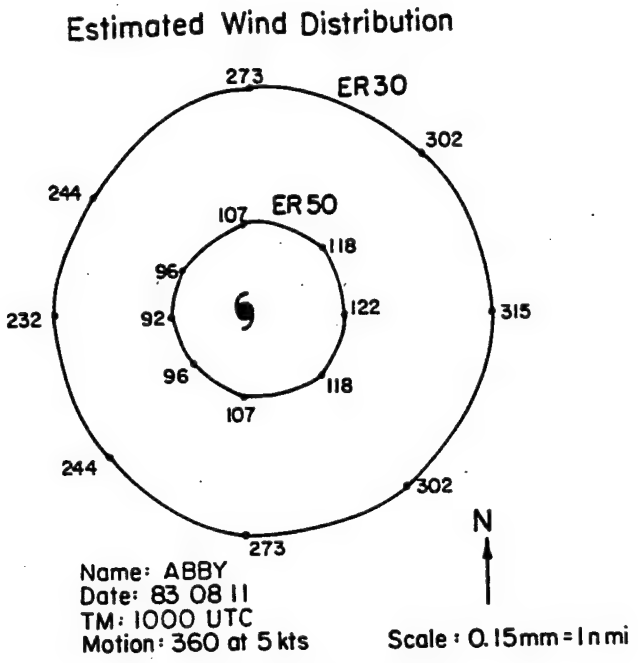


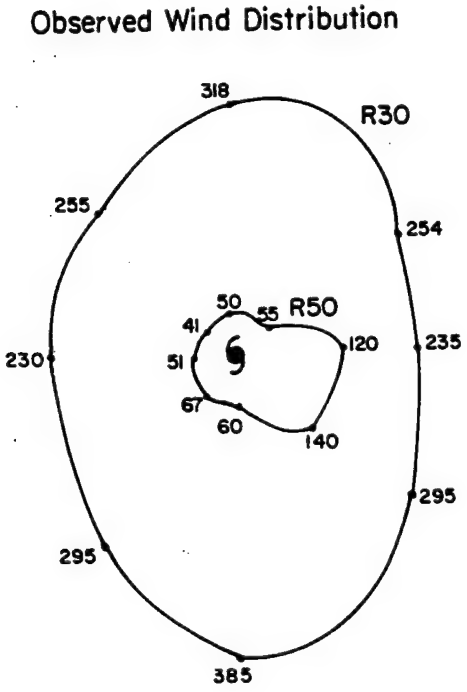


Figure 6.11: Same as Fig. 6.5.

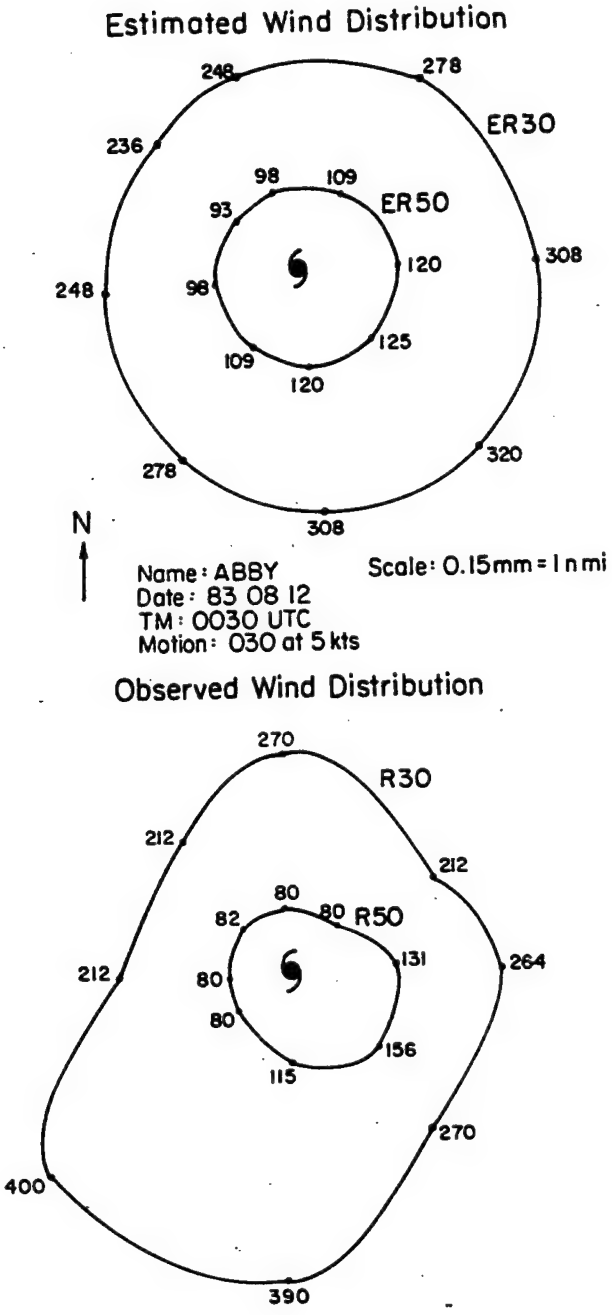


Figure 6.12: Same as Fig. 6.5.

# Chapter 7

# CONCLUSION

## 7.1 Summary

Using both aircraft reconnaissance and synoptic data, the outer wind profile of tropical cyclones were studied. Early on it became apparent that the tropical cyclones used in this study should be divided into three classes. Delayed cyclones showed increases in their outer wind radii for at least one day pat MI. Simultaneous cyclones showed decreases in their outer wind radii either prior to or at MI. The other class contained cyclones that were exceptionally large all during their life cycles, and these were called gyres. Gyres tended to have R30 profiles similar to simultaneous cyclones except the magnitude of R30 is much larger. All cyclones tended to experience periods of steady, slow, negative or no growth in the radius of R30, R50 and R65. It was found that the synoptic size variable, ER04, followed the trend in growth of R30. In Chapter 3, it was found that delayed and gyre cyclones were more likely to occur during the summer and early fall, while simultaneous cyclones were more likely to occur during fall and winter. The locations of simultaneous cyclones at MI were on average much further south than delayed or gyre cyclones. Simultaneous cyclones tended to travel more westward than both delayed and gyre cyclones. Both of these findings leads one to speculate that the change in the seasons leads to different synoptic weather patterns which in turn lead to the different outer wind profiles. There was no real preference in size or intensity for delayed and simultaneous cyclones. By definition, gyre cyclones were always large. Although gyre cyclones have outer wind profiles like simultaneous ones, the motion and seasonal climatology are more like delayed cyclones.

Chapter 4 showed that the life cycle of R30 for simultaneous cyclones tended to follow the life cycle of central pressure, while delayed cyclones continued to grow past MI. Differences in the outer wind radii between these two cyclone types decreased close to the center. The life cycle of central pressure in simultaneous and delayed cyclones were very similar. This implied that an external forcing is causing the differences in the outer wind profiles after MI. The life cycle of the eye size clearly expands after MI for delayed cyclones. Simultaneous ones show a relatively unchanging eye size until very late in the life cycle. This difference implies that the change in the eye size is also having an effect on the outer wind profile after MI. Gyres, when compared to simultaneous and delayed cyclones, showed a completely different life cycle of central pressure. Gyres never became very intense. They experience slow and steady falls and rises in central pressure.

Composites of the track of cyclone centers revealed that by the end of their life cycle, delayed cyclone centers were at a higher latitude than simultaneous cyclones. Gyre cyclones were typically at a higher latitude than both simultaneous and delayed cyclones. Center track longitude composites showed simultaneous cyclones were located much further west than delayed cyclones through most of the life cycle. Gyre cyclones were located much further west than simultaneous cyclones initially, but this difference decreased as time passed. Composite surface pressure maps showed that delayed and gyre cyclones were associated with a synoptic pattern found more often in summer and early fall. The subtropical high and a weak high pressure area were located northeast and northwest respectively of the centers of delayed cyclones. This synoptic environment explains the more northward motion for delayed cyclones. As discussed in Chapter 4, this motion may allow for the cyclones inertial stability to increase to the point where it's eye starts to expand. This in turn acts to intensify the delayed cyclone's outer core until the eye disappears.

Gyre cyclones were associated with an unusually broad and deep monsoon trough. This large monsoon trough typically moved northward taking the gyre with it. Simultaneous cyclones were associated with a synoptic pattern found most often in middle to late fall. A strong ridge of high pressure was located from northwest to northeast of center

of simultaneous cyclones. This keeps their motion on a more west-northwest track until late in the life cycle when these cyclones turned more northward. This may also keep the simultaneous cyclones eye from expanding significantly until late in the life cycle. This strong ridge of high pressure north of simultaneous cyclones originated over the Asian continent. This implies an air mass of cooler and drier air in close proximity to simultaneous cyclones. Perhaps some of this air is entrained into the circulation of the cyclone and inhibits the convection. This may also weaken the inner core of these cyclones.

In Chapter 5, various physical parameters were tested to see how well they related to R30. It was found that ER04, MSLP, and SAT24 correlated best with R30. Statistical equations were developed to estimate R30. It was found that R30 related well to R50, and R50 related to R65. Initially statistical equations were developed that used R30 as a variable for R50 and R65 respectively. However, it was discovered that these equations were closely approximated by the formula $V_t * R^x = C$ where $x = 0.5$. This indicates, at least in a statistical sense, the outer wind profile behaved approximately like a Rankine vortex. Using statistical equations and $V_t * R^x = C$ which showed considerable skill, it was possible to estimate R30, R50 and R65.

A forecast scheme was developed in Chapter 6 that allows forecasters to make 12-48 hour forecasts for the outer wind radii in tropical cyclones. It was found that considerable skill existed in predicting R30 out to 36 hours, and R50 out to 24 hours. A relationship was derived to help account for tangential wind asymmetries associated with the cyclone motion. Eight cases were chosen to test this relationship out. It was found that in some cases the applied adjustment gave realistic results. There were, however, other cases where tangential wind asymmetries not related to cyclone motion were found.

## 7.2 Further Research

In fact, further research is needed to understand many aspects of the different outer wind distributions of these cyclone types. Although it was implicitly shown in this study that synoptic forcing causes the change in the R30 profiles, studies need to be made which explicitly show the physical processes behind variations in the outer wind distribution

and all of its asymmetries. For instance, does the importing of momentum occur when cyclones move in between two anticyclones such as Merrill 1982 suggests? There wasn't clear evidence that this was happening for delayed cyclones. There appeared to be a relationship with the overall monsoon trough pattern and those cyclones that grew in size for longer periods of time past MI as they travel northwards. More research is definitely needed here.

The statistical and forecast equations created need to be tested on an independent data set. Research needs to be done to determine how well the current technique complements the microwave scatterometer derived winds. Any bias needs to be corrected? The technique for determining the outer closed isobar on the surface map is somewhat objective. New research might attempt to create a more objective technique for determining the cyclone's synoptic size.

More research should look into the asymmetries in the outer wind that are not due to cyclone motion. Finally, more research should look into the formation and evolution of gyre cyclones. Throughout this study, they distinguished themselves as being fundamentally different than other cyclones. There are many questions to be answered. For instance, is there any mid-latitude forcing connected with the genesis of gyre cyclones? Do monsoon gyres regularly generate gyre cyclones, or only some of the time? Can gyre cyclones evolve into a simultaneous or delayed cyclone and if so how? More research is needed on this topic.

## REFERENCES

Anderson, D. R., D. J. Seeney and T. A. Williams, 1994: Introduction to statistics: Concepts and applications. Third edition, West Publishing CO., St. Paul, MN, 331 pp.

Brand, S., 1972: Very large and very small typhoons of the western North Pacific Ocean. *J. Meteor. Soc. Japan*, 50, 332–341.

Dvorak, V. F., 1984: Tropical cyclone intensity analysis using satellite data. NOAA Technical Report NESDIS 11, US Dept. of Commerce, Washington, DC, 47 pp.

ESCAP/WMO Typhoon Committee Annual Review, 1985.

Frank, W. M. and W. M. Gray, 1980: Radius and frequency of $15ms^{-1}$ (30 kt) winds around tropical cyclones. *J. Appl. Meteor.*, 19, 2, 219-223.

Harr, P. A. and R. L. Elsberry, 1991: Tropical cyclone track characteristics as a function of large scale circulation anomalies. *Mon. Wea. Rev.*, 119, 1448–1468.

Hawkins, J. D., P. G. Black, 1983: SEASAT scatterometer detection of gale force winds near tropical cyclones. *J. Geophys. Res.*, 88, 1674–1682.

Holland, G. J., 1980: An analytical model of the wind and pressure profiles in hurricanes. *Mon. Wea. Rev.*, 108, 8, 1212-1218.

IMSL, 1987: Fortran subroutines for statistical analysis. International Mathematical and Statistical Fortran Library, 1232 pp.

Jones, W. L., L. C. Schroeder, D. H. Boggs, E. M. Bracalente, R. A. Brown, G. J. Dome, W. J. Pierson and F. J. Wentz, 1982: The SEASAT-A satellite scatterometer: The geophysical evaluation of remotely sensed wind vectors over the ocean. *J. Geophys. Res.*, 87, 3297–3317.

JTWC, 1979: Discussion on tropical cyclone Tip. Annual Typhoon Report, JTWC, Guam, Mariana Islands, 72-77.

JTWC, 1993: Western North Pacific tropical cyclones and tropical cyclone support summary, 1993. Annual Typhoon Report, JTWC, 19-35 and 225-228.

Kidder, S. Q., W. M. Gray and T. H. Vonder Haar, 1978: Estimating tropical cyclone central pressure and outer winds from satellite microwave data. *Mon. Wea. Rev.*, 106, 10, 1458-1464.

Kidder, S. Q., W. M. Gray and T. H. Vonder Haar, 1980: Tropical cyclone outer surface winds derived from satellite microwave sounder data. *Mon. Wea. Rev.*, 108, 2, 144-152.

Kidder, S. Q. and T. H. Vonder Haar, 1995: Satellite Meteorology: An introduction. Academic Press Inc., 255 pp.

Lander, M. A., 1994: Description of a monsoon gyre and its effects on the tropical cyclones in the western North Pacific during August 1991. *Wea. and Forecasting*, 9, 640–654.

McBride, J. L. and W. M. Gray, 1980: Mass divergence and vertical velocity in tropical weather systems, Part I: Diurnal variation. *Quart. J. Roy. Meteor. Soc.*, 106, 449, 501-516.

McElroy, C. A., 1996: Of the causes of tropical cyclone motion and propagation. Dept. of Atmos. Sci. M.S. Thesis, Colo. State Univ., Ft. Collins, CO, 124 pp.

Ohshima, T., H. Uchida, T. Hamada and S. AOsano, 1991: A comparison of GMS cloud motion winds with ship observed winds in typhoon vicinity. *Geophys. Mag. J. Meteor. Agency Japan*, 44, 27-35.

Riehl, H., 1954: Tropical meteorology. McGraw-Hill Book Company, New York, N.Y., 392 pp.

Riehl, H., 1963: Some relations between wind and thermal structure of steady-state hurricanes. *J. Atmos. Sci.*, 20, 276–287.

Rodgers, E., R. C. Gentry, W. Shenk and V. Oliver, 1979: The benefits of using short interval satellite images to derive winds for tropical cyclones. *Mon. Wea. Rev.*, 107, 575-584.

Rupp, J. A. and M. A. Lander, 1996: A technique for estimating recurrence intervals of tropical cyclone related high winds in the tropics: Results for Guam. *J. Appl. Meteor.*, 35, 627–637.

Sadler, J. C., M. A. Lander, A. M. Hori, L. K. Oda, 1987: Tropical marine climatic atlas. NOAA, Volume III.

Schroeder, L. C., D. H. Boggs, E. M. Bracalente, R. A. Brown, G. J. Dome, I. M. Halberstam, W. L. Jones, W. J. Pierson and F. J. Wentz, 1982: The relationship between wind vector and normalized radar cross section used to derive SEASAT-A satellite scatterometer winds. *J. Geophys. Res.*, 87, 3318–3336.

Shea, D. J., 1972: The structure and dynamics of the hurricane's inner core area. Dept. of Atmos. Sci. Paper No. 182, Colo. State Univ., Ft. Collins, CO, 105 pp.

Shoemaker, D. N., 1989: Relationships between tropical cyclone deep convection and the radial extent of damaging winds. Dept. of Atmos. Sci. Paper No. 457, Colo. State Univ., Ft. Collins, CO, 109 pp.

Stewart, R. H., 1985: Methods of satellite oceanography. Univ. of California Press, Berkley.

Uchida, H., T. Ohshima, T. Hamada and S. Osano, 1991: Low level cloud motion wind field estimated from GMS short interval images in typhoon vicinity. *Geophys. Mag. J. Meteor. Agency Japan*, 44, 37–45.

Weatherford, C. L., 1985: Typhoon structural variability. Dept. of Atmos. Sci. Paper No. 391, Colo. State Univ., Ft. Collins, CO, 77 pp.

Weatherford, C. L., 1985: Typhoon structural evolution of typhoons. Dept. of Atmos. Sci. Paper No. 446, Colo. State Univ., Ft. Collins, CO, 198 pp.

Wei, D. and W. M. Gray, 1985: Estimation of tropical cyclone outer wind strength from satellite imagery. Unpublished copy available from W. M. Gray, Colorado State Univ., Ft. Collins, CO, 80523.

Zehr, R., 1987: The diurnal variation of deep convective clouds and cirrus with tropical cyclones. Paper presented at the 17th Technical Conference on Hurricanes and Tropical Meteorology, April 7-10, Miami, FL, 4 pp.

Zehr, R. M., 1997: Satellite analysis of tropical cyclones – more quantitative and more thorough techniques. Preprints, 22nd Conf. on Hurricanes and Tropical Meteorology, May 19-23.